UNIVERSIDADE DE AVEIRO

UNIVERSITA' DEGLI STUDI DI CAGLIARI

UNIVERSITY OF PUSHCHINO

ECOLE NATIONALE de l'INDUSTRIE MINERALE

International Ph.D. Program in Environmental

Sciences and Engineering

(Academic Year 2006/07)

MEDITERRANEAN VEGETATION MONITORING BY REMOTELY SENSED DATA:

LAI retrieval and vegetation trend analysis within two forested areas in southern Italy

Advisor

Prof. Alberto Marini

Ph.D. Candidate

Ludovica Giordano

Settore disciplinare: Geo/04

Ciclo XVIII

To Riccardo

Acknowledgements

I would like to thank my research advisors, Prof.Alberto Marini, head of TeleGIS lab of Cagliari University (Italy), who contributed to arouse my curiosity about remote sensing techniques for environmental studies.

I am particularly grateful to Flavio Borfecchia who helped me to formulate my PhD research proposal and kept on offering his scientific support.

I greatly acknowledge Joachim Hill, head of Remote Sensing department of Trier University (Germany), and all his staff for the valuable help and advice especially concerning satellite image pre-processing.

I also thank Claudia Trotta with whom I shared the difficulties and problems related to the Leaf Area Index measurements field survey, Gabriele Schino for the helpful guidelines concerning the statistical analyses, and Luigi De Cecco for his material support and constant encouragement.

I would like to thank the Italian Ministry of Research and ENEA-Italian Institute for Energy, New Technology and Environment, as this work was for the most part financially supported by them. In particular, many thanks to Massimo Iannetta, head of Biotec-DES group of ENEA, who gave me the possibility to undertake this study while coping with all other job's commitments.

Finally, very special thanks go to Riccardo Cinquegrani, who offered his time to give me all his support and understanding.

CONTENTS

INTRODUCTION 7

LIST OF ACRONYMS 11

LIST OF TABLES 13

LIST OF FIGURES 15

1 REMOTE SENSING OF VEGETATION BIOPHYSICAL PROPERTIES: THEORETICAL BACKGROUND 17

1.1 SPECTRAL RANGES FOR VEGETATION DETECTION 17
1.2 LEAF AND CANOPY REFLECTANCE 18
1.3 SPECTRAL VEGETATION INDICES 22
1.4 LEAF AREA INDEX (LAI) 25

2 STUDY AREA 27

3 LEAF AREA INDEX RETRIEVAL 31

3.1 DATASET 31
3.1.1. LAI data *31*
3.1.2. Satellite and ancillary data *37*
3.1.2.1 Satellite data pre-processing *41*
3.2 UPSCALING *IN SITU* LAI MEASUREMENTS TO SATELLITE DATA 46
3.2.1. Individual spectral band analysis *52*
3.2.2. Vegetation Indices (VIs) computation and LAI-VIs regression analysis *58*
3.2.3 Multiple band approach and LAI maps production *66*
3.2.4. Using Ikonos-2 data as subsampling for upscaling LAI field measurements to Landsat medium-resolution *74*
3.3 DISCUSSION 78

4 MULTITEMPORAL ANALYSIS OF SPECTRAL VI AND CORRESPONDING CLIMATIC PARAMETERS 83

4.1. MATERIALS AND METHODS 85
4.1.1 Satellite images *85*
4.1.2. Climatic data *87*
4.1.3. Statistical analyses *88*
4.2. RESULTS 89
4.2.1. Multiannual series of climatic parameters and spectral VIs *89*
4.2.2. Climatic parameters-VIs relationships *89*
4.3 DISCUSSION 92

5. CONCLUSION 95

Introduction

Mediterranean regions are in a transitional climate zone between arid and humid regions (Di Castri & Mooney, 1973) where it has been hypothesised that climate changes may have the most pronounced effect (Palutikof et al. 1994, Cubash et al., 1996, Lavorel et al., 1998). In many areas, the synergistic effects of climate and human activities (inappropriate land use, grazing, fires, urban expansion, land abandonment, air/water/soil pollution) are already showing worrying signs of latent, unforgiving land degradation. Actually, increased research is required to further develop knowledge especially in those fragile heterogeneous ecosystems potentially vulnerable to perturbations, such as coastal Mediterranean areas (Scarascia-Mugnozza et al., 2000, Reichstein et al., 2002, Lanfredi et al., 2004).

In studying global change and long-term monitoring of the environment and man's effect on it, the necessity detailed and reliable spatial distributions of biophysical parameter is rapidly increased. Nevertheless, collecting biophysical measurements over wide areas by means of traditional field surveys is a time-consuming and expensive task. Furthermore, the establishment of monitoring frameworks for environmental problems is frequently based on retrospective, multi-temporal series of data. In particular, interannual variations in phenology of either animals and plants have been already demonstrated to be sensitive observable indicators of biospheric responses to global warming (Peneuelas, 2002). As a result, remote sensing has become a pivotal technology for environmental science, since it offers a unique means to obtain faster, cost-effective, synoptic, consistent and repetitive perspective over large areas, allowing to derive information about current states of geophysical and biophysical variables and to monitor their changes.

In particular, there is a tremendous interest and potential for retrieving vegetation cover characteristics. In fact, vegetation play a unique role in global climate change studies, regulating the energy, water and gas exchanges between the earth-atmosphere interface (Qi et al., 1995, among others). Moreover, the peculiar spectral *signature* of green vegetation, characterised by a strong absorption at the blue and red wavelenghts and a rather strong reflection at the near-infrared wavelenghts, enables one to to distinguish it well from other terrestrial targets. As a matter of fact, in the last

decade, a lot of knowledge has been gained about spatio-temporal variations of vegetation cover through satellite/airborne image processing. Several essential vegetation biophysical characteristics, such as net primary productivity (NPP), phenology, vegetation structure, e.g. Leaf Area Index (LAI), community composition, vegetation condition, canopy roughness length, have been obtained by means of satellite imagery analysis on a landscape or even larger scale with different degree of success (Myneni et al., 1997, Goetz et al., 1999, Gower et al., 1999, Muchoney et al., 2002, Cias et al., 2005).

In particular, estimation of forest biomass and its changes have become an important topic in the global change research. In fact, although it is generally agreement that forest biomass above-ground carbon pool in the Northern Hemisphere has increased in the past decades, and thus acts as the sink for atmospheric CO2, nevertheless the magnitude, location and causes of this increase remain uncertain (Goodale et al., 2002).

Besides, the recent advent of a new class of commercial remote sensing satellites provides unprecedented observations of the earth from space that are both synoptic and detailed in nature. The possibility to resolve features in scenes that coarser resolution data cannot resolve offers the unique opportunity to both validate conclusions derived from coarser resolution systems and to extend results obtained within rather homogeneous areas toward more complex and mixed environments. This is particularly appealing when considering Mediterranean areas where the performance of environmental and climate models is often limited by a too rough description of the Earth's surface heterogeneity.

In this context, the objective of the following research was twofold.

The first one was the production of Leaf Area Index (LAI) distribution maps within two forested study areas, by means of satellite data. The utility of using high resolution satellite data, like Ikonos-2, and both high and medium (Landsat) spatial resolution data when regional-wide map need to be produced, was investigated and results discussed. It is noteworthy that such an investigation considered two years of observation in order to be able to assess to what extent results obtained with data collected at a certain time point (year) matched those related to data collected in other years. In other words, two years of data collection were considered to test whether it is possibile to temporally extrapolate results obtained using a given dataset (i.e. the

empirical relationship calibrated at present) to past and/or future satellite observations of the same area. The choice to focus on LAI derives by the paramount role this vegetation biophysical parameters plays within important processes, such as canopy radiation interception, evapotranspiration and net photosynthesis (Qi J. et al., 2000; Kyung-Ja Ha et. al., 2001; among others), consequently being a key input parameter of many climate (Sellers et al. 1986, Sellers et al. 1997, Chase et al., 1996, Buermann et al., 2001, Tian Y. et al. 2002), hydrological (D'Urso et al., 1999) and ecological models (e.g. Biome-BGC, see also Chen et al, 2000, Asner et al., 2003, Gong et al., 2003).

The second objective concerned a trend analysis, within the same study areas, aimed at improving our understanding of Mediterranean forests' response to changing climatic conditions. In particular, a yearly series of Landsat satellite data and daily local meteorological measurements over a time span of twenty years (1984-2005) were processed and compared in order to evaluate possible relationships between inter-annual variations of vegetation activity/productivity and related temperature and precipitation regimes.

OUTLINE OF THESIS

Chapter 1 contains some theoretical background about the remote sensing of vegetation biophysical properties including vegetation spectral characteristics at leaf and canopy level, Leaf Area Index (LAI) and spectral Vegetation Indexes (VI_s) definitions and rationale.

Chapter 2 provides a description of the two study areas.

Chapter 3 describes the LAI spatial distribution retrieval analysis, including the adopted datasets (*in situ* measurements and satellite radiometric data), methods for local scale and regional-wide scale map production, and the obtained results

Chapter 4 concerns the vegetation retrospective analysis carried out by processing yearly pairs of satellite and corresponding climatic data within a time span of twenty years (1984-2005).

Finally, some concluding remarks are reported in Chapter 5.

List of Acronyms

Some of the acronyms used once or confined in a specific paragraph and falling outside the mean argumentation, are defined in the text/paragraph only (e.g., all spectral vegetation indices and satellite sensors' acronyms).

acronyms	interpretation
ANCOVA	analysis of covariance
BRDF	bidirectional reflectance distribution function
cv	coefficient of variation
DEM	digital elevation model
DN	digital number
EM	electromagnetic spectrum
GCPs	ground control points
GPS	global positioning system
L	radiance
λ	wavelength
LAI	leaf area index
nIR	near-infrared
NPP	net primary productivity
P	precipitation
ρ	reflectance
RMSE	root mean square error
SWIR	short-wave infrared
T	temperature
τ	aerosol optical thickness
VI	spectral vegetation index

List of Tables

Table 1 - Summary statistics for LAI data collected during the 2004 (a) and 2005 (b) in four different vegetation communities.....32
Table 2 – Ikonos-2 and Landsat TM/ETM bands, spatial and radiometric resolution, acquisition dates.....34
Table 3 – Acquisition parameters of the Ikonos-2 images.....36
Table 4 – RMSE (pixel unit) of orthorectification process.....39
Table 5 – Ikonos radiometric calibration coefficients.....40
Table 6 – Landsat TM and ETM+ calibration coefficients.....40
Table 7 – Results of ANCOVA analysis using NDVI as radiometric variable.....44
Table 8 – Results of ANCOVA analysis using individual band as radiometric variable 45
Table 9 – Performance (r2) of band-by-band regressions carried out using different sensors, multi-year or single-year data sets and different averaging pixel windows size 49
Table 10 – Mean coefficient of variation (%) of Ikonos reflectance computed in 3x3 pixel window size 51
Table 11 – Mean coefficient of variation (%) of Ikonos reflectance computed in 23x23 pixel window 51
Table 12 – Mean coefficient of variation (%) of Ikonos 2004 and 2005 reflectance computed in 3x3 pixel window size centred on 2004 plot locations 52
Table 13 – Comparison between the ratios of within-plot coefficients of variations of reflectance derived from 2004 and 2005 data of either ETM and re-sampled Ikonos images 53
Table 14 –Landsat and Ikonos-derived VI 56
Table 15 – Performance (r2) of VI-based regressions carried out using different sensors, pooled data sets and different averaging pixel windows size 59
Table 16 – Performance (r2) of VI-based regressions carried out using different sensors, sinlge year data sets and different averaging pixel window size 59
Table 17 – Multivariate model terms and relative slope and significance, Ikonos and Landsat ETM sensor, year 2004 64
Table 18 – Multivariate model terms and relative slope and significance, Ikonos and Landsat ETM sensor, year 2005 64
Table 19 – Coefficients of variation per each model term coefficient (leave-one-out procedure) 66
Table 20 – Multivariate model terms, and respective slope and significance, for Landsat ETM-sensor 72
Table 21 – List of Landsat images used 81
Table 22 – Results of statistical analysis between climatic parameters and VIs for the two study areas of M.Coppolo and Pantano 86

Table 23 – Results of statistical analysis between climatic parameters and VIs for M.Coppolo study area per vegetation 87
Table 24 – Results of statistical analysis between climatic parameters and VIs for Pantano study area per vegetation typology 87

List of Figures

Figure 1 – Typical spectral response characteristics of a green leaf 15
Figure 2 – Schematic two-dimensional leaf cross section and leaf reflectance properties 16
Figure 3 – Study areas reported on a Landsat ETM+ multispectral image. The overlapped frame on the lower right-hand corner highlights the Basilicata region within a map of Italy 23
Figure 4 – Climatic diagrams of Pantano (a) and Monte Coppolo (b) study areas, (1970-2000) . 25
Figure 5 – LI-COR LAI 2000 Plant Canopy Analyzer and the acquisition scheme of its optical sensor 28
Figure 6 – Field LAI measurement sampling scheme. In the sketch above four reading per plot are supposed 29
Figure 7 – plot locations of LAI measurements carried out in 2004 (yellow dots) and 2005 (red dots), respectively 30
Figure 8 – mean and variance of field LAI per vegetation typology and year 31
Figure 9 - Ikonos-2 and first four Landsat TM bands spectral response curves 34
Figure 10 - Upscaling in situ LAI measurements to satellite data: comparison between Ikonos and Landsat data performances (hypothesis 1 - orange versus green arrow); comparison between direct Landsat calibration and a two-stage calibration procedure (hypothesis 2 - orange and blue arrows versus green arrow) exploiting Ikonos-derived LAI spatial distributions as intermediate stage for ETM data calibration 48
Fig. 11 - IKONOS-derived LAI maps over the two study sites Pantano and Monte Coppolo, for 2004, August 2 acquisition dates 68
Fig. 12 - IKONOS-derived LAI maps over the two study sites Pantano and Monte Coppolo, for 2005, June 22 acquisition dates 69
Fig. 13 – LAI values distribution for Monte coppolo and Pantano sites, in 2004 ((a) and (b)) and 2005 ((c) and (d)), respectively 70
Figure 14 – Interannual climatic fluctuations - Valsinni and Policoro ground stations 85
Figure 15 – Interannual VI fluctuations observed for M.Coppolo and Pantano areas 85

1 Remote sensing of vegetation biophysical properties: theoretical background

1.1 Spectral ranges for vegetation detection

From the electromagnetic (EM) spectrum, three different wavelength regions can be used to provide information on vegetation characteristics: the Visible to Short Wave Infrared, the Thermal Infrared and the Microwave regions:

1) *Visible to Short Wave Infrared (0.40 - 2.50 μm).* Vegetation reflectance in this portion of the EM spectrum provides information on vegetation biophysical parameters such as chlorophyll, physiological structure and leaf cellular water content. Visible and near infrared channels are available on most optical satellite sensors such as: NOAA-AVHRR (National and Oceanic Atmospheric Administration-Advance Very High Resolution Radiometer), Terra-MODIS (MODerate resolution Imaging Spectroradiometer) and ASTER (Advanced Spaceborne Thermal Emission and Reflection radiometer), SPOT (Satellite Pour l'Observation de la Terre) Vegetation, Meteosat, Envisat-AATSR (Advanced Along Track Scanning Radiometer), Landsat ETM+ (Enhanced Thematic Mapper Plus), TM (Thematic Mapper) and MSS (Multispectral Scanner), Ikonos-2, Quickbird, among others.
2) *Thermal Infrared (6.0 - 15.0 μm).* Emittance of this portion of the EM spectrum provides information on the thermal properties of vegetation cover such as sensible heat. Sensible heat[1] is used to estimate evapotranspiration of vegetation canopies, which is closely related to water stress. For instance, thermal infrared wavelengths are available on NOAA-AVHRR, METEOSAT, ERS2-ATSR (Along Track Scanning Radiometer), GOES (Geostationary Operational Environment Satellite), GMS (Geostationary Meteorological Satellite) and LANDSAT-TM sensors.
3) *Microwave (0.1 - 100 cm).* Active and passive microwave approaches have been developed to sense soil water content, which can be highly relevant to vegetation monitoring. Passive microwave sensors provide information on the thermal

[1] Same as *enthalpy*: the heat absorbed or transmitted by a substance during a change of temperature which is not accompanied by a change of state.

properties of water. Examples are: Passive sensor Special Sensor Microwave Imager (SSM/I), currently available on the Defence Meteorological Satellite Programme (DMSP) platform; TRMM Microwave Imager (TMI) of the Tropical Rainfall Measuring Mission (TRMM) and most of all the Advanced Microwave Scanning Radiometer (AMSR), with dual-polarized channels, onboard the Earth Observing System-Aqua platform. Active microwave sensors provide information on the dielectric constant, which may be related to vegetation water content. References can be found in: Moghaddam and Saatchi (1999); Pampaloni (2004), among others. Examples of active sensors include RADARSAT, ENVISAT-ASAR (Advanced Synthetic Aperture Radar) and JERS-1 (Japanese Earth Resource Satellite).

This study will consider only the optical domain ranges from 0.4 to 2.50 µm.

1.2 Leaf and canopy reflectance

Leaf and canopy optical properties encompass an extensive subject, whose extensive discussion is outside the scope of this thesis, hence here only some basic knowledge are introduced. The spectral response of a leaf can be conveniently divided into three parts, as reported in Figure 1:

- the visible (400-800 nm) characterized by a strong absorption of light by photosynthetic pigments (chlorophyll *a* and *b*, and carotenoids) in a green leaf[2] (Chappelle et al. 1992, Gitelson et al., 1996 (a); Gitelson et al.,1997, Lichtenthaler et al., 1996); eventually, 70-90% of the incoming radiation in blue and red wavelength is absorbed;
- the near infrared plateau (800-1100 nm) where absorption is limited to dry matter but where multiple scattering within the leaf, related to the arrangements and fraction of air spaces between the cells (Danson, 1995), i.e., to the internal structure, drives the reflectance and transmittance levels; the scatter of light in this part of the leaf is very effective because of the high contrast in the index of refraction between the water-rich cell contents and the intercellular air spaces; moreover, in the spectral range 700-1300 nm plants are very bright because this is a spectral region between

[2] the pigments absorb both blue and red light for use in the photosynthesis, while somewhat more of the green light is reflected

the electronic transitions, which provide absorption in the visible and molecular vibrations which absorb in longer wavelengths;

- the middle infrared (1100-2500 nm), which is also a zone of strong absorption, primarily by water in a fresh leaf (Aoki et al., 1988, Hunt et al. 1987, Hunt et al. 1989, Inoue et al., 1993; Peñuelas et al., 1993; Ceccato et al., 2001) and secondarily by dry matter when the leaf wilts;

The water absorption bands are located both in near infrared and middle infrared at approximately 1950, 1450, 1175, 970 nm. Minor absorption also occurs at different wavelength by other biochemical constituent in leaves such as protein, lignin, cellulose and nitrogen (Curran & Kupiec, 1995).

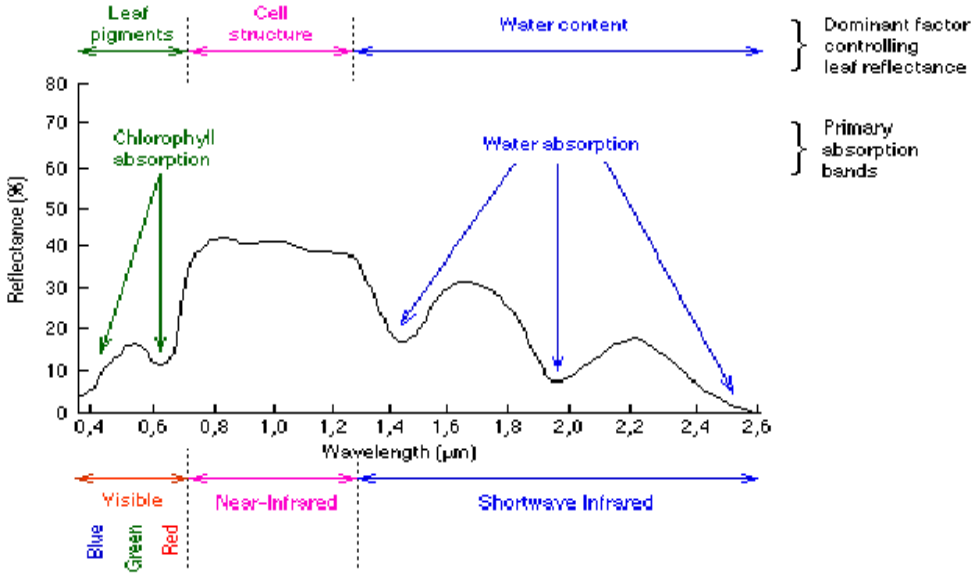

Figure 1 – Typical spectral response characteristics of a green leaf (after Hoffer, 1978)

Light attenuation inside leaves results from complex phenomena related to biochemical composition and anatomical features (Fourty et al., 1996, Ustin et al., 2001, Carter et al., 2001), while the epidermis determines the bidirectional reflectance. As shown in Figure 2 the upper layer of a leaf, called epidermis, is made up of specialized cells arranged so that no gaps or openings exist. On the surface of these cells there is a wax layer called the cuticule, which prevents moisture loss from within the leaf. Both are very transparent to infrared radiation and the majority of the radiation is transmitted to the more internal layer of spongy mesophyll tissue, with irregularly shaped cells

separated by interconnected openings, which scatters the infrared radiation both upward and downward and only a fraction is absorbed.

Furthermore, to fully explain the spectral behaviour of a canopy, information on the leaves' spectral characteristics alone is not sufficient. In fact, it is the combination of multiple factors that gives rise to the canopy reflectance in vegetated pixels. A canopy consists of a set of plants; each plant has usually many leaf layers, e.g. many branches which have many leaves. The leaves may differ in type, age, size, orientation and shape, creating together with the ground, shadowing and structural variables as stems and branches, a complex of elements that influences the canopy reflectance as a whole. Canopy structure is also dynamic, changing on timescales ranging from minutes to years. Heliotropic leaves track the sun throughout the day. Other species fold, droop, or drop their leaves in response to water stress, light, or season.

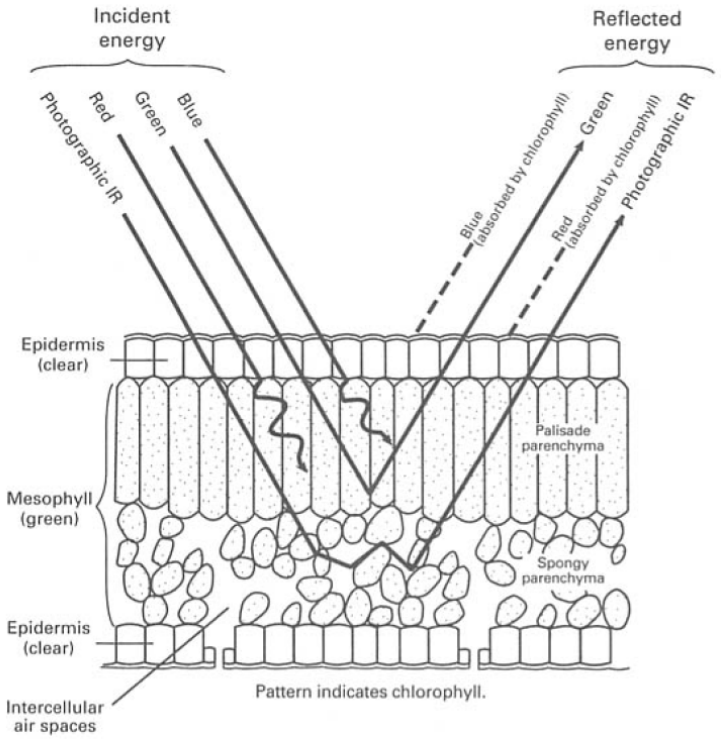

Figure 2 – Schematic two-dimensional leaf cross section and leaf reflectance properties (Sabins, 1996)

Thus, in addition to leaf optical properties, e.g. reflectance, transmittance and absorptance, among the most important elements affecting canopy reflectance (in a certain period) are: green biomass cover percentage (i.e. the proportion between

vegetated and non-vegetated surface) and density, structural/architectural properties, such as leaf dimension; leaves location, e.g. vertical and horizontal distribution, and orientation in three-dimensional space, e.g. leaves inclination and azimuth angle distribution; illumination angle; reflectance of the understorey layer (litter, soil or other background).

Particularly, it must be stressed that changing viewing (i.e. sensor) and/or illumination (i.e. sun) direction changes the proportion of light reflected towards the observer. This is a general statement not only referred to vegetation but to any surface since only an ideal and perfectly diffuse (Lambertian) surface would irradiate exactly the same in any directions and would be independent on light incoming direction. Therefore, this is another element which should be taken into account when using radiometric data to infer whatever information. The "Bidirectional reflectance" is a term first used by Nicodemus et al., 1977 to refer to this dependency of radiometric measurements from both viewing and illumination angles. However, although it is currently part of the established nomenclature for the reflectance products derived by in situ, air- and spaceborne sensors, to be rigorous it must be said that the bidirectional reflectance is not a physically measurable variable[3]. It can only be approximated by measurements and it is rather sensitive to different sensor sampling schemes, preprocessing, atmospheric correction, and angular modelling (see the excellent review on the basic concept and definitions of reflectance quantities by Schaepman-Strub et al., (2006) for further details). Anyway, here it will be referred to as the broadly accepted and used bidirectional reflectance approximated concept. Therefore, the Bidirectional Reflectance Distribution Function[4] (BRDF) describes the scattering of incident light

[3] It is defined as the ratio of the reflected radiance from an infinitesimal surface area in the direction ($\vartheta r,\Phi r$) to the incident radiance upon the same surface from the direction ($\vartheta i,\Phi i$). ϑ and Φ are azimuth and elevation coordinates of a spherical coordinate system centered on the infinitesimal surface of reflection. Bidirectional reflectance, as geometrically and mathematically defined, can never be directly measured because truly infinitesimal solid angles around the directions of incoming or reflecting radiation do not include measurable amounts of radiant flux.

[4] Since it is not possible to measure bidirectional reflectance, BRDF values reported in practice are actually related to another reflectance property called *bidirectional reflectance factor (BRF)*. This is defined as the ratio of radiant flux actually reflected by a sample surface to that which would be reflected into the same reflected-beam geometry by an ideal, lossless, perfectly diffuse (Lambertian) standard surface irradiated in exactly the same way as the sample. However, it is generally accepted that bidirectional reflectance factor measurements of sufficient angular density provide useful estimates of the true BRDF. The BRDF depends on wavelength and is determined by the structural and optical properties of the surface, such as shadow-casting, mutiple scattering, mutual shadowing, transmission, reflection, absorption and emission by surface elements, facet orientation distribution and facet density.

from one direction in the hemisphere into another direction in the hemisphere. The BRDF is an intrinsic reflectance property of a surface and can be used, when known, to correct view and illumination angle effects. Every non-Lambertian surface has its characteristic BRDF, whereas the BRDF of an ideal Lambertian surface is $1/\pi$. References on vegetation BRDF modelling could be found in Susaki et al. (2004), Gao et al. (2003), Li (2000), Chen et Leblanc (1997), among others. It is worth noting that, given the importance of these two parameters, with the launch of NASA's Terra satellite and the MODerate Resolution Imaging Spectroradiometer-MODIS (Justice et al., 1998) 1-km spatial resolution BRDF and 8-day composite LAI products are routinely made available to the scientific community. However, stage 1 validation[5] concluded that MODIS LAI tends to overestimate field measurements by about 12% in dense vegetation (Fensholt et al., 2004, Cohen et al., 2003, among others).

1.3 Spectral Vegetation Indices

The spectral Vegetation Indices (VIs) are mathematical transformations designed to assess the spectral contribution of green vegetation to multispectral observations. They basically are a ratio or a linear combination of two or multiple spectral bands exploiting the peculiar, aforementioned, spectral pattern of leaf components so as to be more sensitive than individual bands to vegetation parameters.

Band ratioing is a common practice in remote sensing as it reduces many forms of multiplicative noise due to illumination conditions (solar illumination differences, cloud shadows, atmospheric attenuation, certain topographic variations) present in multiple bands.

In particular, VIs exploit the characteristic absorption by vegetation in the visible - particularly in the red - portion of the spectrum, due to the presence of clorophyll and other absorbing pigments in the leaves, and high reflectance of green live vegetation in the near-infrared portion (Tucker, 1979), see also figure 1.

VIs have been variously proposed, modified, theoretically analyzed, compared, summarized, categorized, and criticized. A complete review of the more than 100 published VIs is obviously out of the scope of this thesis, and excellent reviews can be

[5] See MODIS Land team web site http://landval.gsfc.nasa.gov/ProductStatus.php?ProductID=MOD15

found in the literature (e.g. Basso et al. 2004, Verstraete et al., 1996 (a), Rondeaux et al., 1996, Bannari et al. 1995, Qi et al. 1994, Baret and Guyot, 1991, Perry and Latenschlager, 1984). Therefore, here only multispectral VIs' rationale is outlined. The readers interested in further details are referred to the cited original publications.

Most of VIs have been designed on the basis of the *soil-line* concepts. Essentially, it is a hypothetical line in red and nIR spectral space along which bare soils of differing brightness lie[6]. This means that soil pixels in red and nIR spectral space are highly correlated with positive correlation coefficient and functionally related by a linear equation of the form nIR =a*red +b.

Most indices measures the distance of one pixel to the soil line (i.e. orthogonal indices, such as the Perpendicular Vegetation Index $(nIR-a*red-b)/(a^2+1)^2$ proposed by Crippen (1990) or the Weighted Difference Vegetation Index (WDVI=nIr-a*red) developed by Clevers (1989)), whereas several other indices (e.g. the Normalised Difference Vegetation Index=(nIr-red)/(nIR+red) (Rouse et al., 1973), among others) measure the angle of the vegetation pixel in the red/nIR space in reference to the soil line (Liang, 2004 (a)).

The Normalized Difference Vegetation Index, NDVI, is one of the oldest, most widely used ratio-based index and, generally, the common vegetation index referred to. It followed the simple ratio SR=nIR/red developed by Jordan (1969). NDVI has been used at virtually all scales ranging from small plot research to global investigations. Part of its popularity stems from the fact that it uses baseline spectral bands available from virtually all remote sensing systems, including colour infrared photography, and it is computationally very efficient. Numerous studies have shown the wide-ranging utility of the NDVI from climate studies, to famine early warning detection, epidemiology and renewable natural resources management. In particular, various authors found valuable relationships between NDVI and biophysical plant canopy properties, such as biomass (Sannier et al., 2002; among other) and Leaf Area Index (Cohen et al., 2003; Kyung-Ja et al., 2001, among others).

Anyway, NDVI is rather sensitive to atmosphere and canopy background variations and hence it is often difficult to interpret at low LAI (Daughtry et al. 2000). Therefore, a

[6] the soil line concept, originally defined for the red-nIR feature space, can also be transferred into other spectral domains (Thenkabail et al., 2000).

lot of alternative indices, often introducing correction factors or constants, aimed at accounting for or minimising those varying exogenous noises, have been developed.

In general a spectral index optimised for sensitivity to a particular variable will also be sensitive to other variables. In other words, it usually not possible to achieve both optimal sensitivity to a desired process and total insensitivity to all perturbing factors (Verstraete et al., 1996 b). Examples are the Atmospherically Resistant Vegetation Index (ARVI, Kaufman and Tanrè, 1992), which takes advantage of the presence of the blue channel in addition to the red and the nIR included within the NDVI to operate a self-correction process for the atmospheric effect on the red channel based on the difference between the blue and the red channels; and the series of soil adjusted vegetation indices, e.g. the Soil Adjusted Vegetation Index (SAVI, Heute, 1988), the Transformed Adjusted Vegetation Index (TSAVI, Baret et al. 1989), the Modified Soil Adjusted Vegetation Index (MSAVI, Qi et al., 1994), and the Optimised Soil Adjusted Vegetation Index (OSAVI, Rondeaux et al., 1996).

Finally, similar to the principal-component transformation the "Tasseled Cap" transformationwas developed by Kauth and Thomas (1976) for Landsat Multi Spectral Scanner (MSS) data; and its second component has become known as the Greenness Index. The "Tasseled Cap" is an affine transformation[7] which determines a new orthonormal basis for the bands that highlights differences in vegetation and soil, enhancing the underlying structure of the image. Crist and Cicone (1984) have extended the analysis to six bands of Landsat Thematic Mapper (TM) data (excluding the thermal infrared band), Huang et al. (2002) to Landsat ETM+ bands, whereas Horne (2003) provided coefficients for Ikonos-derived Greeness Index.

It must be said that, generally, VI exhibits asymptotic (saturated) signals over high biomass conditions, usually because red does not change much but nIR still increases when canopy become denser. Therefore, many authors found that most indices have an exponential relationship with vegetation biophysical parameters (e.g. Carlson& Ripley, 1997; Broge and Mortensen, 2002, Wang et al., 2005, Anderson et al., 2004, among others).

In this thesis the predicted ability of multiple VIs have been tested either in relation to their capacity to provide a quantitative estimate of vegetation structural

[7] A function on a linear space to itself, which is the sum of a linear transformation and a fixed vector.

characteristics (Leaf Area Index) and with regard to their utility in monitoring inter-annual possible changes of vegetation productivity in response to occurring different climatic conditions.

1.4 Leaf Area Index (LAI)

The LAI is broadly defined as one-half of the total area of all leaves in the canopy per unit ground area, within a defined region (m^2/m^2). It is a dimensionless, structural vegetation parameter, which can be measured, analyzed and modelled across a range of spatial scales, from individual tree crowns or clusters to whole regions or continents. Therefore, the LAI is profitably used for scaling between leaf and canopy measurements of vegetation biophysical parameters and it has become a central and basic descriptor of vegetation cover/condition in carbon, water and energy balance studies.

Traditionally, two common approaches have been currently utilized for estimating LAI from optical remotely sensed data:

1) statistical methods, e.g. empirical relationships established by statistically fitting observed LAI values and correspondent remotely sensed data, mainly in form of spectral Vegetation Indices (see next sections);

2) physical algorithms, relying on inverting canopy reflectance model.

Both approaches have advantages and limitations (Qi et al. 2000). Empirical relationships vary substantially in mathematical forms and in their empirical coefficients when different vegetation type are considered. Moreover, they are sensitive to soil background characteristics, bidirectional properties (solar and viewing geometries), atmospheric conditions, chlorophyll concentrations and topography. Additionally, in situ calibration measurements of LAI over regional or global scales are impractical.

On the other hand, biophysical inversion of remotely sensed data is constrained by the complexity of the remote sensing process. Variations in sensor response associated with solar and sensor geometries, surface directional reflectance, topography, atmospheric absorption and scattering, and sensor electrical-optical engineering interact in complex manners that are difficult to decouple and quantify in individual images or in time series of images. Moreover, there is no universally applicable canopy reflectance

model for all vegetation types, thus making model selection problematic. Model selection is often a compromise between model complexity, invertibility, and computational efficiency (Jacquemoud et al., 1995). One-dimensional radiative transfer models are best suited to inversion, but they often have the tendency to oversimplify. In general, associated problems can include lack of convergence, sensitivity of results to initial values chosen for the solution, and difficulty in estimating model input parameters that cannot be directly measured. Finally, the retrieval of LAI through inversion of physically based canopy reflectance models is computationally very cumbersome for large geographic areas (Walthall et al., 2004, Deng et al., 2006).

In this thesis the statistical approach was explored in order to assess to what extent the availability of high resolution remotely sensed data and LAI field measurements can produce appropriate results, by simple regression analysis, in heterogeneous Mediterranean vegetation.

2 Study area

One of the peculiarities of Mediterranean area is the great diversity in endemic plant species (Cowling et al., 1996). However, many of them are now confined to very small areas and thus are extremely vulnerable to habitat loss, overgrazing, and urban/crops expansion. The two study areas were selected as partially representative of these conditions. They are both located in the southern part of Matera Province, Basilicata region (South of Italy) along the Ionian Sea coast (see Figure 3, yellow rectangles).

Figure 3 – Study areas reported on a Landsat ETM+ multispectral image. The overlapped frame on the lower right-hand corner highlights the Basilicata region within a map of Italy.

The first site, showed in the right-hand part of Figure 3 and hereafter referred to as Pantano, represents the last residual of an ancient humid forest which covered 1600 hectares up to the 1930's. Nowadays, it extends about 500 hectares. Also, it have been progressively losing its marked hygrophilous characteristics because of aquifer subsidence (Fascetti, 1996). However, it has recently become a protected area because of its natural, ornithological and entomological importance (e.g. Bavusi et al., 1992). It is a flat area, with an altitudes ranging from 0 to 5 m a.s.l., characterized by present dunes, alluvial deposits with alternating sands and clays and intercalations of gravels mainly near the water courses. The vegetation of the inner part of this area is mainly represented by an azonal hygrophilous forest (*Fraxinus oxycarpa* Bieb., *Populus canescens* L., *Ulmus minor* Miller and *Alnus glutinosa* L.) with middle-European

characteristics (Fascetti, 1996), whereas, next to the shoreline, the vegetation is characterized by typical psammophilous[8] communities (*Agropyron junceum* (L.) Beauv., *Ammophila littoralis* (Beauv.) Rothm., *Eryngium maritimum* L., *Cyperus kalli* (Forsskal) Murb.) of sand dunes. Between the psammophilous vegetation and the hygrophilous forest there are patches of halophilous[9] communities (*Juncus acutus* L., *Erianthus ravennae* (L.) Beauv., *Schoenus nigricans* L., *Plantago crassifolia* Forsskal) and maquis of Mediterranean sclerophyllous vegetation consisting of evergreen shrubs (mainly *Rosmarinus officinalis* L., *Phillyrea latifolia* L., *Pistacia lentiscus* L., *Juniperus oxycedrus* L.). In the open areas of maquis and along the pathways, arid grass communities (*Aegilops geniculata* Roth, *Plantago psyllium* L., *Lagurus ovatus* L., *Medicago polymorpha* L.) are found.

The second site, reported in the left side of Figure 3 and hereafter referred to as Monte Coppolo (after Coppolo Mountain included within the area), is a forested area located about 15 kilometres from the coast in a topographically more complex territory with altitudes ranging from 500 m to 800 m a.s.l.. The area, extending about 800 ha, is part of the Monte Pollino National Park. Alternating sandstones, marls and limestone, with large outcrops of scaly shale complex, represent here the geological substrate. In the valley floors are deposited slope debris composed of arenaceous or calcareous elements. In this study area, mainly four vegetation communities can be distinguished: a live oak forest *(Quercus ilex* L.), a mixed broadleaf forest *(Quercus cerris* L., *Q. pubescens* Willd. and *Carpinus orientalis* Miller), a high maquis consisting of shrubs with an average height of about 2-3 m (predominantly *Q. ilex* L., *Juniperus oxycedrus* L., *Phillyrea latifolia* L., *Pistacia lentiscus* L. and *Spartium junceum* L.) and a garrigue (*Cistus salvifolius* L., *Calicotome spinosa* (L.) Link, *Cistus monspeliensis* L. and *Erica arborea* L.).

Both sites are characterised by a typical Mediterranean climate in which rainfalls are concentrated during autumn and winter and decrease in summer, when a period of dryness takes place from May to September. Figure 4 shows the climatic diagrams, based on a 30-year dataset (1970-2000) provided by two meteorological stations close to the study sites, reporting the monthly mean air temperature (red line) and

[8] living in sandy habitats (specialized condition)
[9] salt-tolerant vegetation

precipitation (blue line). The dotted area represents the dry period. The annual average rainfall is 535 mm and 726 mm for Pantano and Monte Coppolo sites, respectively, whereas the average annual air temperature is around 16 °C for both sites. Mean minimum and maximum air temperatures occur in January and in August, respectively.

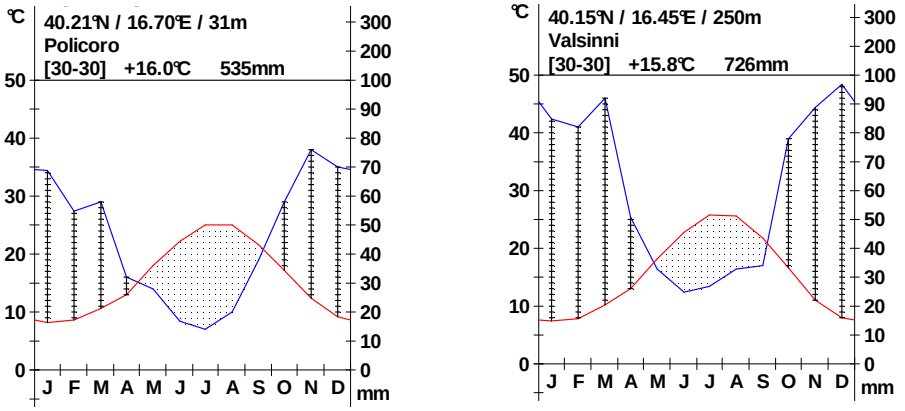

Figure 4 – Climatic diagrams of Pantano (a) and Monte Coppolo (b) study areas, (1970-2000).

3 Leaf Area Index retrieval

3.1 Dataset

3.1.1. LAI data

LAI data were collected during two field surveys carried out in 2004 and in 2005 within 110 plots in all (55 independent plots per year, respectively).

Two previous field surveys, made in October 2003 and April 2004, provided the necessary practical knowledge of the study areas and the opportunity to select and locate the plots wherein performing the LAI measurements later on. In general, the sampling locations were chosen in order to consider the most representative vegetation typologies characterising the study sites (in relation to only forested areas) and to minimise vegetation structural and species heterogeneity within a surrounding area of about 12x12 metres, corresponding to a 3x3-pixel area of Ikonos-2 data. Obviously, plots were located in order to avoid plot overlapping. In both years, four vegetation classes were investigated: *maquis, live oak forest, mixed oak forest* (deciduous forest) and *hygrofilous forest*.

For each sampling plot, the central geographical coordinates were recorded with a handheld *Trimble ProXRS* Geographic Positioning System (GPS) receiver. Once in lab, GPS data were differentially corrected using *Pathfinder* postprocessing software achieving an average horizontal position precision of about 1,5-2 meter. A LAI-2000 *PCA-Plant Canopy Analyzer* (Li-COR, Lincoln, NE, USA) was used to determine indirect LAI values. It is one of the numerous commercially available optical instruments (Jonckheere et al., 2004), such as Decagon ceptometers, DEMON, and TRAC, which infer LAI indirect estimates from measurements of light transmission through a plant canopy.

In particular, PCA is designed to be used under diffuse lightening, and provides effective LAI (LAI retrieved under the assumptions of a random spatial distribution of leaves, Chen & Black, (1991). It is based on a fish-eye light sensor that measures diffuse radiation simultaneously in five distinct angular bands ranging from 0° to 75°, see figure 5. From the differences in diffuse radiation measured above and below the canopy it estimates the canopy gap fraction per angular band. The canopy gap fraction is the fraction of view in a certain direction from beneath a canopy that is not blocked by foliage. Finally, under the assumptions of a random spatial distribution of leaves, canopy gap fraction data are inverted to obtain LAI estimates (LI-COR, 1992).

Figure 5 - LI-COR LAI 2000 Plant Canopy Analyzer and the acquisition scheme of its optical sensor.

In taking the measurements, some practical considerations, according to the operating manual and the logistic constraints, have been taken into account. Thus, all measurements were made:

a) under diffuse lighting condition in order to prevent direct beam radiation, reflecting off upper leaves, from causing these leaves to be confused with gaps (multiple scattering effects), that is during early morning or late afternoon or with uniformly overcast sky so as to avoid rapid change in the incoming radiation intensity;

b) using a 315° view cap wedge blocking 3/4 of the sensor view in order to reduce sensor footprint[10] and relate it to the set plot area (about 3x3 Ikonos pixel on an average) also preventing sensor-operator interference;

[10] The single, sampled area (A) per reading depends on canopy height (H), as $A=f\pi H^2$; where A is a cylindric area with radius roughly equal to the canopy height, f is the field of view fraction, which

c) at all plots, below canopy readings were measured at each of at least four subplots and these were averaged to provide a single LAI value for each plot; specifically, to this aim the sampling scheme sketched in figure 6 was adopted, where the four black dots indicate the four subplot sensor locations each accounting for a sampling area (sensor footprint) of a quarter of circle (striped areas) of about 5-10 m radius, depending on canopy height; above and below canopy readings were performed maintaining the same relative orientation between sun illumination direction and sensor's field of view;

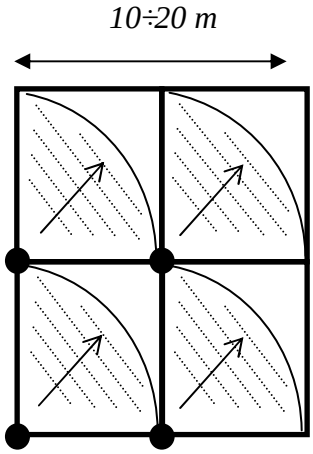

Figure 6 – Field LAI measurement sampling scheme. In the sketch above four reading per plot are supposed.

d) if sky conditions were not sufficiently stable, two above canopy readings were taken, one before and the other at the end of the below canopy measurements, in order to get a final average value. Since above canopy readings (as frequently happens in forested areas) were difficult to be carried out, they were performed within the nearest[11] clearings (open field, roads).

It is worth highlighting that is rather important to exactly report what kind of definition and protocol is adopted in determining LAI values. In fact, from the review of the scientific literature it appears that several definitions and measuring technique, direct or indirect, can be found (Welles, 1990; Welles and Norman, 1991; Welles and

depends on the utilised cap-view. The potential field of view of the sensor is larger than this but the effective range of view is reduced by foliage (Li-Cor, 1992).

[11] the nearer the better, since time between the two readings had to be as short as possible, so as to ensure the same illumination conditions (sun elevation and atmospheric conditions). Alternatives are possible with two linked-instruments, performing synchronous readings.

Cohen, 1996; White et al., 2000; Hall et al., 1995). Regrettably, although they do not always lead to the same quantitative results, many reports fail to provide any details of the LAI definition assumed, and a significant fraction do not describe the methodology used (Asner et al., 2003).

Following the above-reported criteria, 55 LAI ground measurements were taken during early July 2004 and 55 new ones were carried out, over spatially independent plots, at the end of May 2005 (see figure 7).

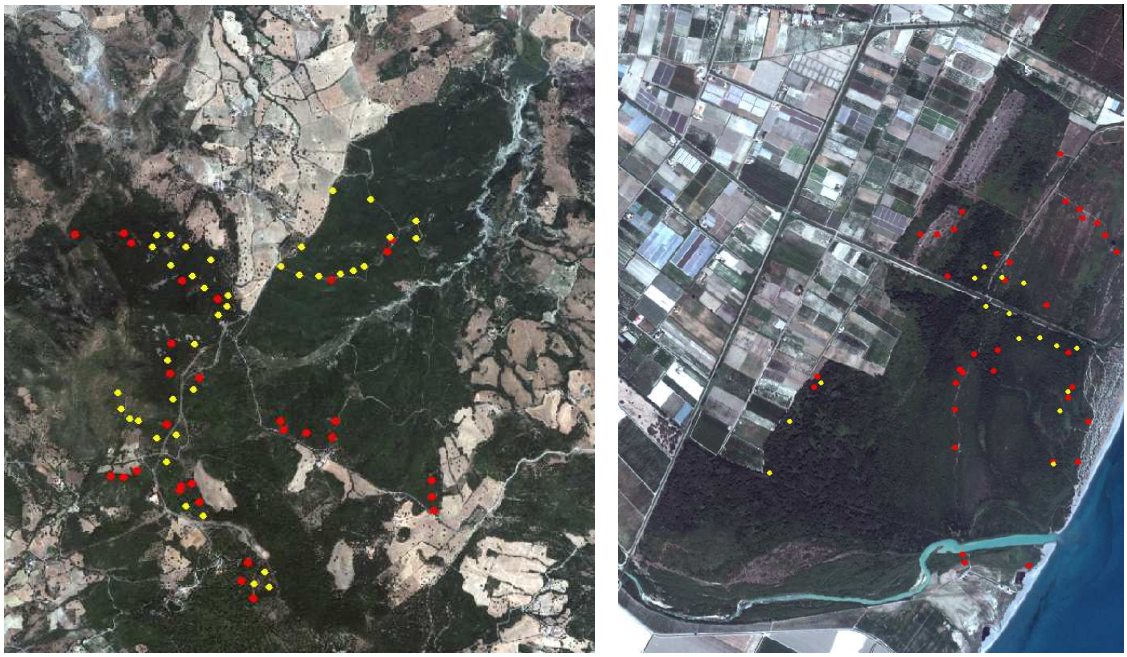

Figure 7 – plot locations of LAI measurements carried out in 2004 (yellow dots) and 2005 (red dots), respectively.

The summer season was selected to focus on LAI distribution corresponding to the maximum photosynthetic capacity of the vegetation being observed. Finally, raw LAI data were post-processed using C2000 software. Not only multiple above canopy readings were averaged but also the most external ring readings were excluded according to Cutini et al., 1998 who have found that PCA tends to underestimate actual LAI values in comparison with direct methods (e.g. littertraps) especially if LAI>5. The underestimation of PCA was supposed to be related to an actual non-random distribution of the foliage within the canopy (clumping effect), characterised by a higher foliage density in the upper layer with respect to the lower ones where woody vegetation prevail (Breda, 2003). In fact, the fifth ring reading exclusion was assumed

to minimising the woody vegetation contribution of lower layer. It caused a nearly 12% LAI increasing on average.

The difference in LAI values of Monte Coppolo area reflected the difference in vegetation typology growing here. The highest values were those of measurements carried out within the live oak and maquis, which were characterised by rather close vegetation canopies and were less disturbed than the deciduous forest wherein some low values locally observed were apparently due to recent fires and underwood grazing (the latter strongly reducing the forest renewing capacity).

LAI values of hygrofilous deciduous forest of Pantano were similar to those of deciduous forest of Monte Coppolo. The lowest LAI values related to plots located within degraded, neighbouring areas surrounded by crop land.

Furthermore, LAI field data were examined in order to investigate whether there was a statistically significant dependency on year of observation and/or on vegetation typology. Summary statistics of LAI data collected during the 2004 and 2005 surveys are reported in figure 8 and table 1 (a) and (b), respectively.

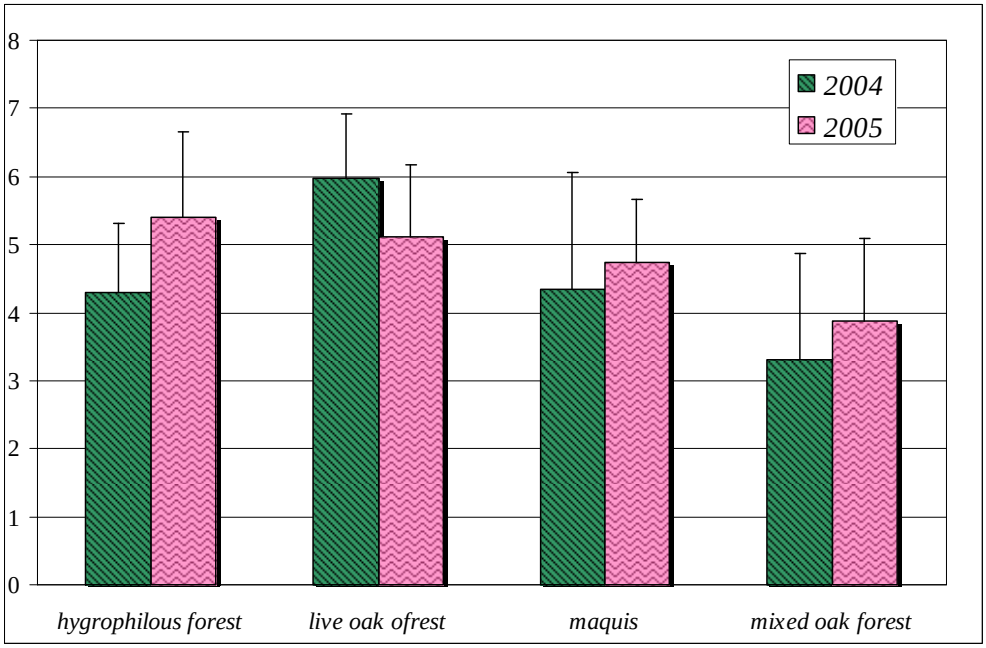

Figure 8 – mean and variance of field LAI per vegetation typology and year

Table 1 - Summary statistics for LAI data collected during the 2004 (a) and 2005 (b) in four different vegetation communities

Vegetation class	**N plot**	**Mean**	**StDev**	**Min**	**Max**
Hygrofilous forest	15	3,96	1,33	1,19	6,20
Live oak forest	11	5,98	0,93	4,72	7,71
Maquis	12	4,80	1,34	2,82	7,10
Mixed broadleaf forest	16	3,30	1,56	1,0	5,44
Tot	**55**				

(a) Year 2004

Vegetation class	**N plot**	**Mean**	**StDev**	**Min**	**Max**
Hygrofilous forest	11	5.41	1.24	3.17	7.37
Live oak forest	12	5.02	0.97	3.38	6.98
Maquis	13	4.76	0.94	3.73	7.09
Mixed broadleaf forest	19	3.88	1.38	1.73	7.14
Tot	**55**				

(b) Year 2005

Then, an analysis of variance (ANOVA) of LAI having as independent variables the year of observation and the vegetation typology, considering their interactions, was performed. Results showed that singularly the year of observation didn't affect significantly *in situ* LAI measurements ($F=3.52$, $df=1/102$, $p=0.06$) whereas the vegetation typology did ($F=10.94$, $df=3/102$, $p<0.0001$). Also, it didn't result a significant interaction between vegetation typology and year of observation ($F=2.45$, $df=3/102$, $p<0.07$). Moreover, repeating the analysis on two subsets related to 2004 and 2005 data, respectively, differences due to vegetation typology were significant for both years (2004: $F=8.59$, $df=3/51$, $p<0.0001$; 2005: $F=5.50$, $df=3/51$, $p<0.0024$).

In other words, if we consider the full data set (2004 and 2005) then results showed that there was no difference between LAI values collected in 2004 and those measured in 2005. Conversely, LAI of a particular vegetation typologies significantly differ from LAI of others, both pooling 2004 and 2005 data and separately considering each single year dataset.

3.1.2. Satellite and ancillary data

System[12]-corrected Landsat Temathic Mapper (TM) and Enhanced Temathic Mapper Plus (ETM+) and *bundle*[13] multispectral and panchromatic Ikonos-2 images, as synchronous as possible to the LAI field surveys, were acquired.

Ikonos-2 data were selected because the high spatial resolution observations provided are at a spatial scale equivalent to field measurements typically carried out in ecological and land cover research and can be directly related to the spatial structure of vegetation (Consoli et al., 2006).

In addition, Landsat TM/ETM+ images, on board of Landsat 5 and 7 platform, respectively, were collected in order to both compare the possible differences in direct LAI retrieval with respect to Ikonos-based estimates and assess the potentiality and economic effectiveness of using high spatial resolution-derived LAI maps for scaling from LAI field data to the Landsat medium resolution when regional-wide LAI spatial distributions need to be produced.

Ikonos-2 sensor has several similar measurement characteristics to the Landsat TM or ETM+. These include a nominal descending orbit at about 10 AM local solar equatorial crossing time on the sunlit side of the Earth and multispectral bandwidths - measured at full width at half maximum – that are similar to the first four of TM and ETM+, though band passes (sensor relative spectral response) slightly differ among different sensors[14] (Figure 9). In particular, the near-infrared (nIR) band is a slightly modified Landsat TM band that minimizes atmospheric water absorption. Also, an other difference relates to the radiometric resolution as Ikonos acquires 11-bit digitized radiometry versus 8-bit of TM and ETM+. Lastly, mention must be made about the two alternate gain (high and low gain) used in ETM+ radiometric acquisition in order to optimise 8-bit available levels. Detailed information on Landsat and Ikonos history and characteristics are out of the scope of this thesis and could be easily found in Markham (2004) and in Dial et al. (2003), respectively, as well as in official web sites, e.g.

[12] Landsat level 1G product and Ikonos-2 Geo products (i.e. the minimum level of processing generally offered to commercial Ikonos customers)

[13] *Bundle* images are panchromatic and multispectral synchronously collected images, which ensure radiometric consistency.

[14] ETM band passes are not shown. However, differences between TM and ETM are considerably smaller than those between Landsat (TM or ETM) and Ikonos sensor.

http://landsat.usgs.gov/technical_details/ and http://www.spaceimaging.com/products/ikonos/.

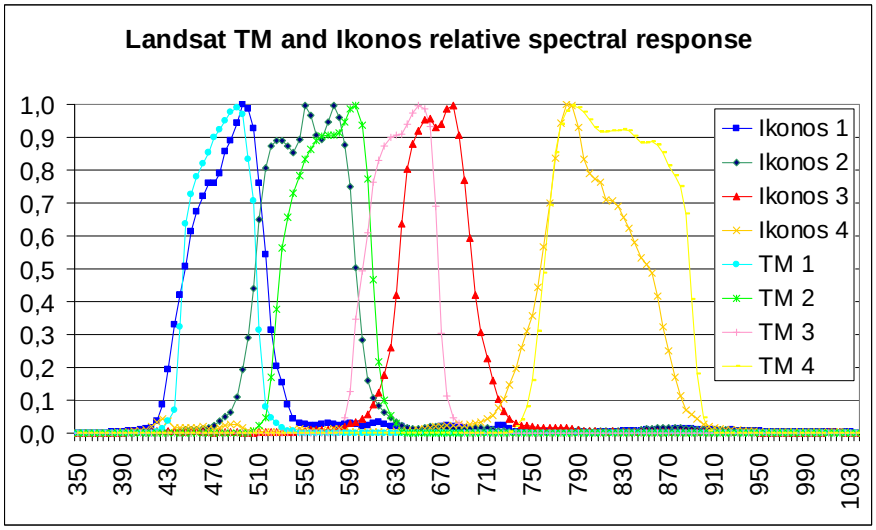

Figure 9 - Ikonos-2 and first four Landsat TM bands spectral response curves

Four Ikonos-2 images, one image per study area per year, four Landsat TM images (orbit track: path 188, row 32), two images per year[15], plus two multispectral and one panchromatic ETM images, were used. In Table 2 the band's interval, spatial and radiometric resolution (Digital Number bit-quantization), as well as the acquisition dates and percent cloud cover of all satellite images are reported.

Table 2 – Ikonos-2 and Landsat TM/ETM bands, spatial and radiometric resolution, acquisition dates

Sensor	Band	Wavelength (μm)	spatial resolution [16] (m)	radiometric resolution (bit)	Acquisition Date[a]
Ikonos	b1 - blue	0.445-0.516	4	11	08/02/2004
	b2 - green	0.506-0.595	"	"	
	b3 - red	0.632-0.698	"	"	
	b4 - NIR	0.757-0.853	"	"	
	panchromatic	0.526-0.929	1	"	06/22/2005

[15] Ikonos SWAT is 11.3 km at nadir, 13.8 at 26° off-nadir, whereas Landsat TM/ETM+ SWAT is about 170x183 km.
[16] After spatial re-sampling in orthorectification process

Landsat TM/ETM		b1 - blue	0.45-0.52	30	8	TM 05/26/04 TM 08/30/04 TM 05/13/05 TM 06/30/05 ETM 21/07/04 ETM 22/06/05
		b2 - green	0.52-0.60	"	"	
		b3 - red	0.63-0.69	"	"	
		b4 - NIR	0.76-0.90	"	"	
		b5 - SWIR 1	1.55-1.75	"	"	
		b6 - thermal	10.40-12.50	120/60	"	
		b7 - SWIR 2	2.08-2.35	"	"	
		Landsat ETM[c] Panchromatic	0.52-0.90	15	8	04/21/2000

[a] Also, Ikonos acquisition time is about 9.50 whereas Landsat TM/ETM+ is around 9:20
[b] In case of Landsat TM/ETM, values are referred to the lower right part of the frame (wherein the study areas are located)
[c] It was used in Landsat co-registration process (see next paragraph)

Specifically, Ikonos-2 *Geo* products were requested to be generated without the Dynamic Range Adjustment, whereas a Modulation Transfer Function Compensation (MTFC) was typically applied by the provider[17]. MTFC is an edge sharpening technique (see Ryan et al. (2003)), aimed at partially restore image degradation due to finite detector size, optical aberrations, motion, diffraction, and electronic effects.

Goward et al. (2003) found that Ikonos MTFC-on product, at their original 4-m spatial resolution, appears to have minor radiometric artefacts as a result of the process. Anyway, over relatively uniform vegetative areas Pagnutti (2003) observed little radiometric difference with either MTFC-on/ MTFC-off option.

Furthermore, when the Ikonos observations were aggregated to 30 m, even Goward et al. (2003) noticed that this problem was essentially absent. Off-nadir viewing was requested to be limited to 20°, in order to guarantee the spatial resolution also minimizing viewing differences with Landsat near-nadir viewing (± 7.5° scan angle).

Detailed information about the Ikonos-2 acquisition configuration are reported in Table 3.

[17] The MTFC is their standard product.

Table 3 – Acquisition parameters of the Ikonos-2 images.

Ikonos-2 images	08-02-04 **Pantano**	08-02-04 **Monte Coppolo**	06-22-05 **Pantano**	06-22-05 **Monte Coppolo**
Nom. Collect. Azimuth	63	87	36	125
Nom. Collect. Elevation	73	75	69	80
Sun Angle Azimuth	141	141	180	137
Sun Angle Elevation	63	63	68	68

Ideally, all datasets should refer to the same date. Actually, this is practically difficult to achieve because of satellite temporal resolution further constrained by the requirement that images need to be cloud free at least over the region of interest. Landsat TM and ETM have 16 days temporal resolution, whereas Ikonos-2 are on-demand data with a local observation repeat frequency of 3 days (depending on the viewing angle constraint) but practically, for a standard order[18], able to guarantee an acquisition within a month temporal window. Unfortunately, during 2004 adverse whether conditions prevent the more synchronous Landsat TM (July, 13th and 29th, and August, 15th) overpasses to be used. Furthermore, a malfunctioning of the Landsat TM system throughout June caused the closest (in time) images to be those of May, 26th or August 30th. Consequently, also Landsat ETM images were acquired although only partial data (striped images) were available because of the Scan Line Corrector-off acquisition mode from July 14th 2003[19] (see http://landsat.usgs.gov/slc_off.html, for references). We got more synchronous though more cloudy satellite data in 2005. In particular, Ikonos 2004 images were completely cloud free whereas those acquired in 2005 had only 5% cloud cover, respectively. Whereas, Landsat TM data had low cloud cover in 2004 (0% and 5% for 05-26-2004 and 08-30-2004 frames, respectively) but they were appreciably cloudy in 2005, especially the 06-30-2005 frame showing clouds (28%) surrounding the study sites. Finally, 2004-Landsat ETM presented low cloud cover (10%) far from the study sites, and the 2005-Landsat ETM a slightly highest cloud cover (20%) though far from the area of interest.

[18] Depending on order priority (there are different prices related to it) and on number, locations and acquisition dates of already scheduled acquisitions' list. These constraints combines with cloud cover and user viewing angle restrictions.

[19] Scan Line Corrector mechanism malfunctioning starting from 14 July 2003 and still present at time of this study.

In addition, some ancillary and reference data were acquired. A Digital Elevation Model (DEM) with a pixel size of 30m, covering both study areas, was provided by the Advanced Computer System Spa. Additionally, only for the Monte Coppolo study area, a DEM with a pixel size of 10m was derived from 5m-spaced contour lines included within the 1:10.000 scale topographic map (Carta Tecnica Regionale) provided by Regione Basilicata.

Furthermore, reference coordinates to be used in orthorectification procedure were derived by digital coloured orthophotos (Terraitaly-it2000™ ©CGRSpA – Parma)[20]. Also, bidirectional reflectance measurements of three asphalted areas located nearby were carried out, by means of an hand-held Analytical Spectral Device (ASD) FieldSpec Pro Full Range spectroradiometer, to be used as *ground truth* reflectance data on which to reconstruct atmospheric conditions (horizontal visibility) at time of Ikonos-2 satellite overpass (see atmospheric correction procedure in following sections). In particular, those asphalted areas were carefully selected as landscape elements (ground targets) radiometrically constant over time and large enough to be resolved by Ikonos-2 spatial resolution. Each spectrum was set to result from an average of 25 readings and a certain number of evenly spaced spectra, per area, were acquired and averaged. At the start of each measurements ASD were optimized[21] and reflectance Labsphere Spectralon panel measurements were taken to generate output reflectance values.

ASD instrument has a spectral resolution of 1.4 nm in the 350-1000 nm spectral range and have a spectral resolution of 10 nm in the 1000-2500 nm. However, the output of the spectroradiometer is interpolated within ASD software to report data at 1nm sampling across the entire spectral range (references can be found in http://www.asdi.com/products-FSP.asp web site).

3.1.2.1 Satellite data pre-processing

Although the new generation of sensors show improved data acquisition and image quality, some inherent distortions affecting the signal coming from the Earth surface and collected by satellites still remain and require correction before performing reliable analysis. Typical corrections include geometric and radiometric distortions (Toutin,

[20] Coordinates were derived by on-line products available at website www.atlanteitaliano.it hence having a slight degraded spatial resolution with respect to original products

[21] ASD optimization sets the integration time for the visible NIR detector and performs a dark current reading.

2004). Image geometric characteristics are set by the orbit, spacecraft attitude (roll, pitch, yaw), scanner properties and earth rotation and shape. Depending on these features, the changing sensor viewing geometry during data collection ultimately results in wrong relative positions of image pixels. Radiometric data adjustment are mainly aimed at reducing topographic and atmospheric effects. Topography affects illumination conditions whereas atmospheric distortions are due to modification of the electromagnetic radiation, in the solar spectrum, caused by gas and aerosols scattering and absorption.

Since images of multiple sensors and dates had to be used and compared, it was essential to obtain corrected reflectance images. Therefore, the pre-processing of remotely sensed images consisted in image orthorectification, radiometric calibration, atmospheric and topographic corrections. First of all, in order to correct for geometric errors and obtained a co-registered dataset, images were orthorectified starting by processing the higher resolution data. Therefore, initially the two August 2, 2004 panchromatic Ikonos-2 scenes were orthorectified, using *Ground Control Points* (GCPs) derived from coloured digital orthophotos and from the available DEMs (the 10m DEM for Monte-Coppolo and the 30m DEM for Pantano sites, respectively).

Since detailed mathematical description of Ikonos-2 camera is not available, preventing the use of a rigorous relationship between object space (points on the ground) and image space (pixels in the image), the orthorectification process was accomplished through the use of the *Rational Polynomial Coefficient* (RPC) model, provided by Ikonos-2 vendor - Space Imaging – as part of the image metadata. References can be found in Dial & Grodecky (2004).

Afterwards, both the 2005 panchromatic and 2004 multispectral scenes, were orthorectified and co-registered using GCPs derived by 2004 orthocorrected panchromatic images. Finally, 2005 multispectral images were orthorectified using 2004 multispectral images as references. A *nearest neighbour* re-sampling algorithm using 1m/5m spatial resolution was used for panchromatic/multispectral Ikonos-2 data, respectively.

Likewise, orthorectification of Landsat TM and ETM+ scenes was performed according to the same hierarchical approach. To this aim, firstly the April 21, 2000

panchromatic Landsat ETM+ image was orthorectified[22] using GCPs extracted from the orthophotos and from the 30m DEM. Then, this geometrically corrected images served as reference to correct all multispectral images. A *nearest neighbour* re-sampling method using 15m/30m spatial resolution was adopted for Landsat panchromatic/multispectral data, respectively.

Root Mean Square Errors (RMSE), all less than 1 pixel except for Ikonos panchromatic images, are reported in Table 4.

Table 4 – RMSE (pixel unit) of orthorectification process

frame	**multispectral**	**Panchromatic**
08-02-2004 Pantano Ikonos-2	0,45	2,81
08-02-2004 Monte Coppolo Ikonos-2	0,99	2,84
06-22-2005 Pantano Ikonos-2	0,1	0,22
06-22-2005 Monte Coppolo Ikonos-2	0,15	0,32
04-21-2000 Landsat ETM	0,33	0,73
07-21-2004 Landsat ETM	0,61	\
06-22-2005 Landsat ETM	0,07	\
05-26-2004 Landsat TM	0,44	\
08-30-2004 Landsat TM	0,46	\
05-13-2005 Landsat TM	0,1	\
06-30-2005 Landsat TM	0,46	\
06-22-2005 Landsat ETM	0.07	\

The Universal Transverse Mercator (UTM), zone 33, European Datum 1950, was the adopted coordinate system.

Before performing any radiometric rectification, all images were calibrated to at-sensor physical units by converting Digital Numbers (DNs) to Top-Of-Atmosphere (TOA) radiance, L_k ($W/m^2/sr/mm$), using suitable, band-specific calibration coefficients ($L_k = gain_k * DN_k + offset_k$).

In particular, since both sensors showed significant detector sensitivity changes with time, calibration coefficients updated for the respective image acquisition date

[22] It was preferred to the other available ETM panchromatic images since it was acquired before the scan-line mechanism malfunctioning occurred, therefore including all pixels in the frame (no data missing).

were used. Therefore, according to Space Imaging (2001) calibration coefficients referring to Ikonos-2 11 bit products and post February 22, 2001 image production (creation), were used. Whereas, with regard to Landsat TM and ETM images, calibration coefficients according to Chander and Markham (2003) and those included in the header files, were used, respectively. References of approaches to and status of Landsat and Ikonos data calibration can be found in Teillet (2006), Chander et al (2004), Roeder et al. (2005) and Pagnutti (2003). All adopted calibration coefficients are shown in table 5 and table 6.

Table 5 – Ikonos radiometric calibration coefficients

Ikonos-2 band (k)	**11 bit, post 2/22/2001 gain** DN*****[mW/cm^2 sr]$^{-1}$
1	1/728
2	1/727
3	1/949
4	1/843

Table 6 – Landsat TM and ETM+ calibration coefficients

Landsat TM	**Post 05/05/2003**	
Band (k)	**Off-set**	**Gain**
1	-1,52	0,763
2	-2,84	1,442
3	-1,17	1,040
4	-1,51	0,872
5	-0,37	0,120
7	-0,15	0,065

Landsat ETM		
Band (k)	**Off-set**	**Gain**
1	-6,98	0,779
2	-7,20	0,799
3	-5,62	0,622
4	-6,07	0,969
5	-1,13	0,126
7	-0,39	0,044

Finally, atmospheric corrections were performed using the 6S-*Second Simulation of the Satellite Signal in the Solar Spectrum* radiative transfer code (Vermote et al. 1997) in order to derive atmospherically corrected surface reflectance from TOA radiance. The application of radiative transfer code to a specific scene and date requires knowledge of the atmospheric properties at the time, mainly aerosol and water vapour content, which are difficult to acquire even when planned, and were not available in this

case. As a consequence, 6S was firstly iteratively used for retrieving the aerosol optical depth (τ) at time of 2004 and 2005 Ikonos-2 overpass. To this purpose, per band reference reflectance values were provided by the ASD on ground reflectance measurements over the asphalted areas re-sampled to Ikonos-2 relative spectral response. Then, multiple runs were performed each time varying only τ□, until the best agreement between those ground measurements and 6S output reflectance of corresponding areas in the image was achieved[23] (Caraux Garson and Lacaze, 2003). In this way, aerosol optical thickness of τ=0.222 at λ=0.550 μm (i.e., a horizontal visibility of approximately 25 km) and τ=0.316 at λ=0.550 (horizontal visibility of about 15 km) for 2004 and 2005 Ikonos-2 satellite overpass were obtained, respectively.

Next, 6S was run using the so-retrieved τ values and providing atmospherically corrected Ikonos-2 images. All image processing steps, but atmospheric corrections, were performed using *Earth Resource Data Analysis* (ERDAS) Imaging 8.5 image processing software.

The same approach was used to correct Landsat images. However, since the asphalted targets were too small for being spatially resolved at Landsat resolution, the reference reflectance values for Landsat scenes atmospheric characterisation were, in this case, provided by the atmospherically corrected Ikonos-2 images. In particular, a sandy area along the coast was selected since it resulted the most homogeneous and wide among temporally radiometrically stable targets individuated, by visual inspections, within the Ikonos scenes. The Landsat TM and ETM images resulted characterised by an optical thickness of τ=0.1951 (i.e. horizontal visibility of about 30 km)[24].

Finally, different sun illumination conditions due to topographic effects were accounted for by applying a cosine-correction method[25] (Teillet et al., 1982). Therefore, reflectance values in each pixel were divided by the corresponding[26] cosine of the illumination angle $\cos(i)=\cos(90-\alpha)*\cos(\theta)+\sin(90-\alpha)*\sin(\theta)*\cos(\beta-\varphi)$, where i=sun

[23] Standard *medium latitude summer* atmosphere model and *maritime* aerosol model were adopted in each 6S runs.
[24] The different optical thickness related to 2005 Ikonos and Landsat ETM images may be explained in terms of a longer path through the atmosphere (and particularly through the lowest layer) the incoming signal to Ikonos sensor have to do with respect to the Landsat platform because of the off-nadir viewing angle of Ikonos. Moreover, residual differences may be due to the different acquisition time.
[25] Under a firts approximation Lambertian surface assumption.
[26] averaged over the same 12x12 m^2 and 90x90 m^2 windows centered on LAI field plots

illumination angle in relation to the normal on a pixel, α=sun elevation angle, β=sun azimuth angle, θ=terrain slope, φ=azimuth angle of the slope or terrain aspect. Slope and aspect were derived by the available DEMs.

3.2 Upscaling *in situ* LAI measurements to satellite data

The retrieval of LAI from satellite data was performed through a traditional statistical approach: empirical relationships established by statistically fitting field LAI measurements and corresponding satellite reflectance data. In particular, ordinary least square regressions with LAI or ln(LAI) as the dependent variable and each band or spectral Vegetation Indices (VIs) as the independent variable, as well as multiple regressions using multiple spectral bands, were performed. It must be said that models using a log-transformed response variable (ln(LAI)) were tested, too, to account for possible asymptotic nature that the LAI-radiometric data relationship may present (e.g. Broge and Leblanc, 2000).

For all the tests, a probability level at $p \leq 0.05$ was considered to be significant.

To this aim, for each plot a mean reflectance values was derived from atmospherically corrected images. The average for a 3x3 pixel window surrounding the LAI plot centre was used. The use of such mean values is a common practice in quantitative remote sensing studies because of the necessity to account for the (~1 pixel) georeferencing error and related uncertainties between the actual ground measurements locations and its assigned positions on the image.

It must be said that a 3x3 Ikonos pixel window, corresponding to a 12x12 m^2 area, nearly matched the LAI measurements plot area. Whereas, a 3x3 Landsat pixel window corresponded to an appreciably largest surface (90x90 m^2). Therefore, in order to compare Ikonos and Landsat observations and their effectiveness in LAI estimating also aggregation of Ikonos measurements on a 23x23 pixel window (~90x90 m^2) were computed. Once more, aggregation were performed by means of arithmetic average in the attempt to approximate the integrated reflectance energy that Landsat sensors measure (Goward et al. 2003).

Moreover, before carrying out the regression analysis and in order to assess if factors like year of observation, vegetation typology or site affected the LAI-spectral

data relationships (Turner et al. 1999, Chen et al., 2002, Davi et al., 2006) an analysis of the covariance (ANCOVA) of LAI was performed having as independent variables a radiometric variable, i.e. one-by-one some VI were tested (NDVI among others) as well as each individual band, the vegetation typology, and the year of observation, including all possible interactions.

In particular, the significance of *year_of_observation*radiometric_variable*, *vegetation_typology*radiometric_variable* and *year_of_observation*vegetation_typology*radiometric_variable* interactions were examined in order to explore the possible dependency of the LAI-radiometric variable relationship on the year of observation or on the vegetation typology or on both. In other words, a significant interaction between the *vegetation_typology* and the *radiometric_variable* would suggest that the relation between LAI and the radiometric variable differs in the various vegetation typologies. This would imply the necessity to develop separate empirical relationships for each vegetation typology. Similarly, a significant interaction between the *year_of_observation* and the *radiometric_variable* would mean that the functional relationship between LAI and the radiometric variable depends on, and hence change with, the specific year of data acquisition. The latter interaction, therefore, would entail that even if using the same radiometric data source (i.e. satellite sensor), referring to the same study area and, roughly, period of observation (i.e. summer season/near-peak vegetation development) it is not possible to apply an empirical model developed by means of data collected in a certain year to radiometric observations referring to different (past or future) years.

In general, those interactions account for possibly existing differences in vegetation phenological status, sun-target-sensor geometric configuration, background characteristics (due to different acquisitions dates) as well as in the spectral behaviour of different vegetation typology.

An ANCOVA analysis was also carried out by substituting the *site* factor for the *vegetation_typology* one. The site factor was examined, since the two areas, although rather close each other, present significant geographical and ecological differences. For example, they are characterised by different geologic substrate and different vegetation typology, except for *maquis*, which is found within both areas. However, *maquis* presented different vegetation species/structure among the two sites and may present

different phenology within the two areas at the time of satellite overpass, as well. Furthermore, different topographic conditions – a flat terrain at Pantano area and a variable aspect and slope at Monte Coppolo site – may differently affect the spectral signal sensed by satellites.

In particular, ANCOVA analyses of either LAI and ln(LAI) data were performed. Also, either high spatial resolution Ikonos-derived radiometric data referred to the 3x3 Ikonos pixel ($12x12m^2$) averaging window and all available observations (n=110) and medium resolution ETM-derived data referred to the 3x3 ETM pixel ($90x90m^2$) averaging window and n=94 observations[27], were examined to this purposes.

In all cases, the ANCOVA analyses indicated that some interactions were not significant ($p>0.05$). Consequently, the models were reduced[28]. Then, substantially, results showed that only an year effect had to be taken into account in the LAI-VI empirical model developing whereas, conversely, it was possible to pool data related to different vegetation typology and different sites.

For example, table 7 reports results obtained for the reduced models of ANCOVA of ln(LAI) data having as independent variables $Ikonos_{3x3}$[29] or ETM_{3x3} NDVI, respectively, the vegetation-typology and the year of data collection. Whereas, table 8 lists results provided by the ANCOVA analysis (same factors and their possible interactions, reduced models) of ln(LAI) performed using each individual band instead of the NDVI as radiometric variable.

Table 7 - Results of ANCOVA analysis using NDVI as radiometric variable

radiometric data source	**Model**	**df**	**F**	**Prob>F**
$Ikonos_{3x3}$-NDVI	NDVI	1/103	65.80	0.0001
	year	1/103	46.24	0.0001
	Vegetation	3/103	11.85	0.0001
	NDVI*year	1/103	45.66	0.0001
	NDVI	1/87	13.26	0.0005

[27] Since some plots had to be discarded because they were located within the ETM missed data and an additional one in order to avoid including water within the 90x90 m^2 area.
[28] the ANCOVA was performed again by retaining only significant interactions.
[29] The subscripts 3x3 indicate the size (pixel unit) of the averaging window.

ETM_{3x3}-NDVI	year	1/87	9.20	0.0032
	Vegetation	3/87	7.37	0.0002
	NDVI*year	1/87	8.40	0.0047

Table 8 - Results of ANCOVA analysis using individual band as radiometric variable

radiometric data source	**Model**	**df**	**F**	**Prob>F**
$Ikonos_{3x3}$-b_1	b_1	1/97	18.53	0.0001
	year	1/97	33.97	0.0001
	vegetation	3/97	4.67	0.0043
	b_1*year	1/97	26.26	0.0001
	b_1*vegetation	3/97	5.49	0.0016
	year* vegetation	3/97	5.87	0.0010
$Ikonos_{3x3}$-b_2	b_2	1/103	32.62	0.0001
	year	1/103	20.38	0.0001
	vegetation	3/103	7.13	0.0002
	b_2*year	1/100	19.95	0.0001
$Ikonos_{3x3}$-b_3	b_3	1/100	68.65	0.0001
	year	1/100	36.03	0.0001
	vegetation	3/100	1.05	0.3755
	b_3*year	1/100	33.58	0.0001
	year* vegetation	3/100	6.62	0.0004
$Ikonos_{3x3}$-b_4	b_4	1/100	3.13	0.0801
	year	1/100	9.32	0.0029
	vegetation	3/100	11.29	0.0001
	b_4*year	1/100	8.05	0.0055
	year* vegetation	3/100	3.79	0.0128
ETM_{3x3}-b_1	b_1	1/87	15.21	0.0002
	year	1/87	10.23	0.0019
	vegetation	3/87	16.19	0.0001
	b_1*year	1/87	14.89	0.0002

ETM_{3x3}-b_2	b_2	1/87	9.41	0.0029
	year	1/87	5.49	0.0215
	vegetation	3/87	5.89	0.0010
	b_2*year	1/87	7.54	0.0073
ETM_{3x3}-b_3	b_3	1/87	9.66	0.0025
	year	1/87	3.25	0.0748
	vegetation	3/87	4.98	0.0031
	b_3*year	1/87	6.75	0.0110
ETM_{3x3}-b_4	b_4	1/88	4.39	0.0390
	year	1/88	2.27	0.1359
	vegetation	3/88	14.50	0.0001
ETM_{3x3}-b_5	b_5	1/82	0.70	0.4052
	year	1/82	4.86	0.0303
	vegetation	3/82	2.26	0.0876
	b_5* vegetation	3/82	2.95	0.0375
	year* vegetation	3/82	2.82	0.0438
ETM_{3x3}-b_7	b_7	1/87	6.64	0.0117
	year	1/87	1.90	0.1714
	vegetation	3/87	2.86	0.0415
	b_7*year	1/87	5.10	0.0264

Basically, results obtained by using either individual band and NDVI showed the LAI-individual band relationship was not year-invariant but it was substantially vegetation/site-independent. The only two exceptions concerned significant interaction between *LAI -blue Ikonos band-vegetation typology* and between *LAI-SWIR1 ETM band- vegetation typology.*

Therefore, it was established to use two datasets - one per year – in developing the empirical models.

On this basis, a comparative analysis of LAI retrieving capacity between different spectral bands/VIs derived from different satellite sensors (Ikonos, Landsat ETM and TM) was carried out.

Results of regression analysis performed by pooling 2004 and 2005 data (general model) are reported, as well, for comparison purposes. It must be noted that when the pooled dataset was considered since two TM images per year were available the following three possible combination of 2004 and 2005 data were explored: 05262004 and 05152005, 05262004 and 06302005, 08302004 and 05302005 named TM_1, TM_2 and TM_3, respectively. Whereas, in order to synthetically distinguish between TM single-year datasets of different acquisition dates they are reported in the following as TM_M, TM_A and TM_J (M/A/J subscripts indicate the month of acquisition date, May/August/June, respectively). It is noteworthy that possible vegetation phenologic differences had to be taken into account when comparing Ikonos-based and TM-based results whereas they were not considered affecting Ikonos vs ETM comparison since respective acquisition dates were within ten days in 2004 and even matched in 2005.

Finally, the effectiveness of using high-resolution satellite (i.e Ikonos) images as subsampling for scaling from LAI field measurements to moderate resolution sensors (i.e. Landsat TM or ETM), was investigated.

Specifically, the following two hypotheses were formulated, whose related quantitative results are reported in the following sections (see figure 10):

Hypothesis 1: On the basis of the available data, Ikonos high spatial resolution data will explain more of the variability in LAI within the selected highly heterogeneous study area than Landsat (TM/ETM) medium resolution one;

Hypothesis 2: a two-stage procedure including a first upscaling of LAI field measurements to high resolution data in order to produce a 4m spatial resolution LAI map (stage 1) to be used for the calibration of medium resolution data (stage 2) will outperform a direct upscaling of LAI field measurements to Landsat satellite data.

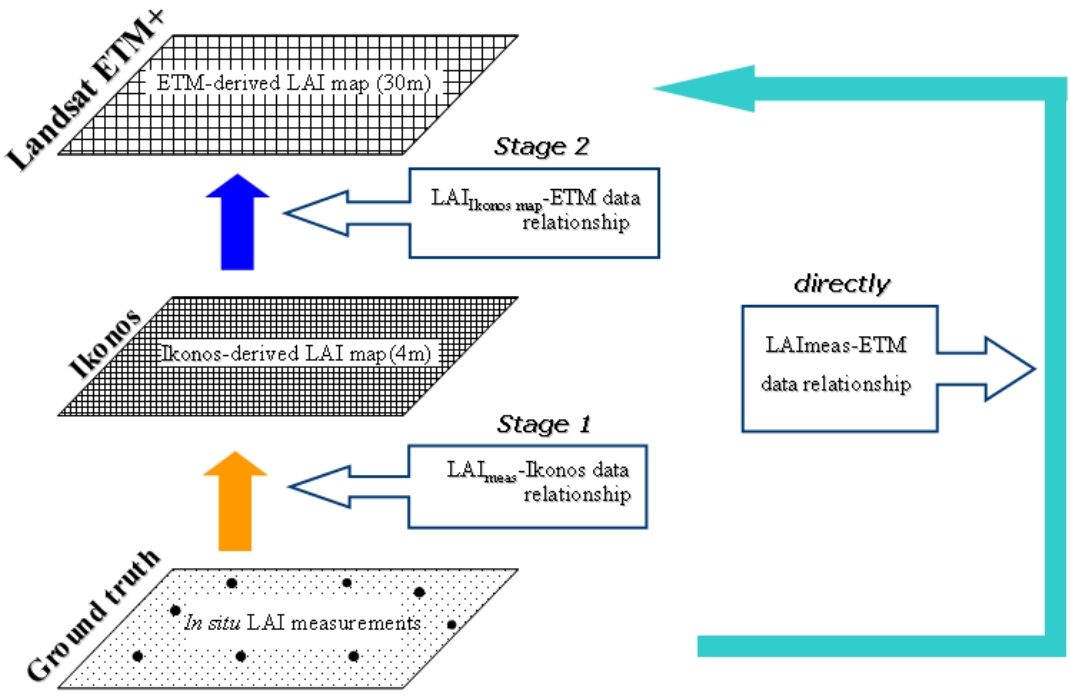

Figure 10 - Upscaling *in situ* LAI measurements to satellite data: comparison between Ikonos and Landsat data performances (hypothesis 1 - orange *versus* green arrow); comparison between direct Landsat calibration and a two-stage calibration procedure (hypothesis 2 - orange and blue arrows *versus* green arrow) exploiting Ikonos-derived LAI spatial distributions as intermediate stage for ETM data calibration.

3.2.1. Individual spectral band analysis

Firstly, an assessment of Landsat, TM and ETM+, and Ikonos sensor observations sensitivity to LAI variation on the per-spectral-band basis was carried out.

To this aim, in order to make possible a comparison of results obtained using all available sources (Ikonos, TM and ETM) data related to plots located within areas of missing data of the striped ETM images were excluded from the analysis. In addition, one more plot was discarded since it was located very close to a river (about 10 m) and the use of a 3x3 Landsat-pixel window would have included water. Therefore, new, on purpose data sets were arranged and they resulted in n=49 and n=45 pairs of LAI field measurements and corresponding radiometric data for 2004 and 2005, respectively.

Table 9 provides a summary of regression models performance (r^2) based on the multi-year data sets, where $band_k$ is the k-spectral band, *n* is the sample size. It is noteworthy that generally the use of LAI/log-transformed LAI values did not make much difference (similar r^2 and p values), though usually slightly better results were provided by the use of the transformed variable. Therefore, for sake of simplicity only the better performing models between those using LAI and those using Ln(LAI) data are reported, the latter in italics. In the following tables, *ns* indicate not significant relationship (at 95% probability level).

Table 9 - Performance (r^2) of band-by-band regressions carried out using different sensors, multi-year or single-year data sets and different averaging pixel windows size

	Ikonos$_{23x23}$	**TM$_1$**	**TM$_2$**	**TM$_3$**	**ETM +**	**Ikonos$_{3x3}$**
acquisition dates:	08022004	05262004	05262004	08302004	07212004	08022004
	06222005	05132005	06302005	06302005	06222005	06222005
pooled data set (n=94)						
band 1	*0.04^{ns}*	*0.01^{ns}*	*0.01^{ns}*	0.00^{ns}	*0.01^{ns}*	*0.03^{ns}*
band 2	*0.15*	0.01^{ns}	0.00^{ns}	0.02^{ns}	*0.11*	*0.11*
band 3	*0.19*	0.00^{ns}	0.00^{ns}	0.03^{ns}	*0.15*	*0.25*
band 4	*0.01^{ns}*	*0.07*	0.05^{ns}	0.00^{ns}	0.00^{ns}	0.00^{ns}
band 5	/	*0.15*	0.11	*0.17*	*0.18*	/
band 7	/	*0.10*	0.07	*0.16*	*0.16*	/
	Ikonos$_{23x23}$	**TM$_M$**	**TM$_A$**	**ETM +**	**Ikonos$_{3x3}$**	
acquisition date:	08022004	05262004	08302004	07212004	08022004	
2004 data set (n=49)						
band 1	0.15	*0.10*	0.20	0.13	0.20	
band 2	0.34	*0.35*	0.32	*0.31*	*0.50*	
band 3	*0.32*	*0.25*	*0.27*	*0.35*	*0.69*	
band 4	0.04^{ns}	0.17	0.03^{ns}	0.00^{ns}	0.02^{ns}	
band 5	/	*0.24*	*0.31*	*0.31*	/	
band 7	/	*0.23*	*0.33*	*0.38*	/	
	Ikonos$_{23x23}$	**TM$_M$**	**TM$_J$**	**ETM +**	**Ikonos$_{3x3}$**	
acquisition date:	06222005	05152005	30062005	06222005	06222005	
2005 data set (n=45)						

band 1	0.00 ^{ns}	*0.06* ^{ns}	*0.03* ^{ns}	0.00 ^{ns}	*0.04* ^{ns}
band 2	0.03 ^{ns}	0.01 ^{ns}	0.00 ^{ns}	0.03 ^{ns}	0.00 ^{ns}
band 3	0.05 ^{ns}	0.00 ^{ns}	0.02 ^{ns}	0.05 ^{ns}	0.02 ^{ns}
band 4	*0.03* ^{ns}	*0.02* ^{ns}	0.00 ^{ns}	*0.01* ^{ns}	*0.05* ^{ns}
band 5	/	*0.09* ^{ns}	*0.14*	*0.09* ^{ns}	/
band 7	/	*0.05* ^{ns}	*0.12*	0.08 ^{ns}	/

ns = not significant at 95% probability level

According to previous work (e.g. Davi et al. 2006, Soudani et al., 2006), when significant relationships were established LAI was, generally, positively correlated with nIR and negatively correlated with visible and SWIR bands.

Also, as expected in those highly heterogeneous Mediterranean environment, generally regression models using $Ikonos_{3x3}$ data sets, which means spectral response of a surface area roughly corresponding to the *in situ* LAI measurements sampled area, out performed Landsat ETM/TM as well as $Ikonos_{23x23}$-based ones.

Generally, $Ikonos_{23x23}$ and ETM (nearly synchronous datasets) yielded rather similar results.

Results reported in table 9 reflected what pointed out by the ANCOVA analysis, in terms of manifest year effect affecting LAI-individual bands relationships.

In fact, regardless of the satellite source utilized - Ikonos, Landsat TM or ETM - and either using LAI or log-transformed LAI data, the use of a general model (pooled data set) provided either not significant or rather poor correlations (all $r^2<0.21$). In particular, no relationships were found between blue or nIR band and LAI except for the very weak one related to TM_1 data set. Furthermore, for all TM-based data sets the red band was not correlated to LAI, whereas Ikonos and ETM red bands were able to explain about 15-20% of variation of LAI. About the same performance were achieved by SWIR bands-based models of TM_3 and ETM data sets ($r^2= 16\div18$).

Furthermore, considerably different performance were obtained between the single-year-based models. In particular, regression results obtained using 2004 data largely outperformed those related to 2005.

Therefore, in order to attempt explaining the unsuccessful result obtained by using 2005 data, all (2004 and 2005) Ikonos-derived data were examined in terms of within-plot variability of spectral signal. In other words, the standard deviation of the

reflectance in each Ikonos band, within the abovementioned pixel windows (plot sizes), was computed. Then, the corresponding coefficients of variations (cv=standard deviation/mean) were calculated and per each band a t-test analysis was used to evaluate possible differences between mean cv of the two years (see table 10 and 11).

It was shown that plots used in 2005 were characterised by significantly higher coefficients of variations of reflectance in all bands, except for nIR band which anyway was shown to be a rather useless one (see table 9), and for both window sizes. In particular, mean cv<10% computed on the 3x3 pixel window characterised 2004 plots whereas appreciably higher cv (except for nIR band) related to 2005 plots.

Also, as expected, highest cv values were observed in the 23x23 pixel window of both years.

Table 10 – Mean coefficient of variation (%) of Ikonos reflectance computed in 3x3 pixel window size

Radiometric band	**Year**	**mean cv**	**t-Test**		
			t ratio	df	Prob<t
band 1	2004	0.05	-7.27	50.05	<0.0001
	2005	0.16			
band 2	2004	0.06	-6.27	56.00	<0.0001
	2005	0.13			
band 3	2004	0.08	-4.95	54.59	<0.0001
	2005	0.17			
band 4	2004	0.09	0.45	91.19	0.67
	2005	0.08			

Table 11 – Mean coefficient of variation (%) of Ikonos reflectance computed in 23x23 pixel window size

Radiometric band	**Year**	**mean cv**	**t-Test**		
			t ratio	df	Prob<t
band 1	2004	0.16	-9.8	79.26	<0.0001
	2005	0.37			
band 2	2004	0.16	-6.26	90.62	<0.0001
	2005	0.27			
band 3	2004	0.26	-4.66	92.03	<0.0001
	2005	0.39			

band 4	2004	0.13	-1.67	85.47	0.0488
	2005	0.15			

Moreover, the coefficients of variation ($cv_{2004plot,2005Ikonos}$) of reflectance corresponding to 2004 plot locations (coordinates) positioned on 2005 Ikonos images were computed. The aim was to assess if the higher radiometric heterogeneity obtained for plots of 2005 field survey ($cv_{2005plot,2005Ikonos}$) reflected a specific characteristic of 2005-plots or rather whether the highest radiometric spatial variability characterised the whole Ikonos images (i.e. the whole area) sensed in 2005. Therefore, a comparison (t-test) between the coefficients of variation of reflectance extracted over the plots of 2004 field survey from the 2004 Ikonos images ($cv_{2004plot,2004Ikonos}$) and the coefficients of variation of reflectance extracted over the same locations from the 2005 Ikonos images ($cv_{2004plot,2005Ikonos}$) was performed. Indeed, results similar to those reported in table 10 were observed, i.e. $cv_{2004plot,2005Ikonos}$ significantly higher than $cv_{2004plot,2004Ikonos}$ (see table 12), meaning that it was not a matter of specific locations of 2005-plots.

Table 12 – Mean coefficient of variation (%) of Ikonos 2004 and 2005 reflectance computed in 3x3 pixel window size centred on 2004 plot locations

Radiometric band	**Year**	**mean cv**	**t-Test**		
			t ratio	df	Prob<t
band 1	2004	0.05	-9.16	61	<.0001
	2005	0.14			
band 2	2004	0.06	-6.52	68	<.0001
	2005	0.12			
band 3	2004	0.08	-5.09	71	<.0001
	2005	0.14			
band 4	2004	0.09	-0.85	93	0.196
	2005	0.09			

Also, the effects of the different Ikonos sun-target-sensor geometries between the two years, mostly related to the difference between sun and sensor-viewing azimuth angles (see table 3), on the highest within-plot radiometric variability

observed in 2005 images was investigated by comparing ETM and 30 m re-sampled Ikonos data. In fact, the Landsat ETM sun-target-sensor acquisition geometry over the same area (frame) can be considered nearly constant over time[30]. Therefore, due to the high synchronicity between Ikonos and ETM acquisition dates, by re-sampling the Ikonos images to the same ETM spatial resolution (30 m) the possible influence of Ikonos different acquisition geometry on the within-plot radiometric heterogeneity was examined as follows.

Per each band, the ratios between 2004 and 2005 ETM-derived cv of reflectance of 3x3 pixel windows centred on 2005 plot locations ($cv_{2004\_ETM\_2005\_plot}/cv_{2005\_ETM\_2005\_plot}$), as well as the ratio between 2004 and 2005 re-sampled Ikonos-derived cv of reflectance ($cv_{2004\_30m\_Ikonos\_2005\_plot}/cv_{2005\_30m\_Ikonos\_2005\_plot}$), were computed. A t-test between these ratios (see table 13), i.e. between $cv_{2004\_ETM\_2005\_plot}/cv_{2005\_ETM\_2005\_plot}$ and $cv_{2004\_30m\_Ikonos\_2005\_plot}/cv_{2005\_30m\_Ikonos\_2005\_plot}$, revealed that the differences between the two sets of data were not statistically significant. In other words, the increase of within-plot radiometric variability observed, in 2005, by ETM sensor was roughly the same observed by (re-sampled) Ikonos one. Therefore, since ETM data were substantially considered not affected by different acquisition geometry, it was concluded that the effects of Ikonos different acquisition geometry on the highest spatial within-plot radiometric heterogeneity of 2005 data were negligible.

Table 13 – Comparison between the ratios of within-plot coefficients of variations of reflectance derived from 2004 and 2005 data of either ETM and re-sampled Ikonos images

Radiometric band	**Sensor**	$\frac{cv_{2004}}{cv_{2005}}$		**t-Test**	
			t ratio	df	Prob<t
band 1	30m-Ikonos	0.6	3.8	83	0.999
	ETM	1.2			
band 2	30m-Ikonos	0.8	2.8	74	0.997
	ETM	1.2			
band 3	30m-Ikonos	0.9	1.2	57	0.878
	ETM	1.1			
band 4	30m-Ikonos	1.1	0.5	83	0.300
	ETM	1			

[30] Only slightly different sun elevation angle due to the different day of the year.

In conclusion, the highest radiometric variability of 2005 images were attributed to the different period of data collection. In particular, it is likely that a different vegetation phenologic status characterised vegetation at time of 2005 data collection with respect to vegetation phenologic status of 2004. It is possible that at the end of May 2005 (i.e. at time of 2005 field survey) forest vegetation had not yet reached the peak of the phenologic cycle[31] (maximum vegetation development) and continued growing during the period between *in situ* LAI measurements and satellite acquisition date. Therefore, phenologic changes might be occurred between *in situ* LAI measurements and image acquisition date in 2005, causing measured LAI to significantly differ from actual LAI values at time of satellite overpass. Conversely, the maximum vegetation development was reasonably reached in late June-early July, 2004, guaranteeing the consistency between LAI measurements and actual LAI values at time of 2004 satellite overpass. Also, background effects, i.e. the impact of understory vegetation on forest canopy reflectance (Eriksson et al., 2006), could have been possibly higher in 2005 than in 2004. In other words, in June 2005 grass might be green in those areas whereas at the beginning of August[32] it was mostly in a senescent status.

3.2.2. Vegetation Indices (VIs) computation and LAI-VIs regression analysis

VIs provide a widely applied, standardised approach to LAI investigation. In particular, the NDVI has been an extremely popular VI for biophysical parameter retrieval. However, since numerous investigations have shown that NDVI is not the best solution for LAI retrieval under all circumstances here a number of VI were computed and their performances compared.

Table 14 (a) and (b) summarise formulae and references of investigated VIs.

[31] In the case of forests and shrub-lands the main greenness peak is associated with the spring green up of vegetation, whereas a second peak may occur in autumn during the months of October and November mainly associated to the precipitation regime which allows for a larger availability of water during the main precipitation season.

[32] Ikonos images were acquired on the 2nd of August in 2004 and on the 22th of June in 2005

In particular, indices based on red and nIR reflectance as well as indices including SWIR bands (the latter obviously only for Landsat TM/ETM data) were tested.

Also, soil-corrected indices using either empirically determined soil line (TSAVI, SAVI2, GESAVI) or pre-defined adjustment factors (SAVI, MSAVI, OSAVI) were used. The, soil line parameters separately derived for the two study areas were represented by the following equations, respectively:

(1) nIR=1.14*red + 0.01 (Pantano site);

(2) nIR= 0.94*red + 0.07 (Monte Coppolo site).

Table 15 and 16 lists results obtained considering the pooled dataset and single year datasets, respectively.

Table 14 (a) –Landsat and Ikonos-derived VI

Index name	Acronym	Equation	Reference
Simple ratio	**SR**	nIR/red	(Jordan, 1969)
Normalized Difference Vegetation Index	**NDVI**	(nIR-red)/(nIR+red)	(Rouse et al, 1973)
Modified Simple Ratio	**MSR**	(nIR/red-1)/√ (nIR/red+1)	(Chen, 1996)
Difference Vegetation Index	**DVI**	nIR-red	(Richardson et al, 1992)
Renormalised Difference Vegetation Index	**RDVI**	√(NDVIxDVI)	(Roujean & Breon, 1995)
Green Normalized Difference Vegetation Index	**GNDVI**	(nIR-green)/(nIR+green)	(Gitelson et al., 1996, b)
Soil Adjusted Vegetation Index	**SAVI**	(nIR-red)(1+L)/(nIR*red*L), L=0.5	(Huete, 1988)
Transformed Soil Adjusted Vegetation Index	**TSAVI**	(nIR-a*red-b)/ (red+a*nIR-a*b) a,b=soil line coefficients	**(**Baret et al., 1989)
Soil Adjusted Vegetation Index 2	**SAVI 2**	nIR/(red+a/b)	(Major et al. 1990)
Modified Soil Adjusted Vegetation Index	**MSAVI**	$nIR+0,5-\sqrt{((nIR+0,5)^2-2*(nIR-red))}$	(Qi et al., 1994)

Optimised Soil Adjusted Vegetation Index	**OSAVI**	(nIR-red)(1+0.16)/(nIR+red+0.16)	(Rondeaux et al., 1996)
GEneralized Soil Adjusted Vegetation Index	**GESAVI**	nIR-b*red-a/red+0,35	(Gilabert et al. 2002)
Global Environmental Monitoring Index	**GEMI**	$\eta*(1-\eta/4)-[(red-0.125)/(1-red)]$	(Pinty & Vestraete, 1991)
Wide Dynamic Range Vegetation Index	**WDRVI**	(c*nIR-red)/(c*nIR+red), c=0.2	(Gitelson, 2004)
Soil and Atmospherically resistant Vegetation Index 2	**SARVI 2**	2.5*(nIR-red)/(1+nIR+6*red-7.5/blue)	(Huete et al. 1997)

L=canopy background brightness correction factor; a and b are the slope and the intercept of soil line: nIR=a*red+b (a=1.1, b=0.01 for Pantano site; a=0.9, b=0.07 for Monte Coppolo site); $\eta=[2*(nIR^2-red^2)+1.5*nIR+0.5*red)]/(nIR+red+0.5)$

Table 14 (b) Additional Landsat-derived VI (using SWIR bands)

Index name	Acronym	Equation	Reference
Normalized Difference Water Index	**NDWI**	(nIR-mIR1)/(nIR+mIR1)	(Gao, 1996)
Tasseled Cap - Greeness Vegetation Index	**GVI**	**TM**: $-0.2728*b_1-0.2174*b_2-0.5508*b_3+0.7221*b_4+0.0733*b_5-0.1648*b_7-0.7310$ **ETM:** $-0.2728*b_1-0.2174*b_2-0.5508*b_3+0.7221*b_4+0.0733*b_5-0.1648*b_7$	(Christ & Cicone, 1984)
Tasseled Cap - Wetness	**WVI**	**TM**: $0.1446*b_1+0.1761*b_2+0.3322*b_3+0.3396*b_4-0.6210*b_5-0.4184*b_7-3.3828$ **ETM:** $0.2626*b_1+0.2141*b_2+0.0926*b_3+0.0656*b_4-0.7629*b_5-0.5388*b_7$	(Christ & Cicone, 1984)

Table 15 – Performance (r^2) of VI-based regressions carried out using different sensors, pooled data sets and different averaging pixel windows size

	Ikonos$_{23x23}$	**TM$_1$**	**TM$_2$**	**TM$_3$**	**ETM +**	**Ikonos$_{3x3}$**
acquisition dates	08022004 06222005	05262004 05152005	05262004 06302005	08302004 06302005	07212004 06222005	08022004 06222005
pooled data set (n=95)						
SR	*0.10*	0.00 ^{ns}	0.00 ^{ns}	*0.05*	*0.12*	*0.08*
NDVI	*0.10*	0.00 ^{ns}	0.00 ^{ns}	0.04 ^{ns}	*0.13*	*0.13*
MSR	*0.10*	0.00 ^{ns}	0.00 ^{ns}	0.05 ^{s}	0.13	*0.09*
DVI	0.00 ^{ns}	*0.06*	*0.04* ^{ns}	0.01 ^{ns}	*0.01* ^{ns}	*0.01* ^{ns}
RDVI	*0.03* ^{ns}	*0.05*	*0.02* ^{ns}	0.03 ^{ns}	*0.05* ^{n}	*0.04* ^{ns}
GNDVI	*0.07*	0.00 ^{ns}	0.00 ^{ns}	0.02 ^{ns}	*0.08*	*0.06*
SAVI	*0.03* ^{ns}	*0.05*	*0.03* ^{ns}	0.02 ^{ns}	*0.03* ^{ns}	*0.03* ^{ns}
TSAVI	*0.04* ^{ns}	*0.04* ^{ns}	*0.02* ^{ns}	0.03 ^{ns}	*0.05*	*0.05*
SAVI 2	*0.04* ^{ns}	*0.04* ^{ns}	*0.02* ^{ns}	0.02 ^{ns}	*0.05*	*0.08* ^{n}
MSAVI	*0.02* ^{ns}	*0.05*	*0.03* ^{ns}	0.02 ^{ns}	*0.03* ^{ns}	*0.11*
OSAVI	*0.05*	*0.04* ^{ns}	*0.01* ^{ns}	0.03 ^{ns}	*0.07*	*0.07*
GESAVI	*0.16*	0.00 ^{ns}	0.00 ^{ns}	0.04 ^{ns}	*0.14*	*0.18*
GEMI	0.00 ^{ns}	*0.07*	*0.05*	0.01 ^{ns}	0.00 ^{ns}	*0.01*
WDRVI	*0.10*	0.00 ^{ns}	*0.04* ^{ns}	0.05	*0.15*	*0.11*
SARVI2	*0.03* ^{ns}	*0.01* ^{ns}	*0.02* ^{ns}	0.00 ^{ns}	0.00 ^{ns}	0.00 ^{ns}
NDWI	/	0.00 ^{ns}	0.01 ^{ns}	*0.26*	*0.23*	/
TC-GVI	0.00 ^{ns}	*0.06*	*0.04* ^{ns}	0.01 ^{ns}	*0.02* ^{ns}	*0.01* ^{ns}
TC-WVI	/	*0.02* ^{ns}	*0.04* ^{ns}	*0.29*	*0.22*	/

ns= not significant at 95% probability level

Table 16 – Performance (r^2) of VI-based regressions carried out using different sensors, sinlge year data sets and different averaging pixel window size

	Ikonos$_{23x23}$	**TM$_M$**	**TM$_A$**	**ETM +**	**Ikonos$_{3x3}$**
acquisition date:	08022004	05262004	08302004	07212004	08022004
2004 data set (n=49)					
SR	*0.29*	*0.01* ^{ns}	*0.18*	*0.25*	*0.58*
NDVI	*0.26*	*0.02* ^{ns}	*0.13*	*0.35*	*0.65*
MSR	*0.30*	*0.02* ^{ns}	*0.17*	*0.28*	*0.60*
DVI	*0.02* ^{ns}	0.14	*0.00* ^{ns}	*0.03* ^{ns}	*0.16*

RDVI	*0.11*	0.10	*0.04* ^{ns}	*0.11*	*0.34*
GNDVI	0.21	*0.11*	*0.10*	*0.30*	*0.37*
SAVI	*0.08* ^{ns}	0.12	*0.02* ^{ns}	*0.08* ^{ns}	*0.29*
TSAVI	*0.12*	0.10	*0.04* ^{ns}	*0.12*	*0.26*
SAVI 2	*0.13*	0.07 ^{ns}	*0.05* ^{ns}	*0.11*	*0.02* ^{ns}
MSAVI	*0.07* ^{ns}	0.11	*0.02* ^{ns}	*0.07* ^{ns}	*0.08* ^{ns}
OSAVI	*0.17*	0.08 ^{ns}	*0.06* ^{ns}	*0.17*	*0.44*
GESAVI	*0.38*	*0.16*	*0.20*	*0.30*	*0.64*
GEMI	*0.01* ^{ns}	0.11	*0.00* ^{ns}	*0.02* ^{ns}	*0.15*
PVI	*0.01* ^{ns}	0.14	*0.00* ^{ns}	*0.02* ^{ns}	*0.12*
WDRVI	*0.29*	0.02 ^{ns}	*0.15*	*0.33*	*0.63*
SARVI2	0.08 ^{ns}	0.10	0.02 ^{ns}	0.03 ^{ns}	0.01 ^{ns}
NDWI		0.00 ^{ns}	*0.35*	*0.38*	
TC-GVI	*0.03* ^{ns}	0.12	*0.15*	*0.04* ^{ns}	*0.12*
TC-WVI		0.00 ^{ns}	*0.34*	*0.38*	
TC-WVI	/	0.02 ^{ns}	0.00 ^{ns}	0.04 ^{ns}	/

	Ikonos$_{23x23}$	**TM$_M$**	**TM$_A$**	**ETM +**	**Ikonos$_{3x3}$**
acquisition date:	06222005	05152005	30062005	06222005	06222005
2005 data set (n=46)					
SR	*0.03* ^{ns}	*0.01* ^{ns}	0.01 ^{ns}	0.04 ^{ns}	0.00 ^{ns}
NDVI	*0.03* ^{ns}	0.00 ^{ns}	0.02 ^{ns}	0.04 ^{ns}	0.00 ^{ns}
MSR	*0.03* ^{ns}	0.00 ^{ns}	0.01 ^{ns}	0.04 ^{ns}	0.00 ^{ns}
DVI	0.01 ^{ns}	*0.02* ^{ns}	0.00 ^{ns}	0.00 ^{ns}	0.03 ^{ns}
RDVI	0.00 ^{ns}	0.01 ^{ns}	0.01 ^{ns}	0.00 ^{ns}	0.01 ^{ns}
GNDVI	*0.01* ^{ns}	0.00 ^{ns}	0.00 ^{ns}	0.02 ^{ns}	0.01 ^{ns}
SAVI	0.00 ^{ns}	0.00 ^{ns}	0.01 ^{ns}	0.00 ^{ns}	0.02 ^{ns}
TSAVI	0.00 ^{ns}	*0.01* ^{ns}	0.01 ^{ns}	*0.01* ^{ns}	0.01 ^{ns}
SAVI 2	0.00 ^{ns}	*0.02* ^{ns}	0.01 ^{ns}	*0.01* ^{ns}	0.01 ^{ns}

MSAVI	*0.03*^{ns}	*0.02*^{ns}	0.01^{ns}	0.00^{ns}	0.02^{ns}
OSAVI	*0.01*^{ns}	*0.01*^{ns}	0.01^{ns}	0.01^{ns}	0.01^{ns}
GESAVI	*0.09*^{ns}	0.00^{ns}	0.01^{ns}	0.08^{ns}	*0.02*^{ns}
GEMI	0.01^{ns}	*0.02*^{ns}	0.00^{ns}	0.00^{ns}	0.03^{ns}
PVI	0.01^{ns}	*0.02*^{ns}	0.00^{ns}	0.00^{ns}	0.03^{ns}
WDRVI	*0.03*^{ns}	0.00^{ns}	0.01^{ns}	0.05^{ns}	0.00^{ns}
SARVI2	*0.01*^{ns}	0.09^{ns}	0.08^{ns}	*0.01*^{ns}	*0.05*^{ns}
NDWI	/	0.03^{ns}	0.14	0.10^{ns}	/
TC-GVI	0.01^{ns}	*0.02*^{ns}	0.00^{ns}	0.00^{ns}	0.04^{ns}
TC-WVI	/	0.05^{ns}	*0.05*^{ns}	*0.03*^{ns}	/

ns= not significant at 95% probability level

In general, the use of indices instead of individual bands didn't provide any improvement when 2004 and 2005 data were pooled. TM_1 and TM_2 dataset-based regressions were even weakest than those related to individual band. Substantially, results for the general model were poor and only some indices provided significant correlations. In particular, VIs including SWIR bands, such as NDWI (e.g. ETM: r^2=0.23, TM_3: r^2=0.26) and Tasseled Cap Wetness (e.g. ETM: r^2=0.22, TM_3: r^2=0.29), showed higher Pearson correlations coefficients than those based on red and nIR bands (e.g. NDVI: r^2=0.13 for both $Ikonos_{3x3}$ and ETM).

Also, when a per year analysis was carried out, results basically confirmed what the analysis on individual bands had highlighted. That is, in 2004, it was possible to explain at least 2/3 of LAI variation by means of high resolution radiometric data (e.g. $Ikonos_{3x3}$) as well as 1/3 of LAI variation if using medium resolution satellite data (e.g. Landsat ETM or $Ikonos_{23x23}$), either using visible band-based indices and SWIR band-based ones. Whereas, in 2005, no significant relationships were found, but for NDWI of TM_3 dataset (r^2=0.14) which basically performed as b_5 and b_7 did in individual band analysis.

The same explanations addressed for individual-band analysis can be extended to VI-based regression results.

In particular, the strongest relationships with LAI were provided by 2004-$Ikonos_{3x3}$–derived NDVI, GESAVI, and WDRVI (r^2=0.63÷0.65) followed by MSR and

SR (r^2=0.60 and r^2=0.58, respectively). In fact, 2004-Ikonos$_{3x3}$ dataset provided higher r^2 than Landsat TM/ETM or Ikonos$_{23x23}$ datasets for almost all tested VI.

With respect to Landsat ETM, TM and TM$_A$ datasets the higher r^2 were found for indices sensible to vegetation water content, NDWI (2004: r^2=0.38 and r^2=0.35 for ETM and TM$_A$, respectively) and TC-Wetness.

On the other hand, for all different radiometric sources considerable differences in terms of performance (r^2) between the various VIs' were observed. For example, among Ikonos$_{3x3}$ soil-corrected indices GESAVI and OSAVI provided correlation coefficients (r^2=0.64 and r^2=0.44, respectively) appreciably higher than SAVI and TSAVI (r^2=0.29 and r^2=0.26, respectively) whereas not significant regressions between LAI and SAVI2 or MSAVI were observed. As well, DVI, GEMI, TC-GVI provided notably lowest correlation coefficients while a not significant relationship was observed for SARVI.

Moreover, for all different radiometric datasets GESAVI always appreciably outperformed the other soil-corrected indices.

3.2.3 Multiple band approach and LAI maps production

The purpose of VIs is to compensate for variable background (e.g. soil and litter) reflectance, different illumination conditions and some forms of atmospheric attenuation while emphasizing vegetation spectral features (Trishchenko et al.. 2002). However, a VI compresses the volume of remote sensing data by a factor equal to the number of channels used and significantly reduces the information contained in the original data set (Verstraete et al.. 1996). Furthermore, univariate regressions using vegetation indices are not able to independently model the red and near-infrared responses. For example, if the red response is curvilinear and the near-infrared is not, a compromise fit is necessary. In other words the use of VIs would seem to unnecessarily constrain the regression analysis. In fact, because different biophysical mechanisms control different band responses, there is no reason to believe the relation of individual bands to ecological variables will necessarily be the same. Thus, the multiple-band regression approach through the decoupling of band permits the analyst to potentially discover different relationships between the response variable and each band (Lawrence et al. 1998).

Therefore, a multiple least square linear regression analysis with LAI/ln(LAI) as dependent variable and all available spectral bands as explicative variables, was

computed. Only explicative variables which contribute significantly to the regression model, were retained.

Also, the predictive ability and stability of the final models was assessed by means of a cross-validation procedure. Cross validation is a technique to estimate the forecast skill of a statistical forecasting model (Michaelsen, 1987). Each member of a given dataset is excluded in turn from the prediction algorithm process (leave-one-out procedure) and then predicted using the algorithm, or fit, or relationship, derived without it. This is done for each member (i.e. the prediction algorithm is computed *n* times, if *n* is the size of the dataset). This avoids separating the dataset into a calibration and test dataset, and allows testing the predictive ability of the algorithm on each member of the dataset. The procedure is repeated n times and the Pearson correlation coefficients and the root mean square error (RMSE) calculated between the predicted and the observed values allow to assess the accuracy of the model. The stability is evaluated by the coefficient of variation (cv) of the different slopes associated to the regression variables (Davi et al., 2006).

On the basis of previous results concerning the ANCOVA of ln(LAI) (see section 3.2) which showed that univariate ln(LAI)-radiometric data relationships (either those using a VI as radiometric variable and those using an individual spectral band) depended on the year of observation, even the LAI-multiple band regression was supposed to be dependent on the year of observation.

Furthermore, in this case, all available LAI measurements were used[33], i.e. 55 observations per year for Ikonos-derived dataset and 49/45 for 2004/2005 ETM-derived dataset, respectively.

Regressions using ln(LAI) outperformed models using LAI for both year-related data sets and both satellite sensors. Therefore, only models developed using log-transformed LAI data are reported and discussed in the following. Table 17 and 18 set forth intercepts and coefficients and relative p-values of multivariate regression models using Ikonos-based 2004 and 2005 data sets, respectively.

[33] For sake of clarity, it must be said that a multivariate analysis performed using Ikonos reduced dataset (including only plots available for ETM) was carried out, as well. Basically, it provided similar results (all bands significant, multiple r^2=0.80 p<.0001 in 2004; only the last three bands significant, r^2=0.37, p<.0001, in 2005, respectively), though obviously slightly different model coefficients were obtained. However, in this case, the main purpose was to work out the best empirical model in order to produce the LAI distribution map rather than to compare Ikonos and ETM performances. Therefore, there were not a priori reason to exclude any observation.

With regard to Ikonos and to both year datasets, either regression models and each model term, except for b_1 in 2005, were highly significant (all band-related p-values<0.01; overall p<0.0001). However, the relative influence of the band was markedly different.

Table 17 – Multivariate model terms and relative slope and significance, Ikonos and Landsat ETM sensor, year 2004

Satellite sensor	Model term	estimate	t	p-value|
$Ikonos_{3x3}$	Intercept	3.41	9.38	<0.0001
	b1	-33.07	-3.77	0.0004
	b2	35.59	2.73	0.0087
	b3	-63.83	-8.26	<0.0001
	b4	2.37	3.25	0.0021

Satellite sensor	Model term	estimate	t	p-value|
ETM_{3x3}	Intercept	2.22	4.66	<0.0001
	b1	-37.77	-3.02	0.0042
	b4	6.02	3.89	0.0003
	b5	-10.04	-5.50	<0.0001

Table 18 – Multivariate model terms and relative slope and significance, Ikonos and Landsat ETM sensor, year 2005

Satellite sensor	Model term	estimate	t	p-value|
$Ikonos_{3x3}$	Intercept	2.49	8.56	<0.0001
	b2	30.43	2.96	0.0016
	b3	-34.57	-3.90	<0.0001
	b4	-2.55	-4.28	0.0001

Satellite sensor	Model term	estimate	t	p-value|
ETM_{3x3}	Intercept	2.38	9.27	<0.0001
	b1	35.64	4.07	0.0002
	b2	-35.88	-4.14	0.0002

For example, the red band had between 12÷20 times (depending on the year) over the influence of nIR band. Also, for 2004-model green and blue[34] coefficients were more than ten times the nIR one. This outcome might be the result of the red band having a much lower asymptote than the near infrared band (Ripple, 1985).

The multiple r^2 were rather different among 2004 (r^2=0.78) and 2005 (r^2=0.33), whereas similar RMSE were obtained for the two years (RMSE=0.22, RMSE=0.25 in 2004 and 2005, respectively). In other words, the relationships worked out in 2004 by means of the multivariate regression allowed to explain about two times more variation of LAI than the model derived from 2005 data.

When regression on all six ETM reflective spectral bands against log-transformed LAI was performed, it resulted in best regression model including bands 1 (blue), 4(nIR) and 5 (SWIR1) in 2004 whereas bands 1 (blue) and 2 (green) in 2005, respectively. This means that a number of bands resulted not contributing at explaining LAI variations. In particular, in 2005, only the first two bands were retained as significant one in the multivariate model. Besides, high overall model significance was observed in both years ($p<0.0001$ and $p<0.0005$ in 2004 and 2005, respectively) though lower multiple r^2 (r^2=0.46 and r^2=0.27), respectively, with respect to Ikonos-related ones, were obtained. Respective RMSE were 0.36 and 0.28 for 2004 and 2005 models, respectively.

With regard to Ikonos-based models, the correlation coefficients and RMSE between predicted and measured values provided by the cross-validation procedure were r^2=0.70 and RMSE=0.90, respectively, for year 2004, and r^2=0.36 and RMSE=1.05 for the year 2005. Whereas, for ETM-based regressions, r^2=0.32 and RMSE=1.36 and r^2=0.22 and RMSE=1.21 for year 2004 and 2005, respectively. Furthermore, either in 2004 and 2005 and for Ikonos as well as ETM related data, rather low coefficients of variation of the coefficients (terms) of multivariate models resulted from the leave-one-out procedure (for all model terms cv <7%) as shown in table 19.

[34] only for 2004 dataset

Table 19 – Coefficients of variation per each model term coefficient (leave-one-out procedure)

Satellite sensor	year	cv (%)						
		intercept	b1	b2	b3	b4	b5	b6
Ikonos$_{3x3}$	**2004**	4.0	- 4.0	6.2	-2.3	7.2	/	/
	2005	2.0	/	5.0	-3.6	-4.1	/	/
ETM$_{3x3}$	**2004**	2.7	-6.6	/	/	4.0	-3.6	/
	2005	1.3	3.9	-3.7	/	/	/	/

In the end, the functional relationships provided by the Ikonos-based multivariate regression models for the two years (i.e. those resulting to provide the highest LAI predictive skill among all tested empirical relationships), respectively, were used to produce 4m resolution[35] LAI spatial distributions, see equation (1) and (2):

(1) LAI=exp(3.41-33.07*b1+35.59*b2-63.83*b3+2.37*b4) (year 2004)

(2) LAI=exp(2.49+30.43*b2-34.57*b3-2.55*b4) (year 2005)

Figure 11 and 12 show the LAI maps, for 2004 and 2005 years, respectively, realised by classifying LAI values into eight classes (for cartographic reasons), displayed over Ikonos panchromatic image background.

Also, in figure 13 the relative percentages per each LAI class computed for the two study sites and the two years of observation, are reported.

In particular, by focusing on 2004 LAI spatial distributions (much accurate and reliable), some interesting information can be drawn. For example, within Pantano site about 2/3 of the area was characterised by LAI values ranging from 0 to 3 while the remaining 1/3 was about almost equally distributed between the 3÷4 LAI range (18%) and 4÷6 one (15%). Only 2% of the territory presented high LAI values (6÷8). Whereas, appreciably higher LAI values characterised Monte Coppolo site, which presented LAI values ranging from 4 to 6 within about 1/3 of the area, from 6 to 8 and from 3 to 4 covering 11% and 16% of the surface, respectively. This findings reflected the differences in LAI due to the different vegetation typologies and characteristics of the two sites, already partially highlighted by *in situ* LAI measurements results (see paragraph 3.1.1.). For instance, rather high LAI values (4÷8) characterised the *maquis* of Monte Coppolo, whereas the same vegetation typology present lowest LAI values (mostly 2÷4) at Pantano

[35] Being applied on a per pixel basis

wherein, in fact, it is generally represented by lowest and less dense vegetation formations. Moreover, the deciduous hygrofilous forest of Pantano showed LAI values similar to those related to the deciduous forest of Monte Coppolo. Finally, it can be noted a forest degradation in some neighbouring areas, near the cultivated land, in terms of lowest LAI values.

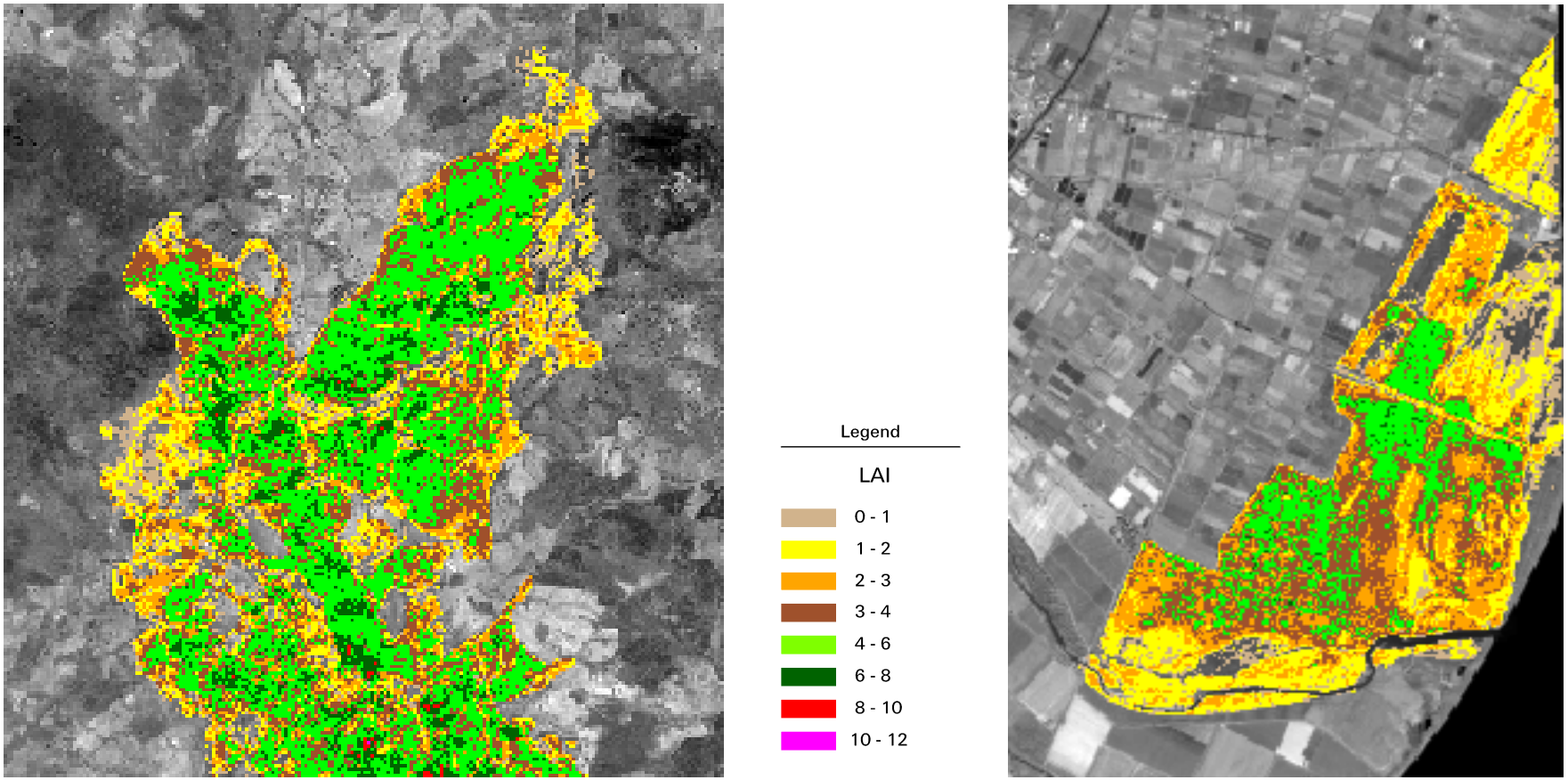

Fig. 11 - IKONOS-derived LAI maps over the two study sites Pantano and Monte Coppolo, for 2004, August 2 acquisition dates.

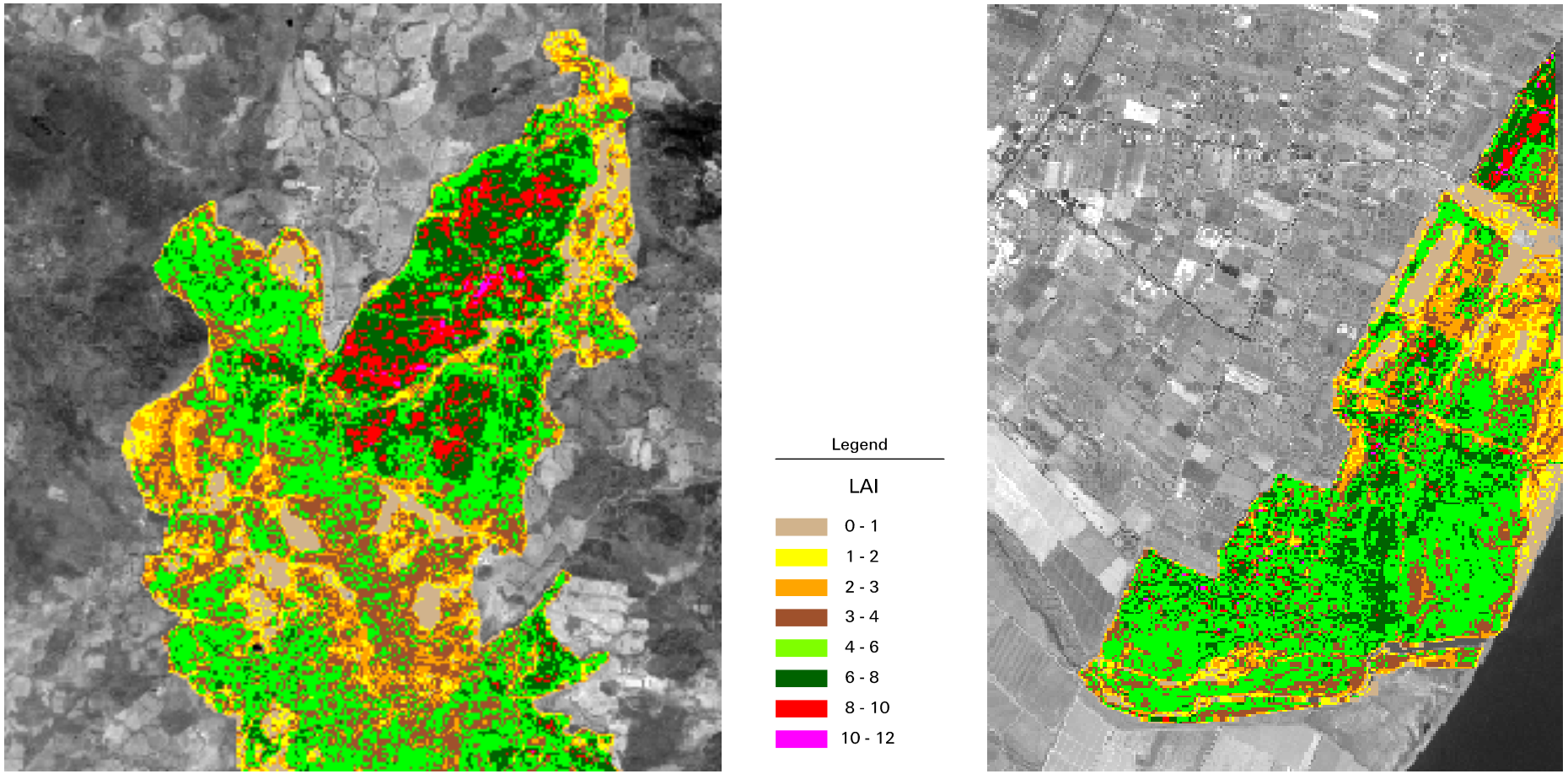

Fig. 12 - IKONOS-derived LAI maps over the two study sites Pantano and Monte Coppolo, for 2005, June 22 acquisition dates.

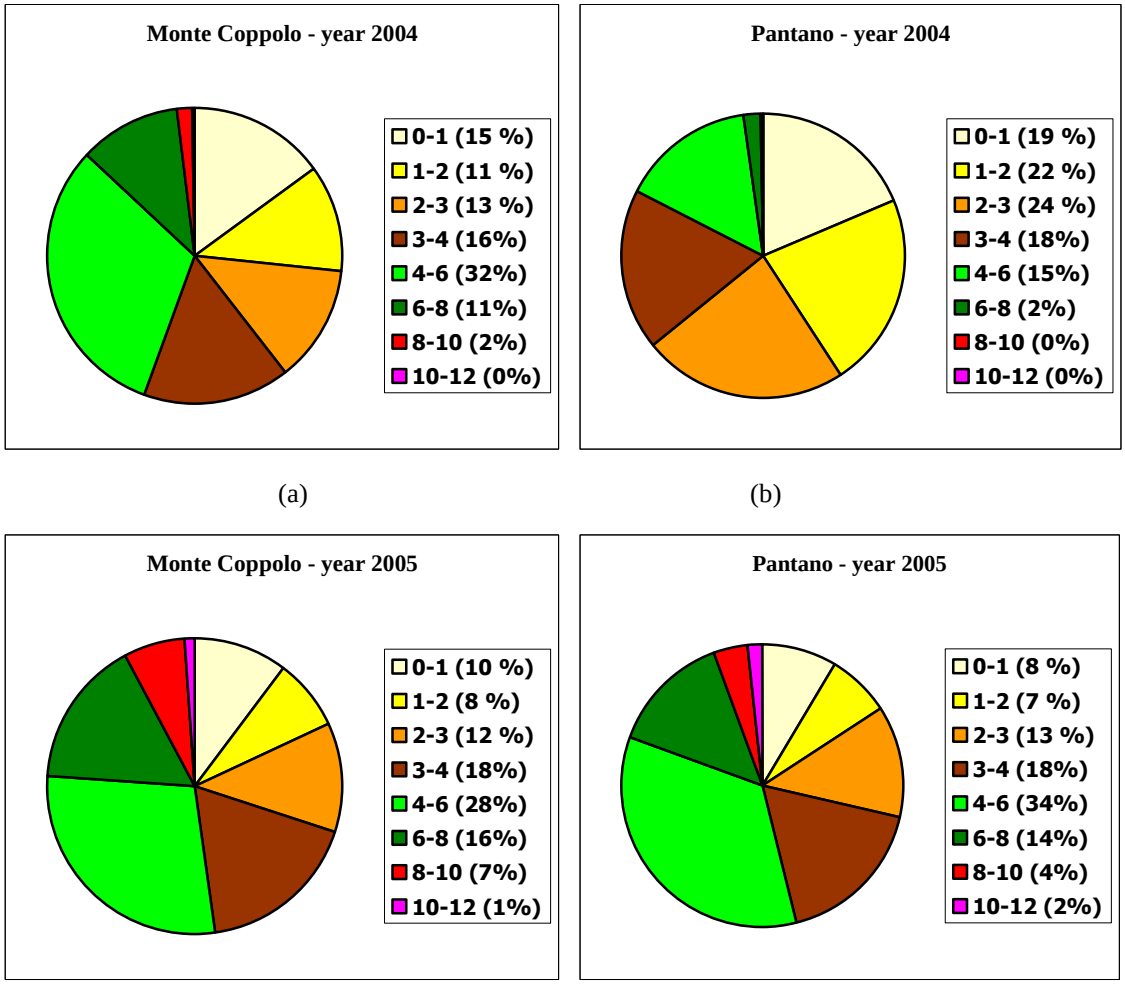

Fig. 13 – LAI values distribution for Monte coppolo and Pantano sites, in 2004 ((a) and (b)) and 2005 ((c) and (d)), respectively.

3.2.4. Using Ikonos-2 data as subsampling for upscaling LAI field measurements to Landsat medium-resolution

The retrieval of land surface characteristics, such as LAI, from satellite data through empirical model calibrated on "point" measurements needs an appropriate density of ground observations. This means that the variability of the deriving products within a single pixel (or better a 3x3 pixel window considering also the georeferencing uncertainties) should be accounted for by the adopted sampling scheme (Liang, 2004 b). In highly heterogeneous vegetation this implies that an extremely large number of ground observations have to be collected, which is a time consuming, expensive and ultimately not always easy/possible condition to satisfy for practical/logistic constraints (e.g.

impenetrable areas). Particularly, the number of measurements increases as the spatial resolution of satellite data decrease.

In this section a comparison between direct LAI measurements-Landsat ETM[36] data calibration and a two-stage procedure, based on the use of Ikonos images as intermediate calibration, as described in the following, is reported. The purpose was to examine the effectiveness of using a high resolution image as subsampling for upscaling LAI field data to a coarse resolution satellite image as an alternative to collecting an adequate, hence very large, number of *in situ* measurements theoretically necessary to well characterise a Landsat 3x3 pixel window.

As sketched in a general form in figure 9 (left-hand side), Ikonos data are firstly used to produce a LAI map based on the best relationship established between *in situ* LAI measurements (LAI_{meas}) and Ikonos high resolution data (stage 1). From those maps, mean LAI values over a 23x23 pixel window (about 90x90 m^2) are calculated ($LAI_{Ikonos\ map}$) to be used in $LAI_{Ikonos\ map}$-Landsat ETM radiometric data empirical model developing (stage 2). To this aim, a set of 128 non-overlapping plots, the size of 23x23 Ikonos pixels, were selected within the two study areas avoiding as much as possible noise effects due to near edge positions. The selection of plots was supported by visual inspection of orthophotos and Ikonos both panchromatic and multispectral images as well as by the knowledge of the study sites gained during the multiple field surveys.

However, specifically, stage 1 was here accomplished by the best performing models[37] already provided by regression analysis shown in previous section, i.e. the Ikonos-derived LAI maps produced by using the multivariate regression models (see equation (1) and (2) within paragraph 3.2.3). As well, the statistical analysis shown in previous paragraph already indicated that the best empirical models[38] for a direct upscaling of field LAI measurements to Landsat ETM data (figure 12 (b)) resulted to be the multivariate models.

Therefore, in this paragraph specifically results related to stage 2 and to the overall performance of the two-stage procedure are examined. In particular, either univariate

[36] Also Landsat TM data were tested but they provided even poorer results than ETM data (data not shown). In fact, the better performance of ETM radiometric dataset was already shown in previous sections.
[37] One model per each year of observation
[38] One model per each year of observation

LAI-NDVI[39] ordinary least square regressions and multivariate LAI-multiple band regressions were tested for Landsat ETM satellite radiometric data calibrations (stage 2). Also, both LAI and log-transformed LAI values were examined in regression analysis. Since regressions using log-transformed LAI data outperformed those using LAI only results relative to the former are reported.

To sum up, two alternatives were investigated for the second stage upscaling:

- case 1: the relationship between $LAI_{Ikonos\ map}$ and Landsat ETM radiometric data provided by NDVI-ln(LAI) $_{Ikonos\ map}$ regression;
- case 2: the relationship between $LAI_{Ikonos\ map}$ and Landsat ETM radiometric data provided by multiple-band regressions.

The effectiveness of the two-stage procedure was assessed by comparing the coefficients of determination (r^2) related to the $ln(LAI_{meas})$-ETM multivariate regressions, with the product of the coefficients of determination of the two stages ($r^2_{tot}=r^2_{stage1}*r^2_{stage2}$).

Results showed that univariate regressions performed between ETM-derived NDVI and corresponding $ln(LAI_{Ikonos\ map})$ data (stage 2, case 1) provided lower coefficients of determination (r^2=0.76, RMSE=0.03 and r^2=0.03, RMSE=0.06 for 2004 and 2005, respectively) than ETM-$ln(LAI_{Ikonos\ map})$ multivariate regressions (stage 2, case 2) for both years (r^2=0.94, RMSE=0.13 and r^2=0.89, RMSE=0.06, for 2004 and 2005, respectively). Detailed outcomes of case 2 analysis are reported in table 20 (a) and (b) for the two year of observation, respectively.

Table 20 – Multivariate model terms, and respective slope and significance, for Landsat ETM- sensor

Model term	**estimate**	**t**	**p-value|**
Intercept	3.08	27.99	<0.0001
b1	-38.40	-12.21	<0.0001
b3	-29.66	-7.78	<0.0001
b4	1.91	4.03	<0.0001
b5	-3.00	-3.06	0.0027

(a) year 2004

[39] The NDVI was selected (out of several tested VI in previous sections) since it resulted the best performing spectral vegetation indices in VI-LAI empirical model developing, as shown in paragraph 3.2.2.

Model term	estimate	t	p-value|
Intercept	2.42	43.89	<0.0001
b1	3.88	3.17	0.0019
b2	11.53	5.47	<0.0001
b3	-17.38	-7.14	<0.0001
b4	-1.72	-12.15	<0.0001
b6	-4.77	-6.33	0.0027

(b) year 2005

In particular, for both year datasets, either multivariate regression model and each model term, were highly significant (all band-related p-values<0.003; overall p<0.0001). Furthermore, as already resulted for direct ETM-LAI_{meas} relationship (see paragraph 3.2.3), different bands were retained in the model depending on the year of observation. Moreover, in comparison with direct ETM-LAI_{meas} multivariate regression, a large number of bands were included. In particular, for 2005 dataset, direct ETM-LAI_{meas} multivariate regression had resulted in a two bands model including only b1 and b2 (see paragraph 3.2.3) whereas all ETM bands, but b5, were included in the ETM-$LAI_{Ikonos\ map}$ multivariate regression. As well, for 2004 dataset, with respect to results related to direct ETM-LAI_{meas} the ETM-$LAI_{Ikonos\ map}$ multivariate regression included the additional contribute of b3. Furthermore, the relative influence of each band was notably different. In 2004, b1 (blue) and b3 (red) had between 10÷20 times over the influence of b4 (nIR) and b5 (SWIR1). Whereas, in 2005, b3 (red) and b2 (green) resulted to have the higher sensitivity to LAI variations.

Finally, the overall performance of the two-stage procedure for the two alternative models (i.e. case 1 and case 2) and the two years, resulted to be the following, respectively:

1) <u>case 1</u>:

$r^2_{tot} = r^2_{stage1} * r^2_{stage2} = 0.78*0.76 = 0.60$ (year 2004)

$r^2_{tot} = r^2_{stage1} * r^2_{stage2} = 0.78*0.03 = 0.01$ (year 2005)

2) <u>case 2</u>:

$r^2_{tot} = r^2_{stage1} * r^2_{stage2} = 0.78*0.94 = 0.73$ (year 2004)

$r^2_{tot} = r^2_{stage1} * r^2_{stage2} = 0.78*0.89 = 0.29$ (year 2005)

Therefore, when compared with direct ETM-LAI_{meas} regression analysis (r^2=0.46 and r^2=0.27 for 2004 and 2005, respectively), these results showed the potentiality of using a high resolution satellite data as intermediate stage (stage 1) for upscaling "point"[40] field measurements to medium resolution satellite image calibration (stage 2) in mediterranean environment.

Obviously, the weaker the relationship used for the first upscaling stage (stage 1) the poorer will be the overall result. For example, in 2005, the LAI distribution map used for ETM calibration derived from a model accounting for only the 33% of surface LAI variation (r^2=0.33). Therefore, substantially, no improvement were observed by adopting the two-stage procedure with respect to directly performed a multivariate regression between field LAI measurements and ETM bands and both methods yielded unsatisfactory results (r^2=0.29 and r^2=0.27, respectively).

Conversely, with regard to the 2004 dataset, both regression models tested for the second upscaling (stage 2) allowed to increase the amount of variation of LAI explained by means of ETM data. Namely, such improvement was of about 10% and 25% for NDVI-based model (r^2_{tot}=0.60) and multivariate model (r^2_{tot}=0.73), respectively.

Once more, with data used in this study, the use of multiple band instead of spectral VI (NDVI represented the best performing VI out of several tested ones) allowed to increase the predictive ability of empirical model.

3.3 Discussion

This chapter presented a quantitative analysis aimed at estimating Leaf Area Index (LAI) spatial distributions in Mediterranean forested areas by means of remotely sensed data.

A fundamental challenge to the retrieval of useful biophysical products, such as the LAI, from remote sensing within Mediterranean areas is the fragmented and mixed environment which characterises these zones with respect to other forest ecosystem (e.g. those of northern latitude).

[40] It is meant measurements having a small footprint (plot size) in order to account for the high spatial variability of mediterranean environment.

Therefore, given that older generation sensors have many known limitations with respect to their suitability for studying highly discretized and complex land cover, the need to evaluate the new generation of sensors, providing highest spatial/spectral resolutions is of critical importance.

In particular, high spatial resolution permits proper (reduced) size as well as accurate location of calibration plots, which is a key issue when coping with high spatial variability and diversity.

In this context, the utility of using Ikonos high spatial resolution images was investigated in order to evaluate:

a) the performance of empirical models developed through regression analysis between *in situ* LAI measurements and Ikonos data for producing LAI spatial distributions of two forested Mediterranean areas (Matera Province, South of Italy);

b) the opportunity of using high resolution satellite data, like Ikonos, as subsampling for medium resolution satellite data, such as Landsat TM/ETM, when LAI of wide areas need to be mapped.

To this aim, two LAI field surveys were carried out in early summer 2004 and late spring 2005 in order to collect a certain number of *in situ* LAI measurements, namely 55 plots per year were sampled within four different vegetation typologies (*maquis*, *deciduous* forest, *live oak* forest and *hygrophylous* forest). Besides, as synchronous as possible Ikonos and Landsat TM/ETM satellite images were acquired.

With respect to the first objective and in order to assist in the selection of the best empirical model, the training dataset (110 pairs of ln(LAI)[41] values and corresponding radiometric values) was examined in order to evaluate if a general model developed pooling all data into a unique dataset could be used or, conversely, it would have been necessary to separately develop per species or per year or even per species and per year regression models. Therefore, an analysis of covariance (ANCOVA) of ln(LAI) having as independent variable the radiometric variable, the year of observation and the vegetation typology, and considering all possible interactions, was performed. In particular, a

[41] In order to cope with possible radiometric signal saturation which tends to occur at the higher LAI values (see previous sections) the use of either LAI and log-transformed LAI data was investigated. Respective results showed the superior performance of empirical models developed using the log-transformed variable. Hence, for sake of sinthesis, here it is referred only to results related to the use of the log-transformed variable.

number of radiometric variables were tested, i.e. one-by-one each individual band as well as several spectral vegetation indices (VIs).

Substantially, results of ANCOVA showed that the ln(LAI)-radiometric variable relationship didn't depend on vegetation typology but it considerably depended on the year of observation. It must be stressed that this results highlighted the utility of the empirical models worked out in this way for a spatial extrapolation of field LAI measurements, hence allowing to obtain LAI distribution maps of the study areas in the year of data collection. Conversely, they prevented a temporal extrapolation of the empirical model (i.e. the possibility to apply the empirical model to radiometric observations referring to year different from that used for model calibration) which would have enabled to monitor the LAI dynamic over the years.

According to results provided by the ANCOVA analysis, the full dataset was subdivided into two subsets, each one referring to one of the year of observation, respectively, to be used in regression analysis.

Then, univariate ordinary least square regressions having ln(LAI) as dependent variable and one-by-one each tested radiometric variable (individual band or VIs) as independent variable, as well as multivariate least square regressions exploring ln(LAI)-multiple spectral band relationships, were examined.

The statistical analysis provided three main outcomes which can be summarised as follows:

- multiple-band models were found to offer substantial improvement over single-variable models (either individual band or spectral VI);
- the first LAI maps of the study areas were produced by means of the best performing models. In particular, one four-variable (all available Ikonos bands) model was used to extrapolate the relationship worked out to the landscape in order to produce the LAI maps of the two study areas in 2004;
- empirical models were robust with respect to variations in vegetation typology and other characteristics of the study sites, thus highlighting the reliability of their spatial extrapolation to other areas;
- empirical models were highly sensitive to conditions at time of data collection (e.g., differences in forest vegetation phenological status, background optical properties), thus limiting the possibility of their temporal extrapolation.

In particular, in relation to the last finding, a comparison of within-plot radiometric variability between Ikonos 2004 and 2005 images was performed by means of within-plot coefficients of variation of reflectance in each band. In this way, it was shown that a significantly highest within-plot heterogeneity characterised the spectral signal in 2005. This, in turn, highlighted the diminished suitability of 2005 radiometric data for developing empirical relationships between LAI measurements and satellite data, thus giving reason for the poor results obtained.

Firslty, the following hypotheses were formulated to explain such a result. Firstly, given the early period of 2005 field survey (and related satellite data acquisition) with respect to 2004 one, two main effects might be assumed to significantly affect 2005 data while not, or only to a minor extent, 2004 ones. Specifically, it is likely that forest vegetation had not reach yet the phenological peak (maximum vegetation development) in late May 2005 (i.e. at time of 2005 field survey) and continued growing during the period between *in situ* LAI measurements and satellite acquisition date, causing measured LAI to significantly differ from actual LAI values at time of satellite overpass (2005, 22nd of June). Conversely, the maximum vegetation development was reasonably reached in late June-early July 2004 (i.e. at time of 2004 field survey), guaranteeing the consistency between LAI measurements and actual LAI values at time of 2004 satellite overpass (2004, 2nd of August).

Secondly, it is possible that background effects (i.e. mainly those due to understory herbaceous vegetation and litter) could have been significantly different between 2005 and 2004. For example, during June 2005 grass is mostly green in those areas and hence its spectral signal is more similar to that of forest vegetation than it is at the beginning of August[42] when grass is mainly in a senescent status.

Furthermore, although the LAI measurements footprint (sampled area) used in this study was rather small (about 12x12m^2), i.e. *ad hoc* tailored to the Ikonos resolution in order to account for the high spatial variability present within the mediterranean areas, nevertheless additional regression analysis performed using either Landsat TM/ETM data and Ikonos data aggregated to match Landsat resolution (i.e. 23x23 Ikonos pixel averaging window corresponding to 3x3 Landsat pixel window were used) was carried out for comparison purposes. However, as expected, since 90x90m^2-wide training areas

[42] Ikonos images were acquired on the 2nd of August in 2004 and on the 22th of June in 2005

were in this case characterised by ground sampled surfaces of less than 2% (~12x12m^2), poorest results were generally obtained.

This result highlighted the need for an appropriate characterisation of the variability of the deriving products (e.g., LAI) within the areas (plot) used for calibration (i.e., usually at least a 3x3 pixel window considering the georeferencing uncertainties). Nevertheless, *in situ* LAI measurements are extremely labour-intensive, rendering their use for an extensive sampling rather demanding if not impractical. Moreover, it must be stressed that logistic constraints (e.g. impenetrable areas) may further limits the possibility to accomplish a suitable sampling scheme.

Therefore, and with respect to the second objective, the study indicates an alternative expedient which may offer a practical means to produce LAI distribution maps on a regional scale or above by means of a limited number of LAI ground measurements using both Ikonos and Landsat satellite images. Obviously, the idea is that Ikonos images will cover only some percent of the area to be mapped which will be, in fact, entirely sensed by Landsat sensor. Therefore, field LAI data will firstly be upscaled to Ikonos resolution in order to produce a high resolution LAI distribution map which in turn will be used to calibrate the LAI-Landsat data empirical model.

Specifically, with data used in this study, it was shown that this procedure allowed to increase of about 25% the amount of variation of LAI explained by means of Landsat ETM radiometric data directly calibrated by means of field LAI measurements.

In conclusion, although needs to be further refined and validated, the use of observations at different spatial resolution (field data + Ikonos + Landsat) so as shown in this study can contribute to the validation of MODIS-LAI products, routinely provided as 1-km spatial resolution data and hence not directly compatible with the scale at which ground measurements are usually collected, in highly fragmented and mixed environment.

4 Multitemporal analysis of spectral VI and corresponding climatic parameters

Mediterranean regions constitute a transitional climate zone between arid and humid regions (Di Castri & Mooney, 1973) where it has been hypothesised that climate changes may have the most pronounced effect (Palutikof et al. 1994, Cubash et al., 1996, Lavorel et al., 1998).

Indeed, there is an increasing evidence that climate change affects biological and ecological processes. In particular, it seems to be a main driver of changes in natural vegetation communities' physiology, growth and net primary productivity. Distribution and abundance of either animals and plants are altered, as well as their life cycles, mainly as a consequence of temperature increasing.

However, evidence of such effects has been mostly limited to northern latitude (Penuelas et al., 2002) where temperature is normally the most important climatic factor limiting plant photosynthesis (Yu et al., 2003). Here, the prevalent effect of global warming on vegetation seems to be an anticipation and hence a lengthen of the growing season, ultimately determining an increase of net primary productivity.

Few studies have investigated the effects of climate change on the lower latitude forests and shrublands of Mediterranean areas where both temperature and precipitation play key roles in regulating plant biological processes.

Athough Mediterranean vegetation species present different adaptive mechanisms to water deficit and high summer temperature, nevertheless it is not clear what might be the response of these species to climate change and particularly to the temperature increase and precipitation decrease forecasted for Mediterranean basin (IPCC, 2001, Palutitikof, 2002).

In general, plant response to changing environmental conditions is related to the genetically acquired adaptive strategies and acclimatation which each species has developed in order to survive and successfully compete within its ecological conditions and related variability ranges.

If environmental conditions change within certain limits of tolerance, plants will put into effect their adaptive strategies, but these strategies will differ from species to species and not all species are able to react with the same degree of efficiency to the same type or same intensity and duration of environmental stress (Pereira et al., 1995).

Because of the high level of biodiversity which characterizes the vegetation communities of our area and therefore the different adaptive mechanisms adopted, one can hypothesize that on a long term basis in the Mediterranean ecosystem climate changes will trigger diverse or even contrasting phenomena. For example, an increase in winter temperatures could determine a reduction of the period of dormancy (with heightened risk to the plant of sudden frosts) and therefore a prolongation of the growth phase, whereas an increase in summer temperatures could increase water deficit impact and reduce the summer growth of the vegetation. At the same time, the species with a greater capacity for adaptation could have a competitive advantage over the others (Gratani et al., 2005), meaning that the more vulnerable species could modify their distributional area – migrating to more suitable climates.

Multi-temporal series of satellite data offer a powerful means to monitor vegetation pattern/changes (e.g. Nemani et al., 2003, Turner et al., 2005). There are series now covering a timespan of more than twenty years, which thus constitute a significant window of observation.

In particular, they can be used to gain insight into the complex mechanisms controlling the response of vegetation to climate variability. It is well known that precipitation and temperature have an important influence on the development and condition of vegetation, particularly during the growth season, which determines its condition in all later phases. Temperature is a key factor in determining the various phenologic phases of plants (sprouting, gemmation, leafing, flowering, fruiting, senescence and winter dormancy) whereas precipitation regulates photosynthetic activity and the transfer of organic substances from leaves and branches to the roots (Papanastasis et al., 1997) and consequently the growth of the plant.

Mostly, temporal series of satellite-derived Normalised Difference Vegetation Index (NDVI) have been profitably used to this purpose argueing that changes in NDVI reflect changes in biological activities (Li et al. 2000, Sarkar and Kafatos, 2004, Suzuki et al., 2006, Volcani et al., 2005, Stokli et al., 2004, Zhang and Anderson., 2004, among others). For example, Myneni et al. 1997 using satellite-derived series of NDVI, from 1981 to 1991, showed evidence of an increased plant growth in the northern high latitude (> 40° N) associated with a lenghtening of the growing season due to warmer temperatures.

The objective of this part of the study was to perform a retrospective analysis of yearly vegetation productivity and corresponding climatic conditions of the two selected study areas (see chapter 2), in order to evaluate possible relationships between inter-annual variation of vegetation and associated temperatures and precipitations.

4.1. Materials and methods

4.1.1 Satellite images

A series of Landsat TM/ETM images from 1984 to 2005 was acquired, all referring to the late spring/summer period and thus relating to the seasonal peak of vegetation development period in the area under study (table 21).

The choice of Landsat sensors was made because of the need for either a sufficient spatial resolution allowing distinguishing the main different vegetation species in the study areas (*Live oak forest, Maquis, Mixed broadleaf forest, Hygrofilous forest*) and a sufficiently long image time series.

Table 21 – List of Landsat images used

Acquisition Date	Orbit track (path, row)
06/20/84	188,32
06/13/87	188,32
08/02/88	188,32
05/10/89	187,32
07/18/94	188,32
06/19/95	188,32
06/14/99	188,32
08/03/00	188,32
07/06/01	187,32
05/26/04	188,32
06/30/05	188,32

In fact, since the two study sites are characterised by significantly different environmental conditions (e.g. altitude, distance from the sea) and hence ecosystems (see chapter 2), they were separately analysed. Furthermore, within the same study area, also per vegetation typology investigation were performed, in order to explore possible different response associated with different vegetation typology.

The spectral vegetation index (VI) selected for the multitemporal analysis were the Normalised Difference Vegetation Index (NDVI=(nIR-red)/(nIR+red)) and the Normalized Difference Water Index (NDWI=(nIR-SWIR)/(nIR+SWIR)).

The first one is largely the most used spectral index for remote sensing of vegetation (Kawabata et al., 2001, Maselli et al., 2004, Yang et al., 1998, among others), and responds to changes in amount of green biomass, chlorophyll content, and canopy water stress (Liang, 2004, b). Whereas, the NDWI is substantially a variation of NDVI exploiting the short wave infrared spectral range (1.2-2.5 μm) where the radiation absorption due to water content is enhanced. For Landsat TM/ETM+, nIR and SWIR correspond to bands 4 (0.78–0.90 Am) and 5 (1.55–1.75 mm), respectively. One reason that the NDWI may not have received much attention until recently is that the infrequent temporal coverage of TM and ETM+ make it difficult to estimate the vegetation water content for various applications. Classic operational instruments such as the AVHRR did do not include a SWIR band. However, new satellite sensors such as the Moderate Resolution Imaging Sensor (MODIS) on NASA's Terra and Aqua satellites now make such data routinely available (Jackson et al., 2004). Also, several studies have profitably used the NDWI derived by Landsat bands (e.g. Hardisky et al., 1983, Anderson et al., 2004, Maki, 2004, Healey et al., 2006).

Satellite images were preprocessed in order to obtain a co-registered dataset as well as a consistent radiometric scale. To this aim, firstly all frames were orthorectified (as described in chapter 3) then a data normalisation based on "pseudoinvariant" target approach (Schott et al. 1988, Furby and Campbell, 2001) was performed.

This approach assume that there are some pixels ("pseudoinvariant" targets) in a satellite image whose reflectance are quite stable through time (e.g. deep water, bedrock). Therefore, variations of radiometric measurements of these pixels on different dates can be related to exogenous "noises" which change the at-satellite sensed signal, such as different atmospheric and illumination conditions or even sensor response drift over the years (see paragraph 3.1.2.1.).

The cloud free 2004-26-05 Landsat TM was selected as reference image for both orthorectification and relative normalization. Therefore, it was firstly orthorectified and atmospherically corrected following the same procedure described in paragraph 3.1.2.1. Actually, since the reference image was a corrected reflectance image the performed

procedure allowed to obtained not only a relative normalization of image radiometry but also corrected surface reflectance images.

Then, a number of pseudoinvariant pixels with variable brightness from dark to bright (such as a stone quarry, urban areas, lake and sea water) were selected[43] and corresponding digital number (DN) and surface reflectance were extracted from each band of the image to be corrected as well as from those of the reference one, respectively. In fact, since the atmosphere affect differently each wavelength it was necessary to retrieve normalization coefficients individually per each band (*k*).

Finally, per each image, per band (*k*) linear regressions (see equation 1) between the reflectance (ρ_k) of the reference image and corresponding digital number (DN_k) of the image to be corrected extracted on the pseudoinvariant targets provided the two coefficients (a_k and b_k) to be used for normalizing all other pixels of the image. All highly significant regression were obtained, and Pearson correlation coefficients related to b3, b4 and b5, which were the bands used to calculate the selected VIs for the multitemporal analysis, were all > 0.97.

$$\rho_k = a_k + b_k DN_k \quad (1)$$

4.1.2. Climatic data

The following climatic parameters were computed from daily measurements of precipitation and surface air temperature collected over the period 1983-2005 by two ground meteorological stations, one close to Monte Coppolo and the other to Pantano site, respectively: maximum, mean and minimum temperatures, total precipitation, growing degree days (GDD), and the ratio between cumulative precipitation and mean temperature (P/T).

GDD is a widely used measurement, especially in agriculture, to estimate or predict the length of the various phases of crop development (Bonhomme, 2000) but also to study the phenologic stages of diverse natural species and their use as climatic indicators (Spano et al., 1999). These are usually calculated as the difference between the mean daily temperature and a temperature below which the process of growth and

[43] It must be said that two sets of pseudoinvariant targets were used in relation to the two different satellite image frames used (path 188, row 32 and path 187, row 32, respectively). In particular, eight pseudoinvariant targets were found and used for the 188-32 image frame whereas only six pseudoinvariant targets were found for the overalapping zone between 187-32 and 188-32 frames.

development become significantly inhibited. The present analysis considers three distinct threshold temperatures 0, 10, and 20°C and set to zero possible negative GDD values.

In particular, in order to explore lag and cumulative effects of precipitation and temperature on vegetation activities and development, mean values for daily minimum, mean and maximum temperature, as well as cumulative values for GDD and precipitation were computed for the 180, 90, 30 and 10 days preceding the date of passage of the Landsat satellite. Also, for the same temporal window the P/T indicators was derived using corresponding cumulative precipitation and mean temperature.

It must be said that these periods were chosen with the aim of investigating which, if any, of them best highlighted the relationship between VI (which refers to vegetation peak) and climatic conditions during vegetation development. In fact, these different temporal windows refer to different vegetation phenological stages, which might differently be affected by variations of climatic parameters. Furthermore, potentially, each vegetation species could present a different optimal temporal window for climatic parameter calculation.

Finally, it is noteworthy that since the various climatic indicators were all strongly correlated to mean temperature and cumulative precipitation (statistically redundant parameters) it was decided to report only the results relative to these two indicators.

4.1.3. Statistical analyses

Univariate ordinary least square regressions were performed between the adopted VIs and climatic parameters referring to the abovementioned different temporal windows.

In particular, either per study site (a unique VI value per each study area) and per species (different VI for different vegetation species, in order to investigate possible different behaviour of the diverse vegetation typologies) analysis were carried out.

Furthermore, given the high number of Pearson correlations computed, since per each VI dataset one-by-one all (namely eight) climatic parameters were tested, the related statistical significances were corrected according to Bonferroni procedure (Rom, 1990).

The statistical analyses were performed using Stata 9.2 (StataCorp, 2005) statistical software package.

4.2. Results

4.2.1. Multiannual series of climatic parameters and spectral VIs

Examination of variations over the last twenty years for some climatic parameters revealed consistent interannual variation. Similarly, a significant interannual variation was evident for the VIs studied. Figure 14 and 15 show these variations.

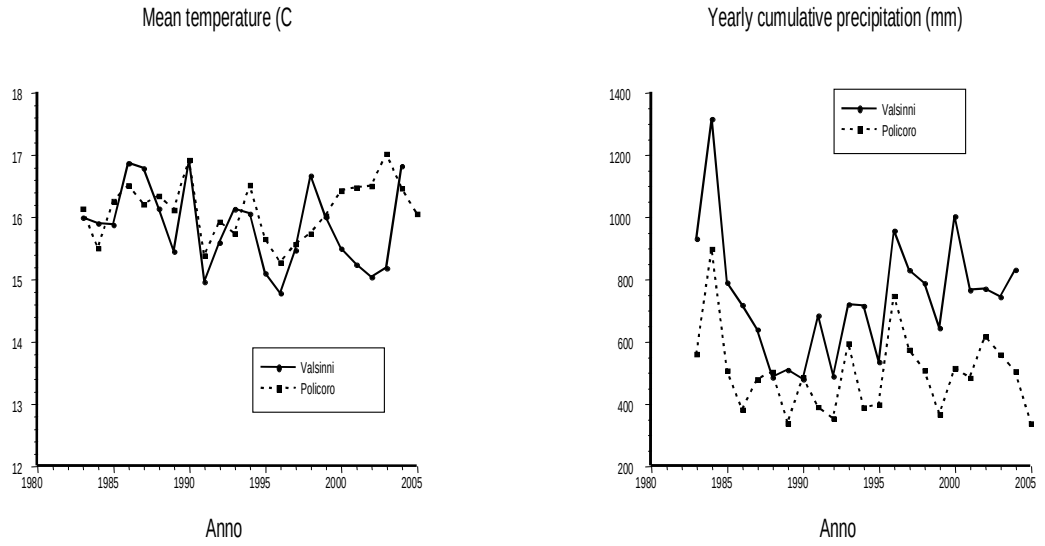

Figure 14 – Interannual climatic fluctuations - Valsinni and Policoro ground stations

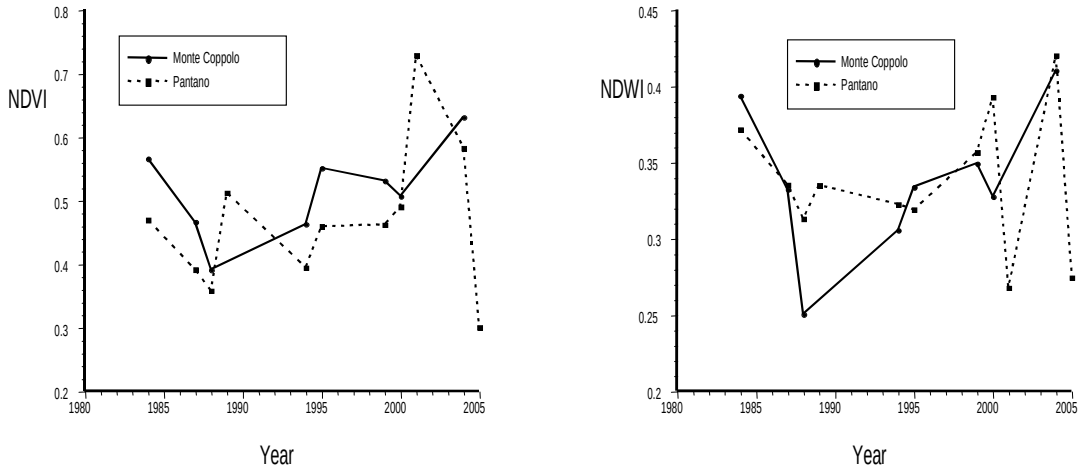

Figure 15 – Interannual VI fluctuations observed for M.Coppolo and Pantano areas.

4.2.2. Climatic parameters-VIs relationships

At first, statistical analyses performed by using a unique, mean VI for the whole study area, were tested. Results are reported in table 22. In Monte Coppolo study site

both NDVI and NDWI resulted inversely correlated with the mean temperature of the preceding 10-30 days. Also, a positive correlation between NDWI and the cumulative rainfall of the preceding three months (P_{90}) was observed. Conversely, within Pantano area none of the relationships resulted to be significant. Afterwards, the same analyses were carried out on a vegetation typology basis, see table 23 and 24.

With regard to Monte Coppolo area, by examining separately each vegetation community, it was highlighted that a temperature effect is particularly evident on deciduous forest and maquis whereas it is weak or even absent on live oak forest. Also, in areas covered by maquis a positive correlation between the NDWI and the cumulative precipitation of the last three months (P_{90}) was observed.

With respect to Pantano study site, once more no significant relationships between any of the tested climatic parameters and VIs were obtained, except for a positive correlation between the NDWI and the cumulative precipitation of the last three months (P_{90}).

Table 22 – Results of statistical analysis between climatic parameters and VIs for the two study areas of M.Coppolo and Pantano (n=number of observations, ns= not significant at 95% probability level)

Climatic parameter	M.COPPOLO		PANTANO	
	NDVI	NDWI	NDVI	NDWI
T_{180}	r=-0.783 n=8 ns	r=-0.831 n=8 ns	r=-0.109 n=11 ns	r=-0.244 n=11 ns
T_{90}	r=-0.807 n=8 ns	r=-0.847 n=8 p<0.1	r=-0.237 n=11 ns	r=-0.224 n=11 ns
T_{30}	r=-0.869 n=8 p<0.05	r=-0.933 n=8 p<0.01	r=-0.333 n=11 ns	r=-0.326 n=11 ns
T_{10}	r=-0.877 n=8 p<0.05	r=-0.911 n=8 p<0.02	r=-0.400 n=11 ns	r=-0.409 n=11 ns
P_{180}	r=0.046 n=8 ns	r=0.150 n=8 ns	r=0.616 n=11 ns	r=0.073 n=11 ns
P_{90}	r=0.753 n=8 ns	r=0.879 n=8 p<0.05	r=0.236 n=11 ns	r=0.513 n=11 ns
P_{30}	r=0.425 n=8 ns	r=0.560 n=8 ns	r=0.327 n=11 ns	r=0.406 n=11 ns
P_{10}	r=0.243 n=8 ns	r=0.313 n=8 ns	r=0.171 n=11 ns	r=0.446 n=11 ns

T= mean temperature, P= cumulative precipitations for the 180, 90, 30 e 10 day temporal windows

Table 23 – Results of statistical analysis between climatic parameters and VIs for M.Coppolo study area per vegetation typology

climatic parameter	M.COPPOLO					
	Deciduous forest		Live oak forest		Maquis	
	NDVI	NDWI	NDVI	NDWI	NDVI	NDWI
T_{180}	r=-0.786 n=8; ns	r=-0.859 n=8; p<0.06	r=-0.757 n=8; ns	r=-0.676 n=8; ns	r=-0.783 n=8; ns	r=-0.798 n=8; ns
T_{90}	r=-0.801 n=8; ns	r=-0.869 n=8; p<0.05	r=-0.778 n=8; ns	r=-0.678 n=8; ns	r=-0.809 n=8; ns	r=-0.816 n=8; ns
T_{30}	r=-0.860 n=8; p<0.05	r=-0.962 n=8; p<0.001	r=-0.823 n=8; p<0.1	r=-0.731 n=8; ns	r=-0.857 n=8; p=0.052	r=-0.880 n=8; p<0.05
T_{10}	r=-0.839 n=8; p<0.1	r=-0.875 n=8; p<0.05	r=-0.848 n=8; p<0.1	r=-0.764 n=8; ns	r=-0.890 n=8; p<0.05	r=-0.901 n=8; p<0.02
P_{180}	r=-0.012 n=8; ns	r=0.068 n=8; ns	r=0.027 n=8; ns	r=0.123 n=8; ns	r=0.055 n=8; ns	r=0.162 n=8; ns
P_{90}	r=0.673 n=8; ns	r=0.780 n=8; ns	r=0.746 n=8; ns	r=0.801 n=8, ns	r=0.794 n=8; ns	r=0.908 n=8;p<0.02
P_{30}	r=0.385 n=8, ns	r=0.567 n=8; ns	r=0.332 n=8, ns	r=0.245 n=8; ns	r=0.441 n=8; ns	r=0.565 n=8; ns
P_{10}	r=0.127 n=8; ns	r=0.105 n=8, ns	r=0.281 n=8; ns	r=0.406 n=8; ns	r=0.337 n=8; ns	r=0.457 n=8,ns

T= mean temperature, P= cumulative precipitations for the 180, 90, 30 e 10 day temporal windows

Table 24 – Results of statistical analysis between climatic parameters and VIs for Pantano study area per vegetation typology

climatic parameter	PANTANO			
	Hygrophilous forest		Maquis	
	NDVI	NDWI	NDVI	NDWI
T_{180}	r=-0.136 n=11 ns	r=-0.294 n=11 ns	r=-0.150 n=11 ns	r=-0.458 n=11 ns
T_{90}	r=-0.264 n=11 ns	r=-0.282 n=11 ns	r=-0.268 n=11 ns	r=-0.424 n=11 ns
T_{30}	r=-0.364 n=11 ns	r=-0.387 n=11 ns	r=-0.350 n=11 ns	r=-0.479 n=11 ns
T_{10}	r=-0.434 n=11 ns	r=-0.484 n=11 ns	r=-0.404 n=11 ns	r=-0.495 n=11 ns
P_{180}	r=0.598 n=11; ns	r=0.094 n=11; ns	r=0.692 n=11; ns	r=0.359 n=11; ns
P_{90}	r=0.226 n=11; ns	r=0.433 n=11; ns	r=0.337 n=11; ns	r=0.855 n=11; p<0.01
P_{30}	r=0.345 n=11; ns	r=0.426 n=11; ns	r=0.372 n=11; ns	r=0.638 n=11;ns
P_{10}	r=0.168 n=11; ns	r=0.335 n=11; ns	r=0.191 n=11; ns	r=0.593 n=11; ns

T= mean temperature, P= cumulative precipitations for the 180, 90, 30 e 10 day temporal windows

4.3 Discussion

Changes in phenology (seasonal plant and animal activity driven by environmental factors) from year to year may be a sensitive and easily observable indicator of changes in the biosphere (Menzel et al., 1999).

In this chapter, the potential of highlighting the inter-annual variation in Mediterranean vegetation activity and productivity using remotely sensed data, i.e. spectral VIs, was shown.

In particular, with data used in this study, in years when mean temperatures were higher a decrease in spectral VIs was observed. This effect was particularly evident for some types of vegetation (*maquis* and *deciduous* forest), whereas it was limited or absent in others (*hygrophylous* and *live oak forest*). In areas of Mediterranean maquis vegetation was also sensitive to rainfall: years with more rainfall showed an increase in VIs.

Reduced sensitivity of *hygrophylous* and *live oak* forest to interannual variations in precipitation and temperature probably had different explanations.

Live oak forest is particularly well adapted to hot dry summers, which are typical of the Mediterranean environment. *Live oak*, apart from having an effective leaf defence mechanism for limiting evapotranspiration and consequent loss of water at high temperatures (Crescente and Gratani, 2002) is a slow growing species possessing a very deep root apparatus (Barbero et al. 1992) allowing it to supply itself with water independently from precipitation. These characteristics explain why in *live oak* areas VIs showed little sensitivity to climatic parameters.

Hygrophylous forest, on the contrary, grows in zones where the soil is almost constantly saturated with water. The overabundance of water can moderate the effects of temperature and rainfall variations over the years.

The *maquis* is partly made up of evergreen sclerophyll like the *live oak*, which has leaf morphology (especially thick and tough) or ecological strategies (stomatal regulations, etc) which are particularly adapted to Mediterranean environments. Some other species of the *maquis*, like semideciduous shrubs, however, show more superficial root apparatus and have a faster growth cycle, having adopted ecological strategies based on the morphological difference between winter and summer foliage (Orshan, 1963, Westman, 1981, Christodoulakis, 1989, Correia et al., 1992, Gratani and Crescente, 1997) and a shortening of the growth phase to take advantage of the most favourable period

(Werner et al., 1999).

Although the Mediterranean *maquis* is made up of a variety of species with diverse adaptive mechanisms, various ecophysiological studies have shown that cumulative precipitation is "the factor which will most influence the response of Mediterranean evergreen species to water conditions on an interannual scale" (Bombelli and Gratani, 2005), in particular during the period of maximum photosynthesis (Gratani and Crescente, 1997, Gratani and Ghia, 2002).

This peculiarity of *maquis* seems to be shown by the NDWI index which is sensitive to cumulative precipitation over the period of 180 days. The effect of temperature, however, was only shown to be of importance for the temporal windows of 30-10 days, showing the relative importance of functional mechanisms to structural attributes. It is difficult to believe that the temperature over a period of 30 days could so strongly influence structural attributes of vegetation such as LAI or biomass. It is more likely that high summer temperatures associated with conditions of water deficit (stress) are compensated by a reduction in photosynthetic activity, especially in the more vulnerable species.

The importance of temperature for the regulation of ecophysiological mechanisms is also found when we analyse *deciduous* forest. Here, in particular the NDWI correlated inversely with the mean temperature calculated for the temporal windows of 90, 30 and 10 days, highlighting a reduction of vegetation water content (but also of background humidity) when temperatures are higher. In addition the NDVI index was inversely correlated to the mean temperature for the 10-30 day periods, probably as a consequence of reduced photosynthetic activity in conditions of thermal stress.

To sum up, the results obtained showed how it is possible to highlight the effect of climatic variations not only on the duration or beginning of the growth period for vegetation, but also on the seasonal peaks that are reached. It is also evident that while studies done on higher latitudes showed a positive effect of increased temperature on vegetation growth, our results showed a reduction of VI when mean temperatures rose.

Therefore, although the correlation nature of the study limits our ability to determine causal factor, nevertheless the available data and the current knowledge of plant and ecosystem functioning allow to draw the following interpretations. Climatic variations can cause changes in the seasonal vegetation peaks measured by the satellite-

derived VI and these changes, in water-limited Mediterranean regions, can be the opposite of those observed in higher latitudes. Furthermore, the study showed the variety of responses of Mediterranean vegetation to climatic change. Even within the same ecosystem different vegetation typologies showed significant diversity in their response to climatic variations. As a result, it is extremely difficult to make quantitative predictions about the possible overall response which climatic change will provoke in Mediterranean ecosystems. Particularly, if we consider that the observed results have been obtained with climatic variations which are much inferior than those expected over the next century. For example, according to the PRUDENCE-*Prediction of Regional scenarios and Uncertainties for Defining EuropeaN Climate change risks and Effect* project (http://prudence.dmi.dk/), whose results represent an essential reference for studies dealing with climate change at the European/Mediterranean regional scale, an increase of summer temperature of 5.5 °C (±1.8 °C) and a decrease in winter precipitation of 50-100 mm (±10 mm) within southern and western Europe may occur in the near future[44] (2071-2100) (Deque et al., 2005).

In the long term (from decades to centuries), changing climate may affect productivity, via species competition, by altering species composition and, ultimately, ecosystem structure and functioning.

It is noteworthy that the different structure and function of terrestrial ecosystems affect those physical mechanisms, such as the exchange of heat, moisture, trace gases, aerosol, and momentum between land surfaces and the overlying air, which may influence the climate system (Pielke et al., 1998). In fact, modelling as well as empirical studies generally indicate that decreases in vegetation increase temperature and decrease precipitation (Nobre et al., 1991, Bounoua et al., 2000, Buermann et al., 2001, Schwartz and Karl, 1990, Bastable et al., 1993), eventually amplifying and/or speeding (positive feed back) the climatic variations up within these areas.

[44] Those climate scenarios were derived according to the emission scenarios A2 defined by the *Intergovernmental Panel on Climate Change* (IPCC, Special Report on Emissions Scenario, 2000 http://www.ipcc.ch/activity/sprep.htm). However, similarly even though less prounanced climatic variations were forecasted if using the B2 scenario.

5. Conclusion

In recent years, the use of satellite imagery in ecological research and ecosystem management has increased significantly. For example, 9 of 10 recent issues of the journal Ecological Applications contain at least one article in which satellite imagery was used to characterize vegetation or land cover. The widespread availability of satellite imagery and image processing software has made it relatively easy for ecologists to use satellite imagery to address questions at the landscape and regional scales. However, as often happens with complex tools that are rendered easy to use by computer software, technology may be misused or used without an understanding of some of the limitations or caveats associated with a particular application. The results can be disappointment when maps are less accurate than expected or incorrect decisions may be derived when they are treated as truth (Fassnacht et al., 2006).

In particular, one of the most important biophysical parameters of vegetated systems is the Leaf Area Index (LAI). It can be used to infer processes (e.g., photosynthesis, transpiration, and evapotranspiration) and estimate net primary production of terrestrial ecosystems. As such, LAI is increasingly desired as a spatial data layer (i.e., map), to be used as input for modelling biogeochemical processes. However, measuring LAI on the ground is difficult and requires a great amount of labour and cost. Therefore, there is a clear need for methods to scale leaf area spatially and temporally under current conditions and environmental change scenarios.

As a result, many studies have sought to establish relationships between LAI and remote sensing data. Most of these studies have relied on empirical relationships between the ground-measured LAI and observed spectral responses, although several have used canopy reflectance models. With few exceptions, such studies used medium resolution multispectral data, like Landsat TM or ETM+ rather than high resolution image, like Ikonos (Johnson et al., 2002, Colombo et al., 2003) and concerned vegetation communities other than mediterranean ones (Lee, 2004).

In fact, a fundamental challenge to the retrieval of reliable vegetation-related information from remote sensing within mediterranean areas is the fragmented and mixed environment which characterises these zones with respect to other one (e.g. those of northern latitude).

Therefore, given that older generation sensors have many known limitations with respect to their suitability for studying highly discretized and complex land cover, the need to evaluate the new generation of sensors, providing highest spatial/spectral resolutions is of critical importance.

On the other hand, it has been hypothesised that climate changes may have the most pronounced effect within the Mediterranean region, especially within the more vulnerable coastal areas where ecosystems are threatened by the synergistic effects of climate change and human disturbances.

In this context, in this study, the utility of using Ikonos high resolution satellite images either for estimating the LAI spatial distribution of typical Mediterranean forests as well as for scaling between in situ "point" measurements and medium resolution Landsat data, when regional-wide LAI maps need to be produced, was quantitatively investigated. Furthermore, some insight into the peculiarities of Mediterranean forests response to possible changing climatic conditions was provided.

To this purposes, a widely used statistical approach for modelling the relationship between satellite-derived radiometric variables and ground measurements of biophysical variables, was utilised.

In particular, with regard to the LAI investigation, the specific selection of the best performing LAI-spectral data empirical model was performed on the basis of results provided by: a) an analysis of covariance (ANCOVA) of LAI having as independent variables the radiometric variables (i.e. one-by-one individual band as well as several spectral VIs were tested), the year of observation and the vegetation typology, and considering all possible interactions; b) a regression analyses between field LAI data and the various tested radiometric variables. Specifically, the ANCOVA analysis, performed using the pooled dataset (both year, all vegetation typologies) in order to explore the possible dependency of the LAI-radiometric data relationship on the year of observation and/or on the vegetation type, showed that only a year effect needed to be accounted for and hence a unique empirical model for all vegetation species, but different models for the two years of observation, had to be sought. Therefore, two separate datasets, one per year, were used in regression analyses. On this basis, comparison between univariate and multivariate least square regressions, performed between *in situ* LAI measurements and single radiometric variable (i.e. individual band or VI) and between *in situ* LAI

measurements and multiple band, respectively, showed the superior performances of the multiple band models, which finally were used to produce the first LAI maps for the areas under study.

However, it must be stressed that with data used in this study results indicated not only an appreciable sensitivity of empirical models to the year of data collection in terms of significantly different model coefficients for the two years but also a substantially different performance results between the two years of investigation.

These outcomes may be important for future investigations, as it indicate that even using images referring to the same areas, acquired during roughly the same season (i.e. for data used in this study in summer when forest vegetation phenological peak is supposed to be reached) of two following years, and under restricted off-nadir Ikonos satellite viewing angle requirements, very different results can be obtained. The last finding was hypothesised to be mainly related to the different period and, particularly, to the different phenological status characterising vegetation at time of 2005 data collection with respect to 2004 one. In particular, the too early period of 2005 observations could have possibly led: to residual vegetation growth between *in situ* LAI measurements and image acquisition date, causing measured LAI to significantly differ from actual LAI values at time of satellite overpass; to a higher impact of understory vegetation on forest canopy reflectance with respect to 2004.

Moreover, the Ikonos-based LAI spatial distributions obtained so far offered the possibility to assess the effectiveness of using high resolution Ikonos data (i.e. Ikonos derived LAI maps) as subsampling for upscaling *in situ* LAI measurements to medium resolution Landsat data in order to limit the extensive, extremely labour-intensive ground sampling needed for a properly characterisation of medium resolution satellite data.

In particular, the proposed strategy is implemented in two sequential steps. In the first step, a reduced number of LAI measurements are scaled to high resolution Ikonos data in order to produce a LAI spatial distribution which, in turn, provide the calibration data for the second upscaling to the medium resolution Landsat image.

Specifically, with data used in this study, it was shown that this procedure allowed an increase of about 25% of the amount of variation of LAI explained by means of Landsat ETM radiometric data directly calibrated by means of field LAI measurements.

In conclusion, while the work carried out showed the potential of using high spatial resolution satellite data (e.g. Ikonos) for LAI retrieval in Mediterranean areas, it is clear that more research is required before LAI of these forests can be routinely remotely estimated with confidence.

In particular, additional research is needed in order to effectively understand the sensitivity of the LAI-radiometric data relationship to the timing of data collection. A key issue of future studies should be to clarify whether, and under which constraints, it is possible to apply empirical relationships calibrated using data collected at a certain time point (year) to satellite data acquired in different years. In fact, in this study, because of the above mentioned differences in the timing of data collection (and hence in the vegetation phenological status) in the two years, it has not been possible to effectively verify the appropriateness of such a temporal extrapolation.

As a result, the retrospective analysis we conducted was limited to qualitative estimates of inter-annual variability in vegetation biomass, as assessed by spectral VIs. Even with these limitations our analyses yielded interesting results. In particular, they showed that it is possible to highlight an effect of climatic variations on the late spring-early summer greenness peak of Mediterranean vegetation by means of remotely sensed data. Furthermore, they pointed out that responses to interannual variations in rainfall and temperature regimes depends on vegetation typology. Even within the same ecosystem different vegetation typologies showed significant diversity in their response to variations in climatic parameters. Finally, our results pointed out that in Mediterranean ecosystems the association between climatic variations and biomass seasonal peaks can differ from what is observed at higher latitudes. In fact, at higher latitudes a positive effect of increased temperature on vegetation growth is observed, whereas our results indicated a reduction of VIs when mean temperatures rose in Mediterranean areas, where water availability is a primary limiting factor for vegetation growth.

Clearly, although the results of this exploratory study are encouraging, much work remains to be done in order to convert the available knowledge into quantitative and operative findings and, more generally, to understand the dynamics of Mediterranean vegetation. In fact, while remote sensing has been shown to provide an effective contribution in these important endeavours, it seems extremely difficult to draw general

conclusions and make quantitative predictions about the possible prevalent or overall response which the forecasted climatic change will provoke in Mediterranean ecosystems. All the more if we consider that the observed results, i.e. the relationships between vegetation productivity and cumulative temperatures and precipitations, have been obtained with climatic variations less extreme than those expected over the next century. In view of the hydric critical conditions of most Mediterranean areas resulting from the more recently forecasted scenarios and the observed different responses of the diverse vegetation typologies it is likely that the latter may alter their competitive ability and thus their ecology and conservation, with possible future changes in structure and functioning of ecosystems.

In refining and validating results obtained so far, future applications may exploit the new generation of high temporal resolution sensors (i.e., MODIS) to monitor the greenness levels along the whole annual phenological cycle at a spatial resolution as fine as 250 m (Zhang et al., 2003). For example, taking advantage of its increased spatial resolution compared to its predecessor (i.e. the 1 km-AVHRR) MODIS observations can be used for evaluating the timing of peak greenness (maximum vegetation activity/productivity) per study sites or even per vegetation community. Also, the investigation should be extended to other, possibly widest areas. Larger data sets should be used to further explore the benefits and robustness of multivariate models, making it possible to use part of the data for developing the empirical relationship (training) and the other part for assessing the predictive ability of the model (validation).

In general, and particularly when dealing with extensive areas, data from satellite images should be integrated with data from the rapidly proliferating volume of spatial information, available at increasingly higher spatial resolutions, e.g., DEM, soil maps, land cover/vegetation maps. Such approach may contributes to improving the capacity of information extraction from satellite data by allowing the design of algorithms that optimally assimilate remote sensing information (Liang 2004, Tuyl 2005). These additional ancillary data might also enhance our confidence in the resultant interpretations. In fact, the correlational nature of most analyses prevent or limit the assignment of causal relations between the observed phenomena, as is typical of experimental studies, and only allow inferential explanations. Thus, the interpretation of results might be strengthened by including in the analyses further environmental data

which are known to influence the processes under study. For example, information on terrain aspect and slope (DEM-derived products), as well as soil characteristics (e.g., depth and texture) would allow to better account for actual water availability at a specific location taking into account both distributed climatic data, i.e. temperature and precipitation, and soil water holding capacity.

Furthermore, a more detailed knowledge of overall ecological conditions might facilitate the extrapolation of results obtained within a specific site to habitat characterised by similar conditions.

Finally, a further step would be the implementation of scaling studies combing remote sensing and physiologically-based process modelling, which represent a rapidly evolving field. A variety of process models now exists which provide forest photosynthesis and primary production estimates, whose reliability obviously depend on the accuracy of input data. These models, applied in a spatially distributed mode, can assimilate a diverse assemblage of environmental data, including information on soils, climate, and vegetation (Turner et al., 2004) and hence might effectively integrate satellite-derived spatial data layer, such as LAI.

6. References

Aoki M.. Yabuki K.. Totsuka T. 1988. Effective spectral characteristics of leaf for the remote sensing of leaf water content. J. Agr. Met.. 44(2):111-117.

Anderson M. C.. Neale C. M. U. Li F.. Norman J. M.. Kustas W. P.. Jayanthi H.. J. Chavez. 2004. Upscaling ground observations of vegetation water content. canopy height. and leaf area index during SMEX02 using aircraft and Landsat imagery. Remote Sensing of Environment. 92. 447-464.

Asner G.P., Scurlock J. M. O.. Hicke J. A. 2003. Global synthesis of leaf area index observations: implications for ecological and remote sensing studies. Global Ecology & Biogeography. Vol. 12. Issue 3. Page 191.

Bannari. A.. Morin. D.. Bonn. F.. & Huete. A. R. (1995). A review of vegetation indices. Remote Sensing Reviews. 13. 95–120.

Barbero, M., Loisel, R., Quezel, P., 1992. Biogeography, ecology and history of Mediterranean *Quercus ilex* ecosystems. Vegetatio, 99–100, 19–34.

Baret F.. Guyot G. and Major D. J.. 1989. TSAVI: a vegetation index which minimizes soil brightness effects on LAI and APAR estimation. in Proceedings of the 12th Canadian Symposium on Remote Sensing. IGARRS ’90. Vancouver. BC. Canada. 10-14 July. Vol.3. pp.1355-1358.

Baret. F.. & Guyot. G. (1991). Potentials and limits of vegetation indices for LAI and APAR assessment. Remote Sensing of Environment. 46. 213– 222.

Basso B.. Cammarano D.. De Vita P.. 2004. Rivista Italiana di Agrometeorologia 1:36-53.

Bastable H.G., Shuttleworth W.J., Dalla rosa R.L.G., Fisch G., Nobre C.A., Observation of climate albedo, and surface radiation over cleared and undisturbed Amazonian forest, 1993. Int.J. Climatol., 12, 783-796.

Bavusi A., Settembrino G., 1992. Il Bosco di Policoro. *Natura in Basilicata*. Alfagrafica Volonnino Lavello. 103-112.

Bicheron. P. and Leroy. M.. 1999. A method of biophysical parameter retrieval at global scale by inversion of a vegetation reflectance model. Remote Sens. Environ.. 67. 251–266

Bombelli A., Gratani L., 2005. Risposte funzionali delle specie sempreverdi della

macchia mediterranea alla disponibilità idrica. Informatore Botanico Italiano, 37 (1A), 182-183.

Bonhomme R., 2000. Bases and limits to using 'degree.day' units. European Journal of Agronomy, 13: 1-10

Bounoua, G., J., Collartz G.J., Los S.O., Sellers P.J., Dazlich D.A.Tucker C.J., Randall D., 2000, Sensitivity of climate to changes in NDVI, J.Clim., 13, 2277-2292.

Breda NJJ. 2003. Ground-based measurements of leaf area index: a review of methods. instruments and current controversies. Journal of Experimental Botany 54 (392): 2403-2417.Campbell B.J.. 1996. Introduction to Remote Sensing (Second Edition). Taylor & Francis. London.

Broge N.H., and Mortensen J.V., 2002. Deriving green crop area index and canopy chlorophyll density of winter wheat from spectral reflectance data. Remote Sens. of Environment, 81, 45-47.

BuermannW., Dong J., Zeng Z., Myneni R.B., Dickinson R.E., 2001. Evaluation of the utility of satellite-based vegetation leaf area index data for climate simulation, J. clim., 14, 3536-3550.

Caraux Garson D. and Lacaze B., 2003. Monitoring Leaf Area Index of Mediterranean oak woodlands: comparison of remotely-sensed estimates with simulations from an ecological process-based model. Int.journal remote sens. 24, , 17, 3441–3456

Carlson T. N.. Ripley D. A.. 1997. On the relation between *NDVI*. Fractional Vegetation Cover and Leaf Area Index. Remote Sens. of Environment. 62:241-252.

Carter G. A. and A. K. Knapp. 2001. Leaf optical properties in higher plants: linking spectral characteristics to stress and chlorophyll concentration. American Journal of Botany 88(4): 677–684.

Chappelle . E.W.. Kim. M.S.. McMurtrey. J.E.. 1992. Ratio analysis of reflectance spectra (RARS) – An algorithm for the remote estimation of the concentration of Chlorophyll-a. Chlorophyll-b and carotenoids in soybean leaves. Remote Sensing of Environment. 39 (3): 239-247.

Chander G.and Markham B., 2003. Revised Landsat-5 TM Radiometric Calibration Procedures and Postcalibration Dynamic Ranges. IEEE Transactions on geoscience and remote sensing, vol. 41, NO. 11, 2674-2677

Chander. G.. D. Helder. B. Markham. J. Dewald. E. Kaita. K. Thome. E. Micijevic. T. Ruggles (2004). Landsat-5 TM reflective-band absolute radiometric calibration. IEEE Transactions on Geoscience and Remote Sensing. vol. 42. no. 12. pp: 2747- 2760.

Chase T. N.. Pielke R. A.. Kittel T. G. F.. Nemani R.. Running S. W. 1996. Sensitivity of a general circulation model to global changes in leaf area index. Journal of Geophysical Research. VOL. 101. NO. D3. pp. 7393–7408.

Chen. J. M.. and Black. T. A. (1991). Measuring leaf area index of plant canopies with branch architecture. Agric. For. Meteorol.. 57:1-12.

Chen, J.M. 1996. Evaluation of vegetation indices and a modified simple ratio for boreal applications. Can. J.Remote Sens.22,:229-242.

Chen Jing M. and Leblanc Sylvain G.. 1997. A Four-Scale bidirectional Reflectance Model Based on Canopy Architecture. IEEE Transactions on Geoscience and Remote Sensing. vol. 35. no. 5.

Chen. W.. Chen J.M.. and Chilar. J.. 2000. Integrated terrestrial ecosystem carbon-budget model based on changes in disturbance. climate. and atmospheric chemistry. Ecol.Model. 135:55-79.

Chen J.M.. G. Pavlica. L. Browna.1. J. Cihlara. S.G. Leblanca. H.P. Whitea. R.J. Hallb. D.R. Peddlec. D.J. Kingd. J.A. Trofymowe. E. Swiftf. J. Van der Sandeng. P.K.E. Pellikka. 2002. Derivation and validation of Canada-wide coarse-resolution leaf area index maps using high-resolution satellite imagery and ground measurements. Remote Sensing of Environment. 80. 165-184.

Christodoulakis, N.S., 1989. An anatomical study of seasonal dimorphism in the leaves of *Phlomis fructicosa*. Ann. Bot. 63, 389–394.

Crist. E. P.. and Cicone. R. C. (1984). Application of the Tasseled Cap concept to simulated Thematic Mapper data. Photogramm. Eng. Remote Sens. 50:343–352.

Ciais. M. Reichstein. N. Viovy. A. Granier. J. Ogée. V. Allard. M. Aubinet. N. Buchmann. Chr. Bernhofer. A. Carrara. F. Chevallier. N. DeNoblet. A. D. Friend. P. Friedlingstein. T. Gruünwald. B. Heinesch. P. Keronen. A. Knohl. G. Krinner. D. Loustau. G. Manca. G. Matteucci. F. Miglietta. J. M. Ourcival. D. Papale. K. Pilegaard. S. Rambal. G. Seufert. J. F. Soussana. M. J. Sanz. E. D. Schulze. T. Vesala. R. Valentini. 2005. Europe-wide reduction in primary productivity caused by the heat and drought in 2003. NATURE. Vol. 437. 22 September.

Clevers J.G.P.W. 1988. The derivation of a simplified reflectance model for the estimation of leaf area index. Remote Sens. of Environ. 61:221-228.

Cohen W. B.. Maiersperger T. K.., Yang T. K.. Z., Gower S. T., Turner D. P., Ritts, Berterretche M., Running S. W.. 2003. Comparisons of land cover and LAI estimates derived from ETM+ and MODIS for four sites in North America: a quality assessment of 2000/2001 provisional MODIS products. Remote Sensing of Environment. 88: 233-255

Cohen W. B.. Maiersperger T. K., Gower Stith T., Turner David P., 2003. An improved strategy for regression of biophysical variables and Landsat ETM+ data. Remote Sens. of Environment 84. 561-571.

Colombo R., Bellingeri D., Fasolini D., Marino C.M., 2003. Retrieval of leaf area index in different vegetation types using high resolution satellite data.

Consoli S., D'Urso G., Toscano A., 2006. Remote sensing to estimate ET-fluxes and the performance of an irrigation district in southern Italy. Agricultural Water Management 81 : 295–314

Correia, O., Martins, A.C., Catarino, F., 1992. Comparative phenology and seasonal foliar nitrogen variation in Mediterranean species of Portugal. Ecol. Mediterr. 18, 7–18.

Cowling. R. M.. Rundel. P. W.. Lamont. B. B.. Arroyo. M. K.. & Arianoutsou. M. (1996). Plant diversity in Mediterranean-climate regions. Tree. 11(9). 362–366.

Crescente M.F., Gratani L., 2002. Shoot growth efficiency and production of *Quercus ilex L.* in different climates. Flora, 197, 2-9.

Crippen R.E.. 1990. Calculating the Vegetation Index Faster. Remote Sens. Environ. 34:71-73.

Cubasch U. Von Storch H. Waszkewitz J. Zorita E. 1996. Estimates of climate change in Southern Europe derived from dynamical climate model output. Climate Research 7: 129-149.

Curran P.J. & Kupiec J.A.. 1995. Imaging Spectrometry: A New Tool for Ecology. in Advances in Environmental Remote sensing (Danson F. M.. & Plumme S. E.. Ed.). John Wiley & Sons.

Cutini A.. Matteucci G.. Scarascia Mugnozza G..1998. Estimation of leaf area index with the Li-Cor LAI 2000 in deciduous forests. Forest Ecology and Management.105. 55-65.

D'Urso G.. Menenti M.. Santini A.. 1999. Regional application of one-dimensional water flow models for irrigation management. Agricultural Water Management, 40: 291±302.

Danson F.M.. 1995. Development in the Remote Sening of Forest Canopy Structure . in Advances in Environmental Remote sensing (Danson F. M.. & Plumme S. E.. Ed.). John Wiley & Sons.

Daughtry C.S.T.. Walthall C.L.. Kim M.S.. de Colstoun E.B.. McMurtrey J.E. 2000. Estimating Corn Leaf Chlorophyll Concentration from Leaf and Canopy Reflectance. Remote Sens. Environ. 74: 229-239.

Davi H., K. Soudani, T. Deckx, E. Dufrene, V. Le Dantec and C. Francois, 2006. Estimation of forest leaf area index from SPOT imagery using NDVI distribution over forest stando. International Journal of Remote Sensing, Vol. 27, No. 5, 885–902.

Deng F.. Chen J. M.. Plummer S.. Chen M.. and Pisek J.. 2006. Algorithm for Global Leaf Area Index Retrieval Using Satellite Imagery IEEE Transactions on geoscience and remote sensing. VOL. 44. NO. 8. 2219

Déqué, M., R.G. Jones, M. Wild, F. Giorgi, J.H. Christensen, D.C. Hassell, P.L. Vidale, B. Rockel, D. Jacob, E. Kjellstrom, M. de Castro, F. Kucharski and B. van den Hurk, 2005: Global high resolution versus Limited Area Model climate change scenarios over Europe: quantifying confidence level from PRUDENCE results. Climate Dynamics, vol.25, issue 6: 653-670.

Di Castri. F.. & Mooney. H. A. (Eds.). (1973). Mediterranean-type ecosystems. Origin and structure. Ecological Studies. vol. 7. New York7 Springer-Verlag. ISBN: 0-387-06106-1.

Dial. G.. Bowen. H.. Gerlach. F.. Grodecki. J.. & Oleszczuk. R., 2003. IKONOS satellite. imagery. and products. Remote Sensing of Environment. 88. 23– 36.

Dial G.. Grodecky J.. 2004. RPC Replacement Camera Model. The International Archive of Photogrammetry. Remote Sensing and Spatial Information Sciences. Vol.34.). Also in http://www.spaceimaging.com/techpapers/default.htm

Eriksson H. M., Eklundh L., Kuusk A., Nilson T., 2006. Impact of understory vegetation on forest canopy reflectance and remotely sensed LAI estimates. Remote Sensing of Environment (in press).

Fassnacht K.S., Cohen W. B., Spies T. A., 2006. Key issues in making and using satellite-based maps in ecology: A primer. Forest Ecology and Management 222:167–181.

Fascetti S.. 1996. Alcune fitocenosi caratteristiche del paesaggio vegetazionale della Basilicata. Monografia su Risorsa natura in Basilicata. Notizie Regione Basilicata. 9 . n. 5-6. pp. 143-146.

Fensholt R.. Sandholt I.. Rasmussen S.M. . 2004. Evaluation of MODIS LAI. fAPAR and the relation between fAPAR and NDVI in a semi-arid environment using in situ measurements. Remote Sensing of Environment 91: 490-507

Fourty. Th.. Baret. F.. Jacquemoud. S.. Schmuck. G.. Verdebout. 1996. Leaf Optical Properties with Explicit Description of Its Biochemical Composition: Direct and Inverse Problems. Remote Sensing of Environment. Vol: 56. Issue: 2.

Furby S. L.. Campbell N. A.. 2001. Calibrating images from different dates to "like value" digital count. Remote Sensing of Environment. Vol. 77. issue 2. pag. 186-196

Gao, B. C., 1996. NDWI—a normalized difference water index for remote sensing of vegetation liquid water from space. Remote Sensing of Environment, 58, 257– 266.

Gao F.. Schaaf C.B.. Strahler A.H.. Jin Y.. Li X.. 2003. Detecting vegetation structure using a kernel-based BRDF model. Remote Sensing of Environment 86. 198–205.

Gilabert MA, Gonzalez-Piqueras J, Garcia-Haro FJ, Melia J, 2002. A generalized soil-adjusted vegetation index. Remote Sensing of Environment, 82 (2-3): 303-310

(b) A.A.. Merzlyak M.N., 1997. Remote estimation of chlorophyll content in higher plant leaves. Int.J. Remote Sens.. 18(12):2691-2697.

Gitelson. A. A.. Merzylak. M. N.. & Lichtenthaler. H. K., 1996 (a). Detection of red edge position and chlorophyll content by reflectance measurements near 700 nm. Journal of Plant Physiology. 148. 501– 508.

Gitelson A., Kaufman Y.J., Merzylak M., 1996. Use of green channel in remote sensing of global vegetation from *EOS-MODIS*. Remote Sensing of Environment, 58: 289-299.

Gitelson. A. A, 2004. Wide Dynamic Range Vegetation Index for Remote Quantification of Biophysical Characteristics of Vegetation. J. Plant Physiol. 161. 165–173

Goetz. S.J.. Prince. S.D.. Goward. S.N.. Thawley. M.M.. Small. J.. and Johnston. A. (1999). Mapping net primary production and related biophysical variables with remote sensing: Application to Boreas region. J. Geophys. Res. 104:27719-27733.

Gong P.. Pu R.. Biging G.S.. Larrieu M.R.. 2003. Estimation of forest leaf area index using vegetation indices derived from Hyperion Hyperspectral data. IEEE Transaction on Geoscience and Remote Sensing. vol.41. no.6. 1355-1362.

Goodale, C.L., Apps, M.J., Birdsey, R.A., Field, C.B., Heath, L.S., Houghton, R.A., Jenkins, J.C., Kohlmaier, G.H., Kurz, W., Liu, S.R., Nabuurs, G.J., Nilsson, S., Shvidenko, A.Z., 2002. Forest carbon sinks in the Northern Hemisphere. Ecol. Appl. 12, 891–899.

Goward S. N., Davis P. E., Fleming D., Miller L., Townshend J. R., 2003. Empirical comparison of Landsat 7 and IKONOS multispectral measurements for selected Earth Observation System (EOS) validation sites

Gower S. T.. Kucharik C. J. and Norman J. M.. 1999. Direct and indirect Estimation of Leaf Area Index. fAPAR. and Net Primary Production of Terrestrial Ecosystems. *Remote Sens. of Environ*. 70:29–51.

Gratani, L., Crescente, M.F., 1997. Phenology and leaf adaptative strategies of Mediterranean maquis plants. Ecol. Medit. 23, 11–19.

Gratani L., Ghia E., 2002. Changes in morphological and physiological traits durino leaf expansion of *Arbutus unedo*. Envir. Exp. Bot., 48, 51-60.

Gratani L., Varone L., Bombelli A., 2005. Modelli adattativi di specie sempreverdi mediterranee. Informatore Botanico Italiano, 37 (1°), 216-217.

Hall F..Townshed J. R.. Engman E. T.. 1995. Status of Remote Sensing Algorithms for Estimation of Land Surface State Parameters. Remote Sensingof Environment. 51. 128-156.

Hardisky, M. A., Lemas, V., & Smart, R. M., 1983. The influence of soil salinity, growth form, and leaf moisture on the spectral reflectance of Spartina alternifolia canopies. Photogrammetric Engineering and Remote Sensing, 49, 77–83.

Healey S. P, Yang Z., Cohen W. B., Pierce D. J., 2006. Application of two regression-based methods to estimate the effects of partial harvest on forest structure using Landsat data. Remote Sensing of Environment 101, 115–126

Horne. 2003. A tasseled cap transformation for ikonos images. ASPRS Annual Conference Proceedings

Howard J.A.. Remote Sensing of Forest Resources – Theory and applications. Chapman & Hall. London 1991.

Huang C.. Wylie B.. Yang L.. Homer C.. and Zylastra G. (2002). Derivation of a tasseled cap transformation based on Landsat-7 at-satellite reflectance. Int. J. Remote Sens.23:1741-1748.

Huete. A. R. (1988). A soil-adjusted vegetation index (SAVI). Remote Sens. Environ. 29:295–309.

Huete. A. R., Liu H.Q., Batchily K., and van Leeuwen W., (1997). A comparison of vegetation indices over a global set of TM images for EOS-MODIS. Remote Sens. Environ. 59:440-451.

Hunt E.R.. Rock B.N.. Nobel P.S. (1987). Measurement of leaf relative water content by infrared reflectance. Remote Sens. Environ.. 22:429-435.

Hunt E.R.. Rock B.N. (1989). Detection of changes in leaf water content using near and middle-infrared reflectances. Remote Sens. Environ.. 30(1):43-54.

Hurcom J.. Harrison A. R.. 1998. The NDVI and spectral decomposition for semi-arid vegetation abundance estimation. International Journal of Remote Sensing. Volume 19. Number 16 / November 1. 3109 – 3125

IPCC. 2001: Climate Change 2001: The Scientific Basis. Contribution of Working Group I in The Third Assessment Report of Intergovernmental Panel on Climate Change. eds.: Houghton. J.T.; Ding. Y.; Griggs. D. J.; Noguer. M.; Van Der Linden. P. J.; Dai. X.; Maskell. K. & Johnson. C A. – Cambridge University Press.

Jackson T. J. Chen D.. Cosh M.. Li F.. Anderson M.. Walthall C.. Doriaswamy P.. Hunt E. R.. 2004. Vegetation water content mapping using Landsat data derived normalized difference water index for corn and soybeans. Remote Sensing of Environment. 92. 475–482.

Jacquemoud, S., Baret, F., Andrieu, B., Danson, F. M., & Jaggard, K.(1995). Extraction of vegetation biophysical parameters by inversion of the PROSPECT + SAIL models on sugar beet canopy reflectance data. Application to TM and AVIRIS sensors. Remote Sensing of Environment, 52, 163–172.

Johnson, L. F., Roczen, D., & Youkhana, S., 2001. Vineyard canopy density mapping with Ikonos satellite imagery. Third International Conference on Geospatial Information in Agriculture and Forestry, Denver, Colorado. 10 pp.

Jordan. C. F. (1969). Derivation of leaf-area index from quality of light on the forest floor. Ecology 50:663–666.

Jonckheere I., Fleck S., Nackaerts K., Muysa B., Coppin P., Weiss M., Baret F., 2004. Review of methods for in situ leaf area index determination Part I. Theories, sensors and hemispherical photography. Agricultural and Forest Meteorology 121, 19–35.

Justice C. O., E. Vermote, J.R. G. Townshend, R. Defries, D. P. Roy, D. K. Hall, V. V. Salomonson, J. L. Privette, G. Riggs, A. Strahler, W. Lucht, R. B. Myneni, Y. Knyazikhin, S. W. Running, R. R. Nemani, Z. Wan, A. R. Huete, W. van Leeuwen, R. E. Wolfe, L. Giglio, J.Muller, P. Lewis, and M. J. Barnsley, 1998. The Moderate Resolution Imaging Spectroradiometer (MODIS): Land Remote Sensing for Global Change Research, 1998. IEEE Transactions on geoscience and remote sensing, vol. 36, n. 4: 1228:1249.

Kaufman, Y.J. and Tanrè, D., 1992. Atmospherically Resistant Vegetation Index (ARVI) for EOS-MODIS. IEEE Transactions on Geoscience and Remote Sensing, vol.30, n°2, pp.261-270.

Kauth. R. J.. and Thomas. G. S. (1976). The Tasselled Cap—a graphic description of the spectral-temporal development of agricultural crops as seen by Landsat. In Proceedings of the Symposium on Machine Processing of Remotely Sensed Data. Purdue University. West Lafayette. pp. 41–51.

Kawabata A., K. Ichii and Y. Yamaguchi, 2001. Global monitoring of interannual changes in vegetation activities using NDVI and its relationships to temperature and precipitation. Int. J. Remote Sensing, 2001, vol. 22, no. 7, 1377- 1382.

Kyung-Ja Ha. Hyun-Mi Oh. and Ki-Young Kim. 2001. Inter-Annual and Intra-Annual Variabilities of NDVI. LAI and Ts Estimated by AVHRR in Korea. Korean Journal of Remote Sensing. Vol.17. No.2. 2001. pp.111-119.

Inoue Y.. Morinaga S.. Shibayama M. (1993). Non-destructive estimation of water status of intact crop leaves based on spectral reflectance measurements. Jpn. J. Crop. Sci.. 62(3):462-469.

Lanfredi M.. T. Simoniello. M. Macchiato. 2004. Temporal persistence in vegetation cover changes observed from satellite: Development of an estimation procedure in the test site of the Mediterranean Italy. Remote Sensing of Environment, 93, 565–576.

Lavorel S., Canadell J., Rambal S., Terradas J., 1998. Mediterranean terrestrial ecosystem: research priorities on global change effect. Global Ecol. Biogeogr. Lett. 7, 157-166.

Lawrence RL. Ripple WJ (1998) Comparisons among vegetation indices and bandwise regression in a highly disturbed. heterogeneous landscape: Mount St Helens. Washington. Remote Sensing of environment 64: 91–102

Lee K., Cohen W. B., Kennedy R. E., Maiersperger T. K., Gower S. T., 2004. Hyperspectral versus multispectral data for estimating leaf area index in four different biomes. Remote Sensing of Environment 91 508–520

Li, Z., & Kafatos, M. (2000). Interannual variability of vegetation in the United States and its relation to El Nino/Southern Oscillation. Remote Sensing of Environment, 71(3), 239– 247.

LI-COR 1992. LAI-2000 Plant Canopy Analyser: Operating Manual. Lincoln. NE. USA.

Liang S.. 2001. Atmospheric Correction of Landsat ETM+ Land Surface Imagery—Part I: Methods. IEEE Transactions on geoscience and remote sensing. vol. 39. no. 11.

Liang S.. 2004, a. Quantitative Remote Sensing of Land Surfaces. pp. 249, John Wiley & Son Inc., Hoboken, New Jersey

Liang S., 2004, b. Quantitative Remote Sensing of Land Surfaces, pp. 250, John Wiley & Son Inc., Hoboken, New Jersey

Li X.. Gao F.. Wang J.. and Strahler A..(2000). A priori knowledge accumulation and its application to linear BRDF model inversion. J. Geophys. Res. 106:11.925-11.935.

Lichtenthaler H.K.. Gitelson A.. Lang M. (1996). Non-destructive determination of chlorophyll content of leaves of a green and an aurea mutant of tobacco by reflectance measurements. J. Plant Physiol.. 148:483-493

Maki M., Ishiahra M., Tamura M., 2004. Estimation of leaf water status to monitor the risk of forest fires by using remotely sensed data. Remote Sensing of Environment, 90, 441–450.

Markham B.L.. 2004. Landsat Sensor Performance: History and Current Status. IEEE Transactions on geoscience and remote sensing. vol. 42. no. 12.

Maselli F.. Amparo Gilabert M.. Conese C.. 1998. Integration of high and low resolution NDVI data for monitoring Vegetation in Mediterranean Environments. Remote Sensing of Environment. 63. 208-218.

Maselli F., 2004. Monitoring forest conditions in a protected Mediterranean coastal area by the analysis of multiyear NDVI data. Rem. Sensing of Environ. 89, 423–433.

Menzel A. and Fabian P., 1999. NATURE, VOL 397, p.659.

Michaelsen, J., 1987, Cross-validation in statistical climate forecast models. Journal of Climate and Applied Meteorology, 26, pp. 1589–1600

Myneni R. B.. Keeling C. D.. Tucker C. J.. Asrar G. & Nemani R. R.. 1997. Increased plant growth in the northern high latitudes from 1981 to 1991. Nature. vol. 386. 698-702

Moghaddam and Saatchi. 1999. Monitoring Tree Moisture Using an Estimation Algorithm Applied to SAR Data from Boreas. IEEE Transactions on geoscience and remote sensing. vol. 37. no. 2. 901.

Muchoney. D. and Strhaler. A. (2002). Regional vegetation mapping and direct land surface parameterisation fromremotely sensed and site data. Int. J. Remote Sens. 23: 1125-1142.

Nemani R. R., Keeling C. D., Hashimoto H., Jolly W. M., Piper S. C., Tucker C. J., Myneni R. B., Running S. W. 2003. Climate-Driven Increases in Global Terrestrial Net Primary Production from 1982 to 1999. Science Reports vol.300: pp.1560-1563.

Nicodemus. F. E.. et al., 1977. Geometrical considerations and nomenclature for reflectance. Washington. DC: National Bureau of Standards. US Department of Commerce.

Nobre C., Sellers P.J., Shukla J., Amazonian deforestation and regional climate change, 1991, J. Clim., 4, 957-988.

Orshan, G., 1963. Seasonal dimorphism of desert and Mediterranean chamaephytes and its significance as a factor in they water economy. In: Rutter, A.J., Whitehead, F.H. (Eds.), The Water Relations of Plants. Blackwell Scientific, Oxford, pp. 206–222.

Pagnutti Mary. Ryan Robert E.. Kelly Michelle. Holekamp Kara. Zanoni Vicki. Thome Kurtis. Schiller Stephen. 2003. Radiometric characterization of IKONOS multispectral imagery. Remote Sensing of Environment 88. 53–68

Palutikof. J. P.. Goodess. C.. & Guo. X., 1994. Climate change. potential evapotranspiration and moisture availability in the Mediterranean basin. International Journal of Climatology. 14. 853– 869.

Palutikof, J.P., 2002: Analysis of Mediterranean climate data. In Mediterranean Climate Variability and Trends (ed. H.-J. Bolle), Springer, Berlin, 125-132.

Pampaloni P..2004. Microwave radiometry of forests. Waves Random Media 14, S275–S298.

Papanastasis V. P., Platis P. D. and Dini-Papanastasi O.,1997. Productivity of deciduous woody and fodder species in relation to air temperature and precipitation in a

Mediterranean environment. Agroforestry Systems, 37, 187–198.

Peñuelas J.. Filella I.. Biel C.. Serrano L.. Savé R., 1993. The reflectance at the 950-970 nm region as an indicator of plant water status. Int. J. Remote Sens.. 14(10):1887-1905.

Pereira JS, Chaves MM, 1995. Plant responses to drougth under climate change in mediteranean-type ecosystems. In Moreno et al.: Global change and Mediterranean-type ecosystems. Sprinter-Verlag, New York, 140-160.

Perry C. R.. and Lautenschlager L. F. (1984). Functional equivalence of spectral vegetation indices. Remote Sens. Environ. 14:169–182.

Pielke R.A., Avissar R., Raupach M., Dolamn A.J., Zeng X., and Denning A.S., 1998. Interaction between the atmosphere and terrestrial ecosystems: influence on wheather and climate, Global Change Biol.,4, 461-476.

Pinty B. & Vestraete H.M., 1991. GEMI: a non-linear index to monitor global vegetation from satellite. *Vegetatio*, 101:15-20.

PRUDENCE final report Prediction of Regional scenarios and Uncertainties for Defining EuropeaN Climate change risks and Effects., http://prudence.dmi.dk/public/publications/PRUDENCE%20Final%20report.pdf

Qi. J., Chehbouni. A., Huete. A. R., Kerr. Y. H.. and Sorooshian. S., 1994. A modified soil adjusted vegetation index. Remote Sens. Environ. 48:119–126.

Qi. J., Cabot F:, Moran M.S: and Dedieu G., 1995. Biophysical parametr estimations using multidirectional spectral measurements. Remote Sens. Environ., 54, 71-83.

Qi J..Y. H. Kerr. M. S. Moran. M. Weltz. A. R. Huete. S. Sorooshian and R. Bryant. 2000. Leaf Area Index Estimates Using Remotely Sensed Data and BRDF Models in a Semiarid Region. Remote Sensing of Environment. 73. 18-30.

Qiu J. 2001. An Improved Model of Surface BRDF-Atmospheric Coupled Radiation. IEEE Transactions on geoscience and remote sensing. vol. 39. n. 1.

Reichstein M.. Tenhunen J. D.. Roupsard O. Ourcival J.. Rambal S.. Miglietta F. Peressotti A.. pecchiari M.. Tirone G.. Valentini R. Severe drought effects on ecosystem CO2 and H2O fluxes at three Mediterranean evergreen sites: revision of current hypotheses? Global Change Biology Vol. 8: 999.

Richardson A. J., Everitt J.H., 1992. Using spectra vegetation indices to estimate rangelands productivity, Geocarto International. Vlo. 1, pp.63-69.

Ripple, W. J., 1985, Asymptotic reflectance characteristics of grass vegetation. Photogramm. Eng. Remote Sens. 51:1915-1921.

Roeder A., Kuemmerleb T., Hill J., 2005. Extension of retrospective datasets using multiple sensors. An approach to radiometric intercalibration of Landsat TM and MSS data. Remote Sensing of Environment 95, 195–210

Rom D.M., 1990. A sequentially rejective test procedure based on a modified Bonferroni inequality. Biometrika 77 (3): 663-665

Rondeaux. G.. Steven. M.. and Baret. F., 1996. Optimization of soil-adjusted vegetation indices. Remote Sens. Environ.55:95–107.

Roujean J.L. & Breon F.M., 1995. Estimating PAR absorbed by vegetation from bidirectional reflectance measurements. *Remote Sens. Environ.*, 48: 119-126

Rouse. J. W.. Haas. R. H.. Schell. J. A.. Deering. D. W.. and Harlan. J. C. (1973). Monitoring the vernal advancement and retrogradation (greenwave effect) of natural vegetation. NASA/GSFC Type III Final Report. Greenbelt. MD.

Ryan, R., Baldridge, B., Schowengerdt, R. A., Choi, T., Helder, D. L., & Blonski, S., 2003. IKONOS spatial resolution and image interpretability characterization. Remote Sensing of Environment, 88, 37– 51.

Sabins F.F.,1996. Remote sensing: principles and interpretation (3rd ed). New York: W.H. Freeman and Company

Salomon. J.. C. B. Schaaf. A. H. Strahler. F. Gao. Y. Jin. Validation of the MODIS Bidirectional Reflectance Distribution Function and Albedo Retrievals Using Combined Observations from the Aqua and Terra Platforms. IEEE Trans. Geosci. Remote Sens. Vol. 44. No. 6. June 2006.

Sannier C. A. D.. Taylor J. C.. Du Plessis W.. 2002. Real-time monitoring of vegetation biomass with NOAA-AVHRR in Etosha National Park. Namibia. for fire risk assessment. International Journal of Remote Sensing. Volume 23. Number 1 / January 15. 71 – 89.

Sarkar S., Kafatos M., 2004. Interannual variability of vegetation over the Indian sub-continent and its relation to the different meteorological parameters. Remote Sensing of Environment 90, 268–280.

Scarascia-Mugnozza G.. Oswald H.. Piussi P.. Radoglou K.. 2000. Forests of the Mediterranean region: gaps in knowledge and research needs. Forest Ecology and Management 132. 97-109.

Schaepman-Strub G., Schaepman M.E., Painter T.H., Dangel S., Martonchik J.V., 2006. Reflectance quantities in optical remote sensing—definitions and case studies. Remote Sensing of Environment 103 27–42

Schwartz M.D. and Karl T.R., Spring phenology: Nature's experiment to detect the effect of "green up" on surface maximum temperature, 1990. Mon.Weather Rev., 118, 883-890.

Schott, J., Salvaggio, R.C., Volchok, W.J., 1988. Radiometric scene normalization using pseudoinvariant features. Remote Sensing Environ. 26, 1–16.

Sellers P. J.. Mints Y.. Sud Y.C.. Dalcher A., 1986. A simple biosphere model (SIB) for use within general circulation models. *J. Atmos.Sci. 43*: 505-531.

Sellers P. J.. Dickinson R. E.. Randall D. A.. Betts A. K.. Hall F. G.. Berry J. A.. Collatz G. J.. Denning A. S.. Mooney H. A.. Nobre C. A.. Sato N.. Field C. B.. Henderson-Sellers A. (1997). Modeling the Exchanges of Energy. Water. and Carbon Between Continents and the Atmosphere. Science. 275. 502– 509.

Smith J.. LAI inversion using a backpropagation neural network trained with multiple scattering model.. IEEE Trans. Geosci. Remote Sens.. 31. 1102–1106. 1993.

Song C.. Woodcock C.E.. Seto K.C.. Lenney M.P.. Macomber S.A.. 2001. Classification and change detection using Landsat TM data: When and how to correct atmospheric effects?. Remote Sensing of Environment. 75. 230-244.

Space Imaging (2001). IKONOS relative spectral response and radiometric calibration coefficients, document no. SE-REF-016, Rev. A. Thorton, CO: Space Imaging.

Spano D., Cesaraccio C., Duce P., Snyder 1999. Phenological stages of natural species and their use as climate indicators. International Journal of Biometeorology, 42, 124-133.

StataCorp 2005. Stata Statistical Software. College Station, TX: StataCorp LP.

Stockli R. and P. L. Vidale, 2004. European plant phenology and climate as seen in a 20-year AVHRR land-surface parameter dataset. Int. j. remote sensing, vol. 25, NO. 17, 3303–3330

Soudani K., Christophe F., Le Maire G., Le Dantec V., Dufrên E., 2006. Comparative analysis of IKONOS, SPOT, and ETM+ data for leaf area index estimation in temperate coniferous and deciduous forest stands. Remote Sensing of Environment 102 161–175

Susaki J.. Hara K.. Kajiwara K.. Honda Y. (2004). Robust estimation of BRDF model parameters. Remote Sensing of Environment. 89:63–71.

Suzuki R., Xu J., Motosa K., 2006. Global analyses of satellite-derived vegetation index related to climatological wetness and warmth. Int. J. Climatol. 26: 425–438.

Teillet, P.M., Guindon, B. And Goodenough, D.G:, 1982. On the slope-aspect correction of multispectral scanner data. Canadian Journal of Remote Sensing, 8 (2), pp. 1537-1540.

Teillet P.M.. J.L. Barker. B.L. Markham. R.R Irish. G. Fedosejevs. J.C. Storey. 2001. Radiometric cross-calibration of the Landsat-7 ETM+ and Landsat-5 TM sensors based on tandem data sets. Remote Sensing of Environment 78 (2001) 39– 54

Teillet P.M., Markham B.L., Irish R. R., 2006. Landsat cross-calibration based on near simultaneous imaging of common ground targets. Remote Sensing of Environment 102 (2006) 264–270

Thome K.J.. 2001. Absolute radiometric calibration of Landsat 7 ETM+ using the reflectance-based method. Remote Sensing of Environment 78 (2001) 27– 38

Thenkabail P.S., A.D., Lyon J.G., Merry C.J., 1994. thematic mapper vegetation indexes for determining soybean and corn growth-parameters. Photogrammetric engineering and remote sensing 60 (4): 437-442

Thenkabail P. S.. Smith. R. B.. & De Paw. E. (2000). Hyperspectral vegetation indices and their relationships with agricultural crop characteristics. Remote Sensing of Environment. 71. 158– 182.

Tian Y. et al., 2002. Radiative transfer based scaling of LAI retrievals from reflectance data of different resolutions. Remote Sensing of Environment 84. 143–159.

Toutin T., 2004. Review article: Geometric processing of remote sensing images: models, algorithms and methods. International J. of remote sensing, 25 (10): 1893-1924

Trishchenko. A. P.. Cihlar. J.. & Li. Z. (2002). Effects of spectral response function on surface reflectance and NDVI measured with moderate resolution satellite sensors. Remote Sensing of Environment. 81(1). 1– 18.

Tucker. C. J.. 1979. Red and photographic infrared linear combinations for monitoring vegetation. Remote Sens. Environ. 8:127–150.

Turner D.P., Cohen W.B., Kennedy R.E., Fassnacht K.S., Briggs J.M., 1999. Relationships between Leaf Area Index and Landsat TM Spectral Vegetation Indices across Three Temperate Zone Sites. Remote Sens. Environ. 70:52-68.

Turner D.P, Ollinger S. V., and Kimball J. S., 2004. Integrating Remote Sensing and Ecosystem Process Models for Landscape- to Regional-Scale Analysis of the Carbon Cycle, Bioscience, vol.54, n.6, 573-584.

Turner D.P., Ritts W. D., Cohen W. B. , Maeirsperger T. K ., Gower S., Kirschbaum A. A., Running S. W., Zhao M., Wofsy S. C ., Dunn A. L., Law B. E., Campbell J.L., Oechel W. C ., Kwon H. J., Meyers T. P., Small E. E., Kurc S. A . and Gamon J. A . 2005. Site-level evaluation of satellite-based global terrestrial gross primary production and net primary production monitoring. Global Change Biology 11, 666–684.

Tuyl V.S., Law B.E., Turner D.P., Gitelman A.I., 2005. Variability in net primary production and carbon storage in biomass across Oregon forests—an assessment integrating data from forest inventories, intensive sites, and remote sensing. Forest Ecology and Management, 209, 273–291.

Ustin. S. L.. Jacquemoud S.. Y. Govaerts. 2001. Simulation of photon transport in a three-dimensional leaf: implications for photosynthesis. Plant. Cell and Environment. 24. 1095–1103

Vermote et al.. 1997. Second Simulation of the Satellite Signal in the Solar Spectrum. 6S: An Overview. IEEE Transactions on Geoscience and Remote Sensing. vol. 35. no. 3. May.

Verstraete M.M., Pinty B. and R.B. Myneni. 1996 (a). Potential and limitation of information extraction on the terrestrial biosphere from satellite remote sensing. Remote Sensing of Environment. 58. 201:214.

Verstraete M.M. and Pinty B.. 1996 (b). Designing Optimal Spectral Indexes for Remote Sensing Applications. IEEE Transactions on Geoscience and Remote Sensing. vol.34. no.5. 1254-1265

Volcani A., Karnieli A., Svoray T., 2005. The use of remote sensing and GIS for spatio-temporal analysis of the physiological state of a semi-arid forest with respect to drought years. Forest Ecology and Management 215: 239–250.

Yamasaki S.. Dillenburg L.R. 1999. Measurements of leaf relative water content in araucaria angustifolia. Revista Brasileira de Fisiologia Vegetal. 11(2):69-75. 1999.

Yang, L., Wylie, B. K., Thieszen, L. L., & Reed, B. C., 1998. An analysis of relationships among climate forcing and time-integrated NDVI of grasslands over the U.S. northern and central great plains. Remote Sensing of Environment, 65, 25–37.

Yu F., Price K. P., Ellis J., Shi P., 2003. Response of seasonal vegetation development to climatic variations in eastern central Asia. Remote Sensing of Environment, 87, 42-54.

Walthall C., W. Dulaney, M. Anderson, J. Norman, H. Fang, S. Liang, 2004. A comparison of empirical and neural network approaches for estimating corn and soybean leaf area index from Landsat ETM+ imagery. Remote Sensing of Environment, 92, 465–474.

Wang Q., Adikua S., Tenhunena J., Granier A.´, 2005. On the relationship of NDVI with leaf area index in a deciduous forest site. Remote Sensing of Environment, 94, 244-255.

Weiss. Abuelgasim. A.. Gopal. S.. and Strahler. A.. 1998. Forward and inverse modelling of canopy directional reflectance using a neural network. Int. J. Remote Sens.. 19. 453–471.

Welles Jon M.. 1990. Some Indirect Methods of Estimating Canopy Structure. Remote Sensing Reviews. vol. 5(1). 31-43.

Welles Jon M.. Norman J.M.. 1991. Instruments for Indrect Measurement of Canopy Architecture. Agronomy Journal. vol. 83. 818-825.

Welles Jon M.. Cohen S.. 1996. Canopy structure measurement by gap fraction analysis using commercial instrumentation. Journal of Experimental Botany. vol. 47. n. 302. 1335-1342.

Werner C, Correia O, Beyschlag W., 1999. Two different strategies of Mediterranean macchia plants to avoid photoinhibitory damage by excessive radiation levels during summer drought. Acta Oecologica- International Journal of Ecology 20 (1): 15-23.

Westman, W.E., 1981. Seasonal dimorphism of foliage in Californian coastal sage scrub. Oecologia 51, 385–388.

White M. A.. Asner G. P.. Nemani R. R.. Provette J.L. and Running S.W.. 2000. Measuring Fractional Cover and Leaf Area Index in Arid Ecosystems: Digital Camera. Radiation Transmittance. and Laser Altimetry Methods. Remote Sensing of Environments. 74. 45-57.

Zhang X, Friedl MA, Schaaf CB, Strahler AH, Hodges JCF, Gao F, Reed BC, Huete A. 2003. Monitoring vegetation phenology using MODIS. Remote Sensing of Environment 84: 471–475.

Zhang P. and Anderson, 2004. Climate-related vegetation characteristics derived from Moderate Resolution Imaging Spectroradiometer (MODIS) leaf area index and normalized difference vegetation index. Journal of Geophysical Research, vol. 109 : 1-13.

Zhou L., Kaufmann R.K., Tian Y., Myneni R.B., and Tucker C.J., 2003. Relation between interannual variations in satellite measures of northern greenness ans climate between 1982 and 1999. Journal of geophysical research, vol., 108